Center for Environmentally Sustainable Transportation in Cold Climates

Environmental Friendly Pervious Concrete for Treating Deicer-Laden Stormwater Phase I

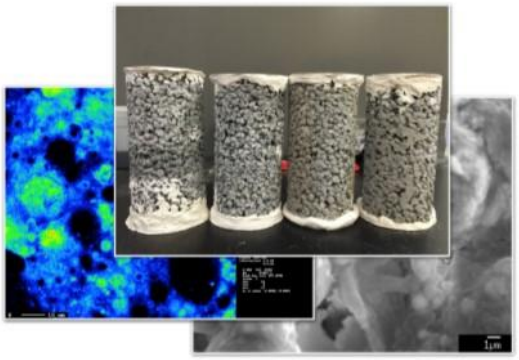

Gang Xu, Xianming Shi
Department of Civil and Environmental Engineering
Washington State University

Anburaj Muthumani

Date: 12/30/2015

Prepared by: Gang Xu, Xianming Shi, Anburaj Muthumani

Center for Environmentally Sustainable Transportation in Cold Climates
University of Alaska Fairbanks
P.O. Box 755900
Fairbanks, AK 99775

U.S. Department of Transportation
1200 New Jersey Avenue, SE
Washington, DC 20590

INE/CESTiCC 101408

Environmentally Friendly Pervious Concrete for Treating Deicer-Laden Stormwater (Phase I Report)

by

Gang Xu, M.Sc., P.E.
Xianming Shi, Ph.D., P.E.

Department of Civil and Environmental Engineering
Washington State University

Anburaj Muthumani, P.E.

Western Transportation Institute
Montana State University

INE/CESTiCC 101408

April 2016

REPORT DOCUMENTATION PAGE

Form approved OMB No.

1. AGENCY USE ONLY (LEAVE BLANK)	2. REPORT DATE	3. REPORT TYPE AND DATES COVERED
	12/2015	Final Report: 07/2014 – 12/2015

4. TITLE AND SUBTITLE

Environmentally Friendly Pervious Concrete for Treating Deicer-Laden Stormwater (Phase I Report)

5. FUNDING NUMBERS

6. AUTHOR(S)

Gang Xu, M.Sc., P.E., Washington State University
Xianming Shi, Ph.D., P.E., Washington State University
Anburaj Muthumani, P.E., Montana State University

7. PERFORMING ORGANIZATION NAME(S) AND ADDRESS(ES)

Laboratory of Advanced & Sustainable Cementitious Materials
Washington State University
405 Spokane Street, Sloan 101, P.O. Box 755900
Pullman, WA, 99164

8. PERFORMING ORGANIZATION REPORT NUMBER

9. SPONSORING/MONITORING AGENCY NAME(S) AND ADDRESS(ES)

U.S. Department of Transportation
1200 New Jersey Avenue, SE
Washington, DC 20590

10. SPONSORING/MONITORING AGENCY REPORT NUMBER

11. SUPPLENMENTARY NOTES

12a. DISTRIBUTION / AVAILABILITY STATEMENT

No restrictions

12b. DISTRIBUTION CODE

13. ABSTRACT (Maximum 200 words)

A graphene oxide-modified pervious concrete was developed by using low-reactivity, high-calcium fly ash as sole binder and chemical activators and other admixtures. The density, void ratio, mechanical strength, infiltration rate, Young's modulus, freeze-deicer salt scaling, and degradation resistance of this pervious concrete were measured against three control groups. The test results indicate that graphene oxide modified fly ash pervious concrete is comparable to Portland cement pervious concrete. While the addition of 0.03% graphene oxide (by weight of fly ash) noticeably increased the compressive strength, split tensile strength, Young's modulus, freeze-deicer salt scaling, and degradation resistance of fly ash pervious concrete, it reduced the void ratio and infiltration rate. The fly ash pervious concrete also showed unfavorable high initial loss during the freeze-deicer salt scaling test, which may be attributed to the low hydration degree of fly ash at early age. It is recommended that durability tests for fly ash concrete be performed at a later age.

14- KEYWORDS:

Fly ash, pervious concrete, graphene oxide, cementitious binder, activators

15. NUMBER OF PAGES

107

16. PRICE CODE

N/A

17. SECURITY CLASSIFICATION OF REPORT	18. SECURITY CLASSIFICATION OF THIS PAGE	19. SECURITY CLASSIFICATION OF ABSTRACT	20. LIMITATION OF ABSTRACT
Unclassified	Unclassified	Unclassified	N/A

DISCLAIMER

This document is disseminated under the sponsorship of the U.S. Department of Transportation in the interest of information exchange. The U.S. Government assumes no liability for the use of the information contained in this document. The U.S. Government does not endorse products or manufacturers. Trademarks or manufacturer names appear in this report only because they are considered essential to the objective of the document.

Opinions and conclusions expressed or implied in the report are those of the author(s). They are not necessarily those of the funding agencies.

METRIC (SI*) CONVERSION FACTORS

APPROXIMATE CONVERSIONS TO SI UNITS

Symbol	When You Know	Multiply By	To Find	Symbol
		LENGTH		
in	inches	25.4		mm
ft	feet	0.3048		m
yd	yards	0.914		m
mi	Miles (statute)	1.61		km
		AREA		
in^2	square inches	645.2	millimeters squared	cm^2
ft^2	square feet	0.0929	meters squared	m^2
yd^2	square yards	0.836	meters squared	m^2
mi^2	square miles	2.59	kilometers squared	km^2
ac	acres	0.4046	hectares	ha
		MASS (weight)		
oz	Ounces (avdp)	28.35	grams	g
lb	Pounds (avdp)	0.454	kilograms	kg
T	Short tons (2000 lb)	0.907	megagrams	mg
		VOLUME		
fl oz	fluid ounces (US)	29.57	milliliters	mL
gal	Gallons (liq)	3.785	liters	liters
ft^3	cubic feet	0.0283	meters cubed	m^3
yd^3	cubic yards	0.765	meters cubed	m^3
		TEMPERATURE (exact)		
ºF	Fahrenheit temperature	5/9 (ºF-32)	Celsius temperature	ºC
		ILLUMINATION		
fc	Foot-candles	10.76	lux	lx
fl	foot-lamberts	3.426	candela/m^2	cd/cm^2
		FORCE and PRESSURE or STRESS		
lbf	pound-force	4.45	newtons	N
psi	pound-force per square inch	6.89	kilopascals	kPa

Note: Volumes greater than 1000 L shall be shown in m^3

These factors conform to the requirement of FHWA Order 5190.1A *SI is the symbol for the International System of Measurements

APPROXIMATE CONVERSIONS FROM SI UNITS

Symbol	When You Know	Multiply By	To Find	Symbol
		LENGTH		
mm	millimeters	0.039	inches	in
m	meters	3.28	feet	ft
m	meters	1.09	yards	yd
km	kilometers	0.621	Miles (statute)	mi
		AREA		
mm^2	millimeters squared	0.0016	square inches	in^2
m^2	meters squared	10.764	square feet	ft^2
km^2	kilometers squared	0.39	square miles	mi^2
ha	hectares (10,000 m^2)	2.471	acres	ac
		MASS (weight)		
g	grams	0.0353	Ounces (avdp)	oz
kg	kilograms	2.205	Pounds (avdp)	lb
mg	megagrams (1000 kg)	1.103	short tons	T
		VOLUME		
mL	milliliters	0.034	fluid ounces (US)	fl oz
liters	liters	0.264	Gallons (liq)	gal
m^3	meters cubed	35.315	cubic feet	ft^3
m^3	meters cubed	1.308	cubic yards	yd^3
		TEMPERATURE (exact)		
ºC	Celsius temperature	9/5 ºC+32	Fahrenheit temperature	ºF
		ILLUMINATION		
lx	lux	0.0929	foot-candles	fc
cd/cm^2	candela/m^2	0.2919	foot-lamberts	fl
		FORCE and PRESSURE or STRESS		
N	newtons	0.225	pound-force	lbf
kPa	kilopascals	0.145	pound-force per square inch	psi

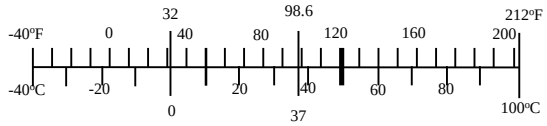

ACKNOWLEDGMENTS

The authors would like to thank the Center for Environmentally Sustainable Transportation in Cold Climates for funding this work. They would also like to thank Dr. Zhengxian Yang, Dr. Mehdi Honarvarnazari, Jiang Yu, Sen Du, and Jialuo He from the Laboratory of Advanced and Sustainable Cementitious Materials; faculty and staff from Peter Hooper GeoAnalytical Lab and Composite Materials and Engineering Center at Washington State University; Dr. Jing Zhong from Harbin Institute of Technology; and Montana State University for its cooperation during the salt scaling tests.

Table of Contents

LIST OF FIGURES

LIST OF TABLES

EXECUTIVE SUMMARY

The objective of this project during Phase I is to advance the scientific knowledge of nanotechnology by using it to expand the use of industrial waste and recycled materials in pervious concrete. This report provides an analysis and evaluation of mortar and pervious concrete that has fly ash as a sole binder. Chemical activators and graphene oxide were chosen to improve the overall performance of mortar and pervious concrete. The method of analysis included a uniform design of experiments to investigate the effects of admixtures and chemical activators on the performance of fly ash binder, and a microscopic investigation to obtain additional insights on the function of graphene oxide and chemical activators in fly ash binder. The results of mortar tests indicated that low-reactivity fly ash could be used as sole binder to form a paste with desirable strength by adopting chemical activation and graphene oxide modification at room temperature.

Following fly ash mortar testing, the property of pervious concrete with fly ash as a sole binder was evaluated. Laboratory evaluation consisted of a density and porosity test, mechanical strength test, modulus of elasticity test, and durability test. It was concluded that graphene oxide-modified fly ash pervious concrete is comparable to cement pervious concrete in terms of desirable density, void ratio, strength, infiltration rate, and durability. Further investigation is needed to improve hydration degree at early age. The results of this study demonstrate an example of a beneficial use of fly ash, a use that diverts fly ash from waste streams in its building material application. The results also show the potential for using such “greener” pervious concrete for treating deicer-laden stormwater in a variety of contaminant-loading scenarios.

CHAPTER 1.0 INTRODUCTION

1.1 Background

This project has two objectives: (1) to advance the scientific knowledge of nanotechnology by applying it to expanding the use of industrial waste and recycled materials in pervious concrete; and (2) to explore the potential of "greener" pervious concrete for treating deicer-laden stormwater in a variety of contaminant-loading scenarios.

Pervious concrete is a special type of high-porosity concrete that allows water from precipitation and other sources to pass through it directly (Figure 1.1). The infiltration effect provided by pervious concrete pavement not only recharges the groundwater, but also reduces the amount of total suspended solids, total phosphor, and total nitrogen and metals in the groundwater (Schaefer et al. 2006). The infiltration effect provided by pervious concrete pavement also meets U.S. Environmental Protection Agency (EPA) stormwater regulations.

Figure 1.1 Pervious concrete demonstration (photo by J.J. Harrison)

Fly ash, a by-product of coal-fired power plants (Figure 1.2a), has been used as partial cement replacement in concrete for decades. However, fly ash is typically used at a replacement rate of less than 35% by mass of cement due to the lack of understanding of its overall

performance (Minkara 2015). Two categories of fly ash are defined by ASTM C618: Class F fly ash (FFA) and Class C fly ash (CFA). Class F fly ash is produced from burning anthracite or bituminous coal and contains less than 20% CaO, so it is pozzolanic in nature. Class F fly ash requires a cement agent or activators to produce cementitious pastes. Palomo et al. demonstrated the potential of alkali-activated FFA as a cement for the future; the glassy silica and alumina contents in FFA were transformed into well-cemented composites by alkali activation (Palomo et al. 1999).

Figure 1.2 (a) Fly ash; (b) air pollution from fly ash (photo by Shaila Dewan)

Class C fly ash is produced from the burning of lignite or subbituminous coal and contains more than 20% CaO. In addition to its pozzolanic properties, CFA has self-cementing properties. Researchers have demonstrated that certain CFA can be used solely as a binder for green concrete production, with similar mechanical and durability performance as Portland cement (Roskos et al. 2015; Berry et al. 2011).

1.2 Problem Statement

A typical pervious concrete mix design in the United States contains Portland cement. It is well known that Portland cement has some environmental concerns related to mining and

manufacture: high-energy consumption and the release of air pollutants (NO_x and SO_2) and greenhouse gases (CO_2). The annual global production of cement is about ***4180 billion metric tons*** in 2014 (Hendrik G. van Oss 2015), which has had an enormous impact on the environment. In this study, to make pervious concrete sustainable, fly ash has been chosen to fully replace Portland cement.

Significant quantities of fly ash are generated every year. In 2013, the United States produced 115 million tons of coal ash. While only 45% of the coal ash was used beneficially, nearly 64 million tons were disposed of (Minkara 2015). In an effort to recycle fly ash from industrial waste and reduce the demand for Portland cement, fly ash has been used as partial cement replacement in concrete for years (Roskos 2011; Harwalkar and Awanti 2014; Palomo et al. 1999; Schneider et al. 2011). A 100% fly ash pervious concrete could reduce the demand for Portland cement and divert fly ash from industrial waste, helping to reduce serious environmental problems (Figure 1.2b)

1.3 Scope of Work

This study consists of two tasks: In Task I, emphasis is placed on the selection of fly ash and an interdisciplinary evaluation of fly ash paste with activators and nanomodifiers. The research plan includes the following:

1. Preparation: review literature on the properties of fly ash and pervious concrete.
2. Selection: adopt criteria for identifying fly ash that could be used as a sole binder in pervious concrete.
3. Interdisciplinary investigation: investigate the fundamental engineering properties and the durability of a pure fly ash paste. Standard mechanical test methods related to Structural

Engineering and Pavement Engineering will be adopted. Scanning electron microscope (SEM)/energy dispersive X-ray spectroscopy (EDS) will be employed to understand the microstructure and the elemental composition of fly ash paste with graphene oxide (GO).

The focus of Task II is a systematic laboratory investigation of pervious concrete with a pure fly ash paste. Based on the Task I evaluation, a mix design of pervious concrete and the selected fly ash will be developed, with a goal of desired workability, compressive strength, and split tensile strength. Laboratory tests (salt scaling, freeze–thaw, and abrasion resistance) simulating many years of field service will be conducted to investigate the durability of pervious concrete.

1.4 Outline of Report

This report is divided into five chapters. Chapter 1 outlines the scope of work. Chapter 2 provides a literature review based on both national and international sources. Chapter 3 contains description and discussion of the different mortar designs with the pure fly ash binder. Chapter 4 addresses the mix design for pervious concrete with the pure fly ash binder. Chapter 5 summarizes the work of this report and gives conclusions.

CHAPTER 2.0 LITERATURE REVIEW

2.1 Introduction

Fly ash has been used as a partial cement replacement in concrete for years; however, it is typically used at a replacement ratio of less than 35% due to a lack of understanding related to its overall performance (Minkara 2015). In particular, fly ash with high free lime content can cause cement stability issues and deleterious concrete expansion (Thomas 2007a). The research presented is based on an idea that carefully selected fly ash can perform as self-cementitious material to create a paste in the presence of water, which forms a thick coating around aggregates and replaces 100% Portland cement in pervious concrete. Activators and nanomodifiers were chosen to facilitate the dissolution of aluminosilicates from fly ash and the polymerization of reaction products around aggregates. The following literature review summarizes recent studies on fly ash characterization and its hydration mechanism to support the idea behind this research; it also includes a review of literature related to the mix design, mechanical and material properties, durability, and permeability of pervious concrete. The information and data gathered from this literature review were used to develop a fly ash pervious concrete that meets the multidisciplinary requirements of Material Science, Structural Engineering, Pavement Engineering, and Environmental Engineering.

2.2 Fly Ash Properties

As a by-product of coal-fired power plants, the physical and chemical characteristics of fly ash are dependent on coal type, the boiler, operating conditions, and post-combustion

conditions. As illustrated in Figure 2.1, mineral matter within coal oxidizes, decomposes, fuses, disintegrates, or agglomerates. Spherical, amorphous (non-crystalline) fly ash particles are formed by rapid cooling in the post-combustion zone. Heating and cooling have a significant effect on the composition and morphology of fly ash particles (Kutchko and Kim 2006), which determine the pozzolanic or cementitious property of fly ash. Fluidized bed combustion (FBC) fly ash is typically produced at lower temperatures (800–1000°C) and is generally considered to have less pozzolanic activity than fly ash produced at higher temperatures (Iribarne et al. 2001). In a pulverized coal-fired boiler, furnace operating temperatures are typically in excess of 1400°C, which produces pulverized fuel fly ash (PFA). Pulverized fuel fly ash can be blended with FBC ash to provide or reinforce pozzolanic activity. One study (McCarthy and Solem-Tishmack 1994) stated that, essentially, all high-calcium fly ash, dry process flue gas desulphurization (FGD) by-products, and clean coal technology by-products that use lime as a sorbent are cementitious, while low-calcium fly ash, wet process FGD by-products, and bottom ash slags are not generally cementitious.

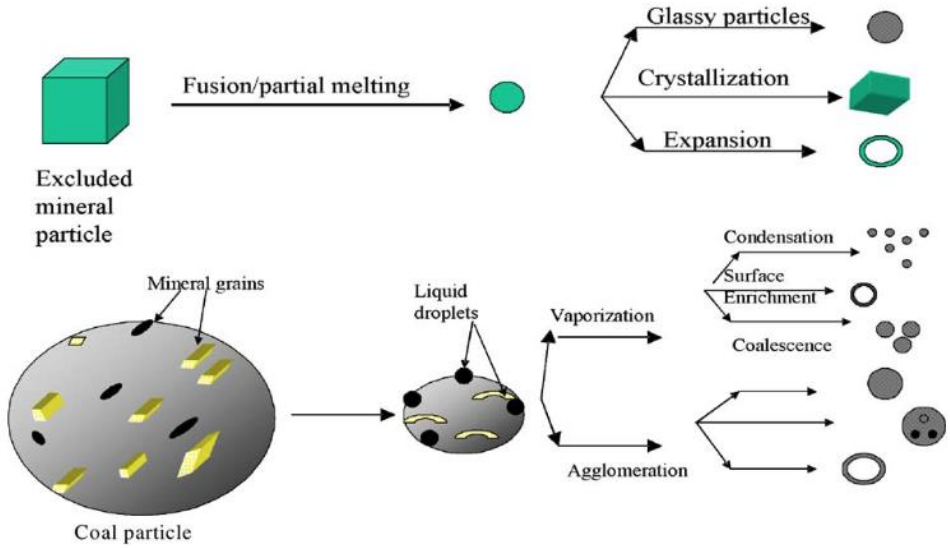

Figure 2.1 General transformation of mineral matter in coal during combustion (reprinted from Kutchko and Kim 2006)

The main chemical composition of fly ash is aluminosilicate compounds (Iribarne et al. 2001); fly ash also contains some iron and calcium oxides (Brouwers and Eijk 2003). Other than SiO_2, Al_2O_3, Fe_2O_3, and CaO as the major constituents of fly ash, the X-ray fluorescence (XRF) technique shows that other elements in fly ash include MgO, Na_2O, K_2O, SO_3, MnO, TiO_2, and C (Ramezanianpour 2014). Based on CaO content, fly ash can be divided into high-calcium fly ash (CaO content > 10%) and low-calcium fly ash (CaO Content < 10%) (Fan et al. 2015). In accordance with ASTM C618, high-calcium fly ash is produced from burning lignite or subbituminous coal, since lignite and subbituminous coal have high CaO content, up to 10%. Low-calcium fly ash typically is produced by the combustion of anthracite or bituminous coal. Fly ash with (SiO_2 + Al_2O_3+ Fe_2O_3) > 70% is classified as Class F, while fly ash with 70% > (SiO_2+ Al_2O_3+ Fe_2O_3) > 50% is classified as Class C (C09 Committee 2012). Low-calcium and high-calcium fly ash show a discrepancy in unburned carbon content. High-calcium fly ash usually has low unburned carbon content (< 1%), whereas low-calcium fly ash has relatively

high unburned carbon content that is able to absorb significant amounts of water and chemical admixtures (Ramezanianpour 2014).

Fly ash is a complex material in terms of mineralogical composition; approximately 316 individual minerals and 188 mineral groups have been identified in it (Vassilev and Vassileva 2005; Vassilev et al. 2004). X-ray diffraction (XRD) and infrared spectroscopy techniques are usually used to determine crystalline phases in fly ash. The low-angle XRD technique is used to determine glass phases. In general, the content of fly ash is mainly vitreous (< 90%) (Ramezanianpour 2014). The content of crystalline material varies, ranging from 11 to 48% (Joshi 1970), and this material may contain one or more of the four major crystalline phases: quartz, mullite, magnetite, and hematite (Ramezanianpour 2014). The presence of a mineral form in high/low calcium fly ash indicates a large difference in crystalline materials. In general, the mineral composition of low-calcium fly ash mainly consists of mullite, quartz, and magnetite. The mineral composition of high-calcium fly ash is relatively complex, usually consisting of lime, mullite, hematite, magnetite, quartz, anhydrite, and gehlenite (Zhao et al. 2010). In addition to the more reactive calcium-rich glass phases, some of the crystalline phases in high-calcium fly ash react with water, which makes high-calcium fly ash react more easily with water than low-calcium fly ash. This characteristic consequently renders fly ash both pozzolanic and hydraulic in nature (Thomas 2007b). Berry et al. (2011) demonstrated the possibilities of using fly ash as the sole cementitious binder to make concrete that has moderate strength, if the calcium content of fly ash is high enough. **Error! Reference source not found.** summarizes the mineral contents of both low-calcium and high-calcium fly ash.

Table 2.1 The minerals in fly ash (adopted from Li 2011)

Low-calcium fly ash	High-calcium fly ash
Mullite {$2Al_2O_3.2SiO_2$}	Calcium, aluminum, magnesium melilite {Ca, Mg, Al (Si_2O_7)}
Quartz {SiO_2}	Ferrite – spinel {(Mg, Fe)(Fe, Mg)$_2O_4$}
Magnetite – Ferrite {Fe_3O_4 - (Mg ,Fe)(Fe ,Mg)$_2O_4$}	Merwinite {$Ca_3Mg(SiO_4)_2$}
Magnetite {Fe_3O_4}	Larnite {Ca_2SiO_4}
Anhydrite {CaSO4}	Lime {CaO}
	Periclase {MgO}
	Cristobalite / quartz {SiO_2}
	Feldspar (Na, Ca, Al) silicate
	Tricalcium silicate {Ca_3SiO_5}
	Tricalcium aluminate {$Ca_3Al_2O_6$}
	Anhydrite {$CaSO_4$}

2.3 Fly Ash Glass Structure and Hydration Reactions

Some crystalline phases (C_2S, C_3A, $CaSO_4$, MgO, and free CaO) in fly ash can react with water to form ettringite, mono sulphoaluminate hydrate, and C-S-H, which contribute to the hydraulic property of fly ash. Ramezanianpour reported that the hydration behavior of C_2S, C_3A in fly ash is the same as that in cement (Ramezanianpour 2014). Since fly ash is composed of 75–90 wt.% of Si-Al bearing glass, fly ash belongs to the silica-alumina-based system. However, the formation rate of C-S-H from the glass phase is relatively low. Aluminosilicate glassy structure in fly ash contains Si-O-Si and Si-O-Al chemical bond, etc., as well as a certain amount of network modifier bond, for example, Ca-O and Mg-O. The bond of network modifiers is much weaker than the Si-O-Si and Si-O-Al bond, while the Si-O-Al bond is more prone to break than the Si-O-Si bond (Duxson and Provis 2008). Diamond (1981) conducted a study of fly ash

glass using XRD. The results indicated that the composition of glass in low-calcium fly ash (< 5wt.% CaO) has diffused halo maxima at 23° (2-theta (Cu Kα radiation)); high-calcium fly ash (10 ~ 20 wt.% CaO) at 28° (2-theta). The glass phases in fly ash can be categorized into Type I and Type II (Hemmings and Berry 1987). The Type I glass phase is aluminosilicate glass (similar to low-calcium glass in Diamond's findings), which has a relatively low content of network modifier ($CaO + MgO + Na_2O + K_2O \approx 8\%$). The Type II glass phase is calcium-aluminosilicate glass (similar to high-calcium glass in Diamond's findings), which has a higher content of network modifier ($CaO + MgO + Na_2O + K_2O \approx 27\%$).

Li (2011), who conducted a study of the composition and structure of glass phases in fly ash, found that low-calcium fly ash presented a lower content of glass phase (≈ 72 wt.%) than high-calcium fly ash presented (≈ 81 wt.%). Since the structure of glass phases in fly ash varies with the element composition, furnace temperature, and cooling speed, the structure of glass phases was studied by Li (2011) as well, using IR-Raman, nuclear magnetic resonance (NMR), and high-resolution transmission electron microscopy (HRTEM) techniques. The results showed that more Si-O-Si(Al) bonds existed in low-calcium fly ash, with Si mainly existing as Q^4 and Q^2 units ($Q^4/ Q^2 = 100/48.46$) and Al existing as both 4-coordinate and 6-coordinate (4CN/6CN ≈ 1, Al exists approximately equally in the glass phases and crystalline phases) (Figure 2.2). In addition, a phase separation in glass was found in the low-calcium fly ash. As for high-calcium fly ash, it was found that Si-O-Si(Al) bonds were less than that of low-calcium fly ash. Si mainly existed as a Q^1 unit with some Q^2 units ($Q^1/ Q^2 = 100/69.95$), while Al also existed as both 4-coordinate and 6-coordinate (4CN/6CN>1, almost all Al existed in the glass phases). Contrary to low-calcium fly ash, no obvious phase separation was found in high-calcium fly ash. All of these

findings suggest that the degree of polymerization is higher in low-calcium fly ash, whereas high-calcium fly ash is more prone to the hydration reaction.

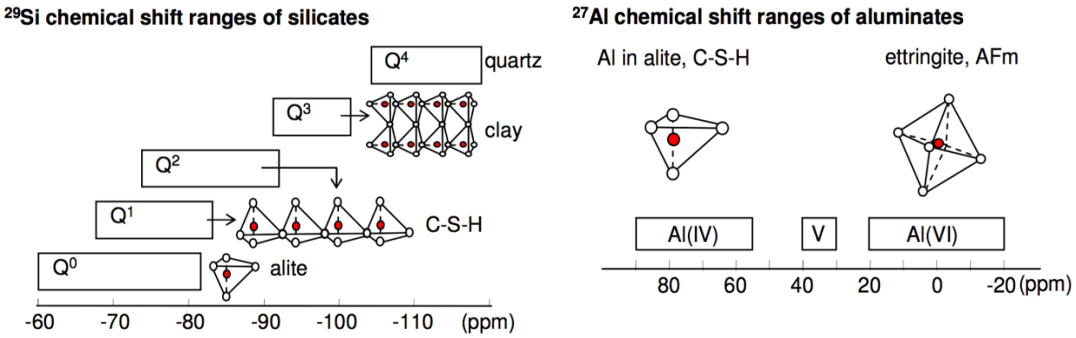

Figure 2.2 Example of NMR analysis of Si and Al structure
(reprinted from Ashbrook, Sharon 2006)

An alkaline solution is often used to activate glass phases in fly ash. Si-O-Al and Si-O-Si bonds in glass phases can rupture and depolymerize, generating $[SiO_4]^{4-}$ and $[AlO_4]^{5-}$ monomers. These monomers can further form into a three-dimensional network structure. Relevant reactions are shown as follows (Joseph Davidovits 1994):

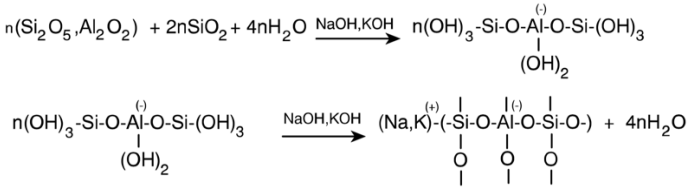

Figure 2.3 provides an illustration of the dissolution mechanism that contains both monovalent and divalent network modifiers in the fly ash glass. In the moderately high pH environment, water molecules break down into H^+, which replaces Ca^{2+} and Na^+ from the glass. With Ca^{2+} and Na^+ leaching, the glass structure is distorted; the replacement of Ca^{2+} gives more distortion to the glass structure than Na^+. With the increase of pH, Si-O-Si and Si-O-Al bonds are attacked by OH^-. Then the breakage of the Si-O-Al bond occurs due to its weak nature. This also

promotes depolymerization of the whole glass structure and, thus, the formation of Si $(OH)^{4-}$ and Al $(OH)^{4-}$ monomers.

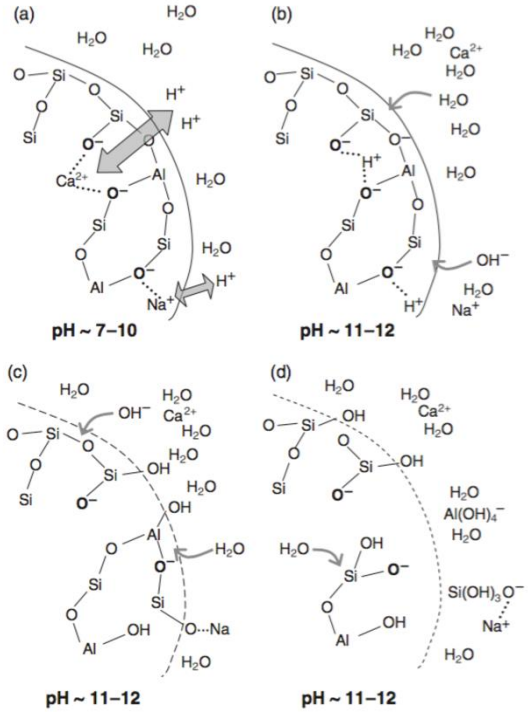

Figure 2.3 Hydration mechanism of vitreous aluminosilicate (reprinted from Kutchko and Kim 2006)

Based on this dissolution mechanism, it is easy to understand that Ca^{2+} and Mg^{2+} ions in the glass structure cause a greater degree of distortion in the aluminosilicate structure. This distortion leads to the formation of a small concentration of weaker Al-O-Al bonds and increases the amount of non-bridging oxygen, which decreases the degree of polymerization (Li 2011; Duxson and Provis 2008). For these reasons, fly ash that is rich in Ca^{2+} and Mg^{2+} shows much higher reactivity than fly ash with fewer alkali ions. All these findings support the idea of using high-calcium fly ash as a sole binder in making a moderate strength concrete such as pervious concrete.

2.4 Pervious Concrete

2.4.1 Aggregates

Pervious concrete uses the same aggregates as conventional concrete; however, it contains little or no fine aggregate, and the size distribution or gradation of the coarse aggregate is kept narrow. The standard aggregates used in pervious concrete are typically crushed stone (angular aggregates) or gravel (rounded aggregates).Typical sizes are from 3/8 in. to 1 in. (Tennis et al. 2004). Smaller aggregates can increase the compressive strength of pervious concrete by providing a tighter bond between aggregates and cement paste (Anderson et al. 2013). The disadvantage of using smaller aggregates in the mix design of pervious concrete is the decrease of void space (Tennis et al. 2004). Although smaller aggregates can increase the void ratio in pervious concrete, use of larger aggregate results in a statistically significant decrease in both compressive strength and static elastic moduli due to the subsequent decrease in paste amount. As it has been reported (Crouch et al. 2007), while compressive strength was higher for pervious concrete containing smaller aggregate sizes, there was no significant difference between the static elastic moduli when different aggregate sizes were used. For a given aggregate size, Ghafoori and Dutta (1995) provided a chart which displays the effects of aggregate cement ratio and compaction energy on the 28-day compressive strength of pervious concrete (Figure 2.4).

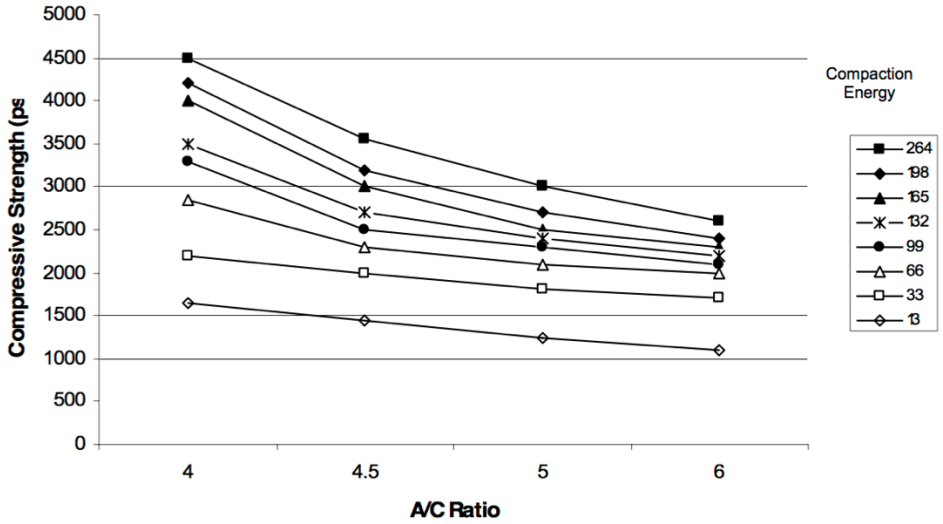

Figure 2.4 28-day compressive strength vs. A/C ratio
(reprinted from Ghafoori, N. and Dutta, S. 1995)

Today, much research effort has been directed toward the use of glass powders as fine aggregates. In one study (Tejaswi, S Sai et al. 2015),it was found that by partially replacing cement with glass powder, the initial strength gain of concrete was less due to the addition of glass powder on the seventh day, but it increased at a later age. It was also found that a 20% addition of glass powder resulted in better strength of the concrete. Glass powder size less than 90 microns was found to be very effective for strength enhancement (Tejaswi, S Sai et al. 2015). Based on these findings, recycled glass powder shows the potential for being used in pervious concrete.

A typical mix design of pervious concrete has no fine aggregates. However, a small amount (5–7%) of fine aggregate is required to increase freeze–thaw durability (Kevern et al. 2010). As shown in Figure 2.5a, a small amount of fine aggregates is also beneficial to the workability of pervious concrete. The initial workability of pervious concrete increases slightly with a sand to coarse aggregate ratio between 0% and 12.5%; however, with a sand to coarse

aggregate ratio between 7.5% and 10%, a significant decrease in compaction energy occurs (Schaefer et al. 2009). The relationship between porosity and 7-day compressive strength is shown in Figure 2.5b. With a fine aggregate amount of less than 10%, the mortar volume increases, creating a thick paste around coarse aggregates. Above 10%, the binder demand from the surface area of the additional fine aggregate begins to negatively impact compressive strength. A 7–10% of fine aggregate to coarse aggregate ratio has been shown to greatly increase compressive strength with a slight decrease in porosity (Schaefer et al. 2009).

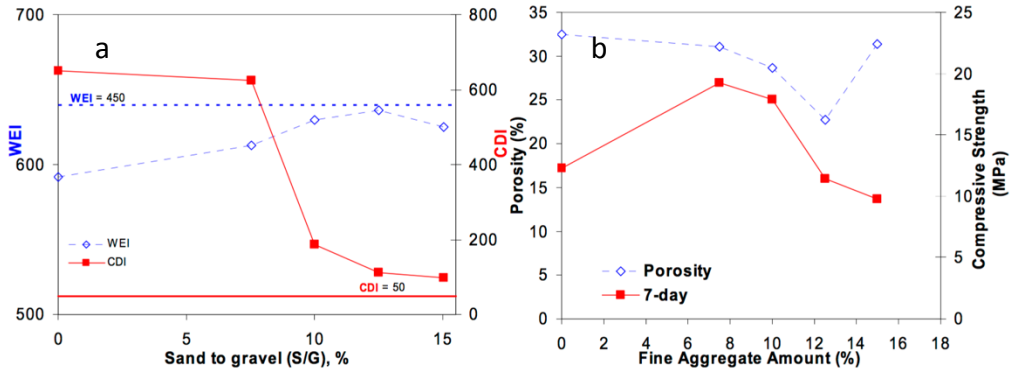

Figure 2.5 (a) Effect of fine aggregate on workability (b) Effect of fine aggregate on concrete properties (reprinted from Schaefer et al. 2009)

2.4.2 Cementitious materials

Although in this study, fly ash was used as cementitious material, a literature review was carried out on conventional cementitious material, that is, Portland cement. The knowledge obtained from the study of Portland cement as cementitious material was transferred into this study of fly ash as cementitious material.

Portland cement, conforming to ASTM C150 and C1157, and blended cements, conforming to ASTM C595 and C1157, were typically used in pervious concrete. Silica fume, fly ash, and ground-granulated blast furnace slag were used as supplementary cementitious

materials (SCM). Since SCM can affect setting time, rate of strength development, permeability, and porosity, SCM should be tested by trial batching (Roy and Ldorn 1982; Thomas 2007b; Holland 2005). The reason to incorporate SCM is to improve the durability of pervious concrete. Silica fume is a by-product of silicone production, and can significantly increase the strength and durability of concrete. Silica fume is normally used to replace 5–12% of Portland cement (Holland 2005). Fly ash is often used to replace 5–65% of Portland cement (Thomas 2007b). Blast furnace slag, which is a by-product of steel manufacturing, also improves the strength and durability of concrete, and can replace 20–70% of Portland cement (Roy and Ldorn 1982).

The water-to-cement ratio is another critical factor for successful mixing of pervious concrete. Water-to-cement ratios between 0.27 and 0.38 are often used with proper inclusion of admixtures such as an air entraining agent water reducer (Tennis et al. 2004). Tennis et al. (2004) indicated that there is no clear relationship between strength and the water-to-cementitious-material ratio for pervious concrete because the total paste volume is less than the voids volume in pervious concrete. Therefore, stronger paste in pervious concrete may not always lead to increased strength. Meininger (1988) studied the relationship between 28-day compressive strength and water-to-cement ratio with different aggregate-to-cement ratios and aggregate sizes. As shown in **Figure 2.6**, the results of these experiments were used to deduce an optimum water cement ratio. Desirable water content can also be inspected visually. **Figure 2.7**a and Figure 2.7c show a sample of pervious concrete that is too dry or too wet to form a void structure, whereas **Figure 2.7**b shows a proper amount of water as a sample of pervious concrete that forms a ball.

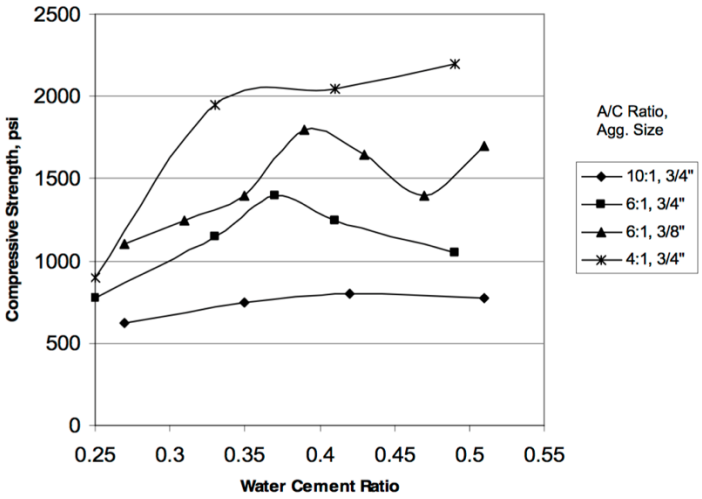

Figure 2.6 28-day compressive strength vs. W/C ratio
(reprinted from Meininger 1988)

Figure 2.7 Samples of pervious concrete with different water contents, formed into a ball: (a) too little water, (b) proper amount of water, and (c) too much water
(reprinted from Tennis et al. 2004)

2.4.3 Admixture

Due to little or no fine aggregates in the mix designs, pervious concrete mix is typically harsh and can create challenges in placement on job sites. To address the challenges, chemical admixtures are used in pervious concrete mainly to improve workability and performance. Good pervious concrete mixtures must discharge from a concrete truck readily, have stable paste without draining to the bottom of the pavement after compaction, have a sufficient setting time,

and obtain adequate strength (Koehler et al. 2009). Chemical admixtures must be selected carefully to achieve these properties.

Cement particles in pervious concrete usually have quick hydration due to a low water-to-cement ratio. In addition, pervious concrete mix dries quickly from the open void structure. Retarders or hydration-stabilizing admixtures (HSA) are commonly used in pervious concrete to control rapid setting time (Tennis et al. 2004). One study indicated that a dosage of 5 fl oz./cwt (325 mL/100 kg) of HSA provides approximately 60–90 minutes of working time at 70°F (21.1°C) ambient temperature conditions from the time of batching (Bury et al. 2006).

Pervious concrete has a very high void volume, which negatively affects its overall strength. To achieve desirable strength, a strong paste is required to bond aggregates. One way to achieve a strong paste is to use low water-to-cement ratios. Therefore, pervious concrete typically has a water-to-cement ratio in the range of 0.27–0.30 for better overall strength. A mid-range water reducing admixture or a high-range water reducing admixture is needed to efficiently disperse cement particles with low water content (Koehler et al. 2009).

Other commonly used admixtures are viscosity-modifying admixtures (VMAs) and air-entraining admixtures (AEAs). A VMA is used to achieve better flow, faster discharge time from a truck, and easier placement and compaction of an otherwise dry, harsh mix (Bury et al. 2006). A VMA prevents clogging that can occur from cement paste that drains to the bottom of the pavement due to gravity, and otherwise reduces the infiltration rate of pervious concrete. A VMA also improves compressive and flexural strength in low-compaction pervious concrete mixes by providing a better paste-to-aggregate bond (Bury et al. 2006). Air-entraining admixtures, which can reduce freeze–thaw damage in conventional concrete, are also used to

control freeze–thaw damage in pervious concrete exposed to certain conditions of freezing and thawing (National Ready Mixed Concrete Association 2004).

Pervious concrete durability is of considerable importance. Many researchers found that mixing of polymeric admixtures, such as styrene–butadiene rubber (SBR) latex, modifies the cement matrix and achieves better durability (Wang et al. 2011; Yang et al. 2009; Zhong and Chen 2002). Yang et al. (2009) found that admixing SBR with a varying SBR/cement ratio of 0–16% led to a denser and more refined microstructure of cement hydrates; this was confirmed by improved chloride penetration resistance along with general ionic permeability resistance. Scanning electron microscopy (SEM) investigation confirmed that SBR forms a network structure with cement hydrate phases to bind aggregate particles. Huang et al. (2010) carried out laboratory experiments and found that a ratio of 10% latex solids to cement slightly decreased the porosity and permeability of conventional pervious concrete, but increased the compressive and split tensile strength of conventional pervious concrete. All these results suggest the beneficial effects of SBR on overall performance of Portland cement pervious concrete; however, no study on mixing SBR with fly ash as a cementitious material was found.

The recent development of nanosize materials presents an opportunity to improve the overall performance of cementitious materials. Among numerous nanomaterials, graphene oxide (GO) (see **Figure 2.8**) shows potential as an admixture for concrete because it is a two-dimensional carbon sheet with an aspect ratio up to 30,000 or higher (Tung et al. 2009), has a Young's modulus of 1 TPa and an intrinsic strength of 130 Gpa, and is highly hydrophilic (Lee et al. 2008).

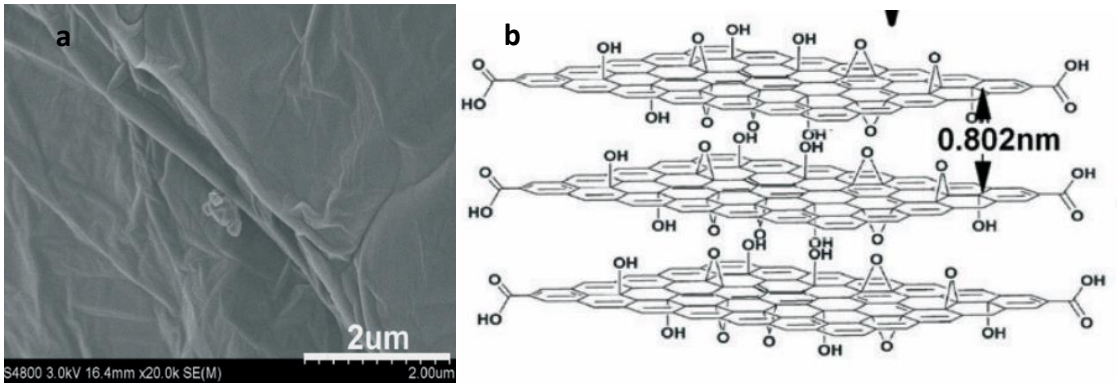

Figure 2.8 (a) SEM image of GO membrane. (b) molecular model of GO (reprinted from Lv et al. 2014).

Gong et al. (2015) indicated that the addition of 0.03% (by weight of cement) GO in plain cement resulted in 13.5% lower total porosity and 27.7% fewer capillary pores compared with cement without GO addition. The 28-day compressive strength and tensile strength of cement paste were increased by over 40%. However, GO reduced the workability of plain cement mix. Lv et al. (2014) observed that different amounts of GO (0.01–0.06% by weight of cement) promoted flower-like and polyhedron-like cement hydration products (**Figure 2.9**), which formed a compact microstructure. As a result, the flexural strength and compressive strength of cement mix with 0.03% GO were considerably improved by 60.7% and 38.9%, respectively. Graphene oxide demonstrated a crack deflection or branching mechanism, which increases a crack path to release stress in cement paste. Ranjbar et al. (2015) found that GO absorbs more energy when under crack bridging or pull out and thus leads to improved toughness.

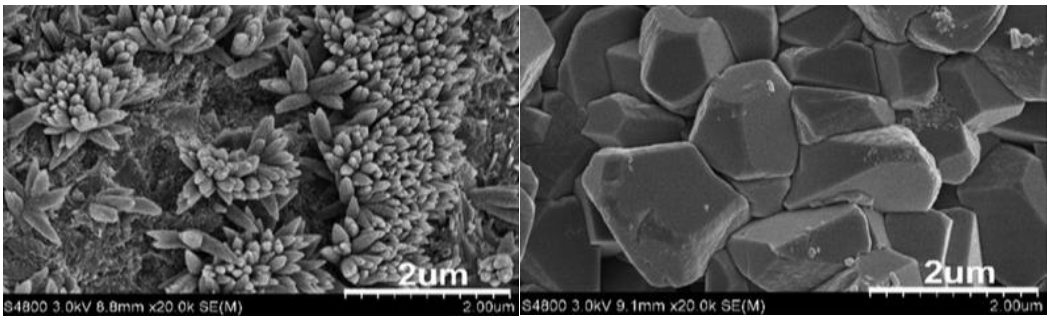

Figure 2.9 SEM image of cement hydrates at 7-days: (a) flower-like shape with 0.01% GO; (b) polyhedron-like shape with 0.05% GO
(reprinted from Lv et al. 2014)

These results suggest that GO can significantly improve the overall performance of cement mix by regulating cement hydration, providing a crack branching and bridging mechanism, and acting as nanofillers. Therefore, GO shows significant potential for practical application in fly ash-based cementitious materials of high strength and durability.

Each admixture may improve the performance of pervious concrete in a specific way. However, lab tests should be used to quantify the effects of individual admixture so that all admixtures used in a pervious concrete system can lead to a positive overall effect. The typical range of material proportions of pervious concrete are listed in Table 2.2.

Table 2.2 Typical ranges of material proportions in pervious concrete (adopted from Tennis et al. 2004)

	Proportions (lb/yd^3)
Cementitious materials	450 to 700
Aggregate	2000 to 2500
Water to cement ratio (by mass)	0.27 to 0.43
Aggregate to cement ratio (by mass)	4 to 4.5:1
Fine to coarse aggregate ratio (by mass)	0 to 1:1

2.4.4 Permeability

The internal interconnected void space of pervious concrete allows water to flow through, thus reducing the amount of runoff. Permeability or the saturated hydraulic conductivity of pervious concrete is an important property in draining water from a concrete surface.

Schaefer et al. (2006) tested pervious concrete permeability by using a falling head permeability test apparatus (**Figure 2.10**). A flexible gum sealed the top perimeter of the samples to inhibit water leakage along their sides. The samples were then confined in a membrane and sealed in a rubber sleeve. The tests were performed with several water heights. The average coefficient of permeability (k) was determined using Equation 1 (Das and Sobhan 2013) .

$$k = \frac{aL}{At} LN\left(\frac{h_1}{h_2}\right) \quad (1)$$

where

k = coefficient of permeability, L/T
a = cross-sectional area of the standpipe, L^2
L = length of sample, L
A = cross-sectional area of specimen, L^2
t = time for water to drop from h_1 to h_2, T
h_1 = initial water level, L
h_2 = finial water level, L

Figure 2.10 Permeameter used to measure the permeability of pervious concrete samples (reprinted from Das and Sobhan 2013)

Flores et al. (2007) proposed a test method to evaluate pervious concrete permeability. A 4 inch by 8 inch (10 × 20 cm) pervious concrete cylinder was used in this method. The perimeter surface of the cylinder was covered with waterproof, non-absorbing material. A plastic cap was attached to the top of the specimen as a constant head at the top surface of the concrete. This test recorded the time it took for water to flow through the entire specimen (**Figure 2.11**).

Figure 2.11 Filtration test apparatus (reprinted from Flores et al. 2007)

The typical water permeability of pervious concrete is 288 in./hr (0.2 cm/s) to 770 in./hr (0.54 cm/s). Although the falling head method (FHM) and the constant head method (CHM) are commonly used to test the water permeability of permeable concrete, Qin et al. (2015) indicated that permeability measured using the FHM was typically lower than that measured using the CHM, because permeability was found to decrease with the applied water head. The authors suggested that the water permeability of pervious concrete should be reported with the applied pressure and the associated testing method.

2.4.5 Void ratio

Pervious concrete typically has a void ratio of 15–40%, depending on its application, whereas conventional concrete has a void ratio of 3–5% (Wanielista and Manoj Chopra 2007). Pervious concrete is usually used for constructing pavement that requires a reasonable flexural

strength. One study indicated that, with void ratios of 20–29%, pervious concrete could achieved desirable flexural strengths of 400 psi to 500 psi (Gong et al. 2015). The void volume in pervious concrete is the summation of effective porosity (open or interconnected porosity) and closed porosity (Neithalath et al. 2010; Neithalath et al. 2006). Effective porosity allows water to flow through, whereas closed porosity contributes little to permeability. Therefore, high porosity may not indicate high permeability in pervious concrete. Effective porosity is more important to permeability and acoustic absorption of pervious concrete (Tong 2011). Tennis et al. (2004) reported the relationship between void ratio and permeability for Portland cement concrete as shown in **Figure 2.12**. The authors also indicated that mixes with a void ratio of between 15% and 19% could achieve a 7-day compressive strength of about 3,000 psi or more, and a permeability between 135 in./hr and 240 in./hr. The 7-day compressive strength decreased lineally with increasing void ratio.

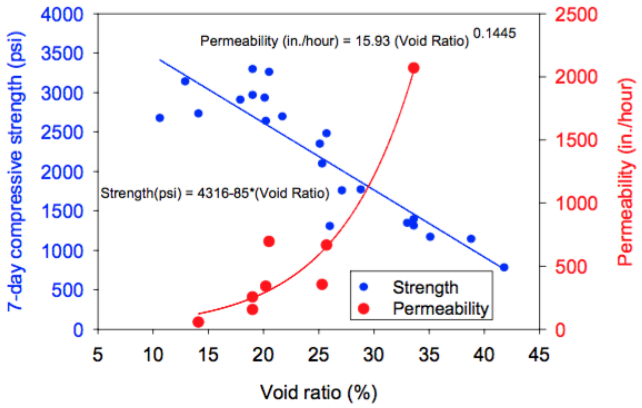

Figure 2.12 Relationship between strength, void ratio and permeability (reprinted from Tennis et al. 2004)

Most testing methods (ASTM D7063 and ASTM C140) to determine the void ratio of pervious concrete are based on the water displacement principle. These test methods involve holding a pervious concrete sample under water and shaking it to remove air bubbles. Void ratio

can be calculated based on the submerged mass and dry mass of samples. However, these methods are not always accurate, since some voids in pervious concrete are not readily accessible to water and the sample shaking is difficult to reproduce. A new test method has been proposed that involves submerging a pervious concrete sample for 30 minutes, tapping the sample against the container 5 times, and inverting it 180°. This method has proven to be sufficient for filling most pores in a sample with an error of 2.2% in void ratio between different operators and testing facilities (Montes et al. 2005).

Some researchers have also studied the effects of void ratio on sound absorption characteristics of pervious concrete. Park et al. (2005) reported that the optimum void ratio for sound absorption is 25%, since compressive strength reduced rapidly when the void ratio exceeded 25%. Kim and Lee (2010) indicated that the maximum acoustic absorption coefficient increased as the void ratio increased, and the acoustic maximum absorption coefficient reached 1.0 when the void ratio exceeded 30%.

2.4.6 Durability

Durability concerns for pervious concrete mainly include freeze–thaw resistance, clogging, salt-scaling resistance, and abrasion resistance.

Freeze–thaw resistance

Pervious concrete can allow for the free transfer of moisture into a concrete matrix, which potentially causes more severe freeze–thaw problems in pervious concrete than in conventional concrete. A mass loss of about 15% after freeze–thaw damage represents a terminal serviceability level for pervious concrete pavement (Vernon R. Schaefer et al. 2006). Air-entrainment has been shown to improve freeze–thaw protection for concrete. The National

Ready Mixed Concrete Association (NRMCA) suggests using 4–8% air entrainment with a spacing factor of 0.01 inches to provide freeze–thaw resistance for pervious concrete in cold weather areas.

While the current ASTM C666 may not be able to simulate the exact in situ freeze–thaw conditions for pervious concrete, many researchers have investigated the freeze–thaw resistance of pervious concrete from various perspectives. Olek et al. (2003) found that the specimens undergoing a more rapid cycle rate had relative dynamic moduli of less than 40% at 80 freeze–thaw cycles, whereas specimens undergoing a slower cycle rate had relative dynamic moduli greater than 90% left. Neithalath (2004) stated that after 80 cycles of slow freezing and thawing (1 cycle per day), pervious concrete samples maintained more than 95% of relative dynamic modulus, while samples with the same mix design at a rapid rate of freezing and thawing (5 to 6 cycles per day) had 50% of dynamic modulus. Schaefer et al. (2006) concluded that freeze–thaw damage of pervious concrete is a result of either aggregate deterioration or cement paste matrix failure. Mix design with sand or latex had better freeze–thaw resistance. The optimum mix design for freeze–thaw resistance was single-sized gravel with 7% sand, which resulted in only 2% mass loss after 300 freeze–thaw cycles.

Although some factors, such as freeze–thaw cycle rate, were evaluated for freeze–thaw resistance, more study is needed to investigate the effects of aggregate properties and compaction energy on the freeze–thaw resistance of pervious concrete.

Clogging

Clogging, which adversely affects the permeability of pervious concrete, is one of the major concerns associated with pervious concrete voids. Joung (2008) performed a clogging test

to measure permeability after clogging. This test involved placing 50 g of clogging material (sand) into 1 kg of water and mixing thoroughly. The clogging fluid was then poured into pervious concrete samples. These two steps were repeated five times until samples became well clogged. The permeability of clogged specimens was measured by a falling-head permeameter. It was found that pervious concrete samples with a void ratio of over 33% were not affected by clogging. Samples with a void ratio from 23% to 31% were clogged and decreased in permeability. Haselbach and Freeman (2006) found that porosity increased significantly from top to bottom for pervious concrete slabs approximately 6 inches in height and placed with an approximately 10% surface compaction technique. This top lower porosity could trap larger clogging particles within the pavement. Therefore, surface washing or vacuum sweeping usually was efficient at removing larger clogging particles trapped in the top layer of pavement.

Salt-scaling resistance

The application of deicers could cause serious damage to pervious concrete pavement. Commonly used deicers are chloride-based salts such as sodium chloride and calcium chloride. The mechanisms for deicer attack on pervious concrete are similar to those on conventional concrete: the chemical reaction between salts and cement hydrates physically and chemically changes the aggregates, aggregate-paste interface, and cement paste, and causes severe paste deterioration (Lee et al. 2000). Studies have shown that low chloride concentrations (2% to 4%) produced more scaling in conventional concrete, irrespective of the w/c ratio (Marchand et al. 1999). However, the porous structure of pervious concrete may make it more susceptible to salt-scaling deep into pavements. Anderson et al. (2013) performed salt-scaling tests on different pervious concrete mix designs; the results are summarized in **Figure 2.13**, where each data point

is averaged from 16 mix designs. Of all the solutions, 4% to 8% of salt solution caused the most serious damage. Those samples with 8% solution failed after tests. Anderson et al. also tested the salt-scaling resistance of pervious concrete using different fly ash content. The results showed that mixes with 10% and 20% fly ash replacement exhibited better salt-scaling resistance than the control specimens containing no fly ash, but mixes of 0% and 30% fly ash replacement had the greatest damage.

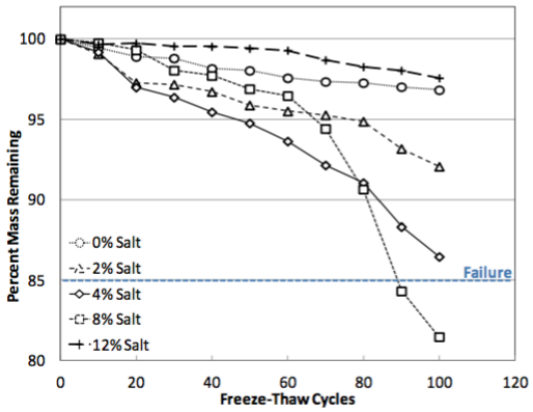

Figure 2.13 Salt-scaling damage for all mix design per salt concentration (reprinted from Anderson et al. 2013)

Abrasion resistance

Surface abrasion is a potential problem for pervious concrete, especially when snowplows and studded tires are used in wintertime, because of its low strength and rough surface from the void structure. Therefore, pervious concrete is not suitable for highway pavements. The standard test method of abrasion resistance is ASTM C944 (**Figure 2.14**a). Other methods include the Cantabro test conducted with the Los Angeles abrasion machine (**Figure 2.14**b) and loaded wheel tester (**Figure 2.14**c). Dong et al. (2013) presented abrasion results of pervious concrete with different methods (see Table 2.3). The comparison showed that the Cantabro test had the lowest coefficient of variation (11.1%), and the ASTM C944 had the

highest (32%). This study also indicated that using small-size aggregates and/or adding latex and fibers generally improved the abrasion resistance of pervious concrete. Amde and Rogge (2013) performed the ASTM C944 test on a pervious concrete mix design with different admixtures. They found that pervious concrete with cellulose fibers had the lowest mass loss of 0.1%. Admixtures such as delayed set modifier and viscosity modifier increased mass loss 0.3–0.4% compared with the control mix mass loss of 0.2–0.3%. Kevern and Sparks (2013) also evaluated low-cost techniques for improving the abrasion resistance of pervious concrete. The results showed that latex paint and epoxy were effective at improving abrasion resistance, whereas super absorbent polymer for internal curing reduced abrasion resistance.

Table 2.3 Comparison of three abrasion tests (reprinted from Dong et al. 2013)

Items	Cantabro loss test	Loaded wheel test	Surface abrasion test[a]
Specimen size	Cylinder, 150-mm diameter by 100-mm height	Beam 300 × 125 × 75 mm	Top ends of 150-mm diameter cylinder (ASTM 2012c)
Test equipment	LA abrasion machine	Asphalt pavement analyzer with studded wheels	Rotating-cutter device
Test period	10 min	1.5 h for 3 specimen	6 min
Weight loss	35 to 80% (Lost weight: 1,200 to 2,800 g)	0.6 to 1.8% (lost weight: 33 to 101 g)	0.2 to 0.5% (lost weight: 11 to 28 g)
Overall coefficient of variation (%)	10	19	32
Ratio of the lowest result to the result of the control mix (%)	62	45	58

[a]According to ASTM C944 (ASTM 2012c), the rotating-cutter surface abrasion test was primarily intended for use on the top ends of 150-mm (6-in.) diameter concrete cores and mortar specimens.

Figure 2.14 Abrasion testing apparatus (a) ASTM C944 method; (b) L.A. abrasion machine; (c) studded steel wheel abrasion test (reprinted from Dong et al. 2013)

2.4.7 Placement and compaction

There are many procedures for placing pervious concrete as pavements. Since most pervious concrete mixes do not flow, pervious concrete cannot be pumped. The placement of pervious concrete on job sites usually requires a single additional shoot attached to a ready-mix truck, and pervious concrete mix is often pulled off the shoot manually (**Figure 2.15**). Mixes that contain a viscosity-modified admixture are more flowable. A full-length shoot can be used to discharge more flowable pervious concrete from a ready-mix truck with fewer workers (Kevern et al. 2006).

Figure 2.15 Pervious concrete placing (reprinted from Kevern et al. 2006)

The compaction of pervious concrete is critical, since it affects the void ratio, permeability, strength, and durability of pervious concrete. A vibratory screed or a weight roller is typically used to compact pervious concrete pavements. Sometimes a plate compactor with plywood placed on top of the pervious concrete pavement is used for compaction (Kevern et al. 2006). Although different compaction techniques are developed for specific jobsite applications, producing specimens that have compaction similar to in-place pervious concrete pavement is still more challenging. Putman and Nepture (2011) studied the differences between laboratory

specimens and pavement cores by using different compaction procedures. They found that the standard Proctor hammer method provided the least variability in compaction and resulted in properties similar to the in-place pavement. The authors indicated that the density of cylinders was generally greater than the pavement; however, 600 × 600 mm slabs with the same thickness of pavement had porosity and density closest to those of pavement.

2.5 Literature Review Summary and Conclusions

Based on previous research, it is possible to use fly ash as a sole cementitious binder in making concrete that has moderate strength, such as pervious concrete. The following conclusions can be drawn from the literature review:

- The physical and chemical characteristics of fly ash depend on the coal type, the boiler, operating conditions, and post-combustion conditions. Other than the coal type, heating and cooling has a significant effect on the composition and morphology of fly ash particles, which determine the pozzolanic or cementitious properties of fly ash.
- Other than SiO_2, Al_2O_3, Fe_2O_3, and CaO as major constituents of fly ashes, the X-ray fluorescence (XRF) technique shows that fly ash also consists of MgO, Na_2O, K_2O, SO_3, MnO, TiO_2, and C.
- According to ASTM C618 standards, high-calcium fly ash is produced from burning lignite or subbituminous coal, since lignite and subbituminous coal have a high CaO content, up to 10%. Low-calcium fly ash typically is produced by the combustion of anthracite or bituminous coal. Fly ash with (SiO_2 + Al_2O_3+ Fe_2O_3)> 70% is classified as Class F fly ash. Fly ash, with 70% > (SiO2+ Al2O3+ Fe2O3) > 50%, is classified as Class C fly ash. One study indicated that essentially all high-calcium fly ash is

cementitious, while low-calcium fly ash is not generally cementitious.

- Fly ash is a very complex material in terms of mineralogical composition. Approximately 316 individual minerals and 188 mineral groups have been identified in fly ash. In general, fly ash mainly consists of vitreous content (< 90%), and the content of crystalline material varies, in the range of 11% to 48%, and may contain one or more of the four major crystalline phases: quartz, mullite, magnetite, and hematite. Some of the crystalline phases (C_2S, C_3A, $CaSO_4$, MgO, and free CaO) in fly ash will react with water to contribute to the hydraulic property of fly ash.
- Fly ash is generally composed of 75–90 wt.% of Si-Al bearing glass, which can be categorized into Type I and Type II glass phases. Type I glass phase is aluminosilicate glass (similar to low-calcium glass), which has a relatively low content of network modifier ($CaO + MgO + Na_2O + K_2O \approx 8\%$). Type II glass phase is calcium-aluminosilicate glass (similar to high-calcium glass), which has a higher content of network modifier ($CaO + MgO + Na_2O + K_2O \approx 27\%$).
- Low-calcium fly ash has a lower content of glass phase than high-calcium fly ash has. In low-calcium fly ash, Si mainly exists as Q^4 and Q^2 units and Al exists almost equally in the glass phase and crystalline phase as both 4-coordinate and 6-coordinate. A phase separation in glass was also found in low-calcium fly ash. In low-calcium fly ash, Si mainly exists as Q^1 and Q^2 units and almost all Al exists in the glass phase as both 4-coordinate and 6-coordinate. It is suggested that the degree of polymerization is higher in low-calcium fly ash, and high-calcium fly ash is more prone to hydration reaction.

The following are conclusions based on the pervious concrete literature review:

- Pervious concrete typically contains little or no fine aggregate, and the size distribution or gradation of the coarse aggregate is narrow. Smaller aggregates will decrease the void space of pervious concrete. The use of larger aggregate results in a statistically significant decrease in both compressive strength and static elastic moduli.
- A small amount (5–7%) of fine aggregate is required to increase the freeze–thaw durability of pervious concrete, which is beneficial to the compressive strength of pervious concrete. A 7–10% fine aggregate to coarse aggregate ratio has been shown to greatly increase compressive strength with a slight decrease in porosity, but additional fine aggregates above 10% negatively impacts the compressive strength. Glass powder size less than 90 microns, used as a fine aggregate, is very effective at enhancing pervious concrete strength.
- Portland cement and blended cement are usually used as cementitious materials for pervious concrete. Silica fume, fly ash, and ground-granulated blast furnace slag are typically used as supplementary cementitious materials, and have a great impact on setting time, rate of strength development, permeability, and porosity of pervious concrete. Water-to-cement ratios of between 0.27 and 0.38 are used with proper inclusion of admixtures such as an air-entraining agent, water reducer for pervious concrete, but there is no clear relationship between strength and water to cementitious materials ratio for pervious concrete.
- Pervious concrete mix is typically harsh and can create a challenge in placement on job sites. To address this challenge, chemical admixtures are used in pervious concrete,

mainly to improve workability and performance. Retarders or hydration-stabilizing admixtures (HSA) are commonly used in pervious concrete to control rapid setting time. A mid-water- or high-range water reducing admixture is needed with low water content. A viscosity-modifying admixture (VMA) is used to achieve better flow and faster discharge time. Air-entraining admixtures are also used to control freeze–thaw damage in pervious concrete.

- Graphene oxide (GO) can improve the overall performance of cement mix significantly by regulating cement hydration, providing a crack branching and bridging mechanism, and acting as nanofillers. Therefore, GO shows significant potential as an admixture in pervious concrete of high strength and durability.
- Typical water permeability of pervious concrete is 288 in./hr (0.2 cm/s) to 770 in./hr (0.54 cm/s). The falling head method (FHM) and constant head method (CHM) are commonly used to test the water permeability of permeable concrete. The water permeability of pervious concrete should be reported along with the applied pressure and the associated testing method.
- Pervious concrete typically has a void ratio of 15%–40%, depending on its application. The void volume in pervious concrete is the summation of effective porosity (open or interconnected porosity) and closed porosity. The water displacement principle is used to determine the void ratio of pervious concrete (ASTM D7063 and ASTM C140).
- Durability concerns for pervious concrete mainly include freeze–thaw resistance, clogging, salt-scaling resistance, and abrasion resistance. The National Ready Mixed Concrete Association (NRMCA) suggests using 4% to 8% air entrainment with a spacing

factor of 0.01 inches to provide freeze–thaw resistance for pervious concrete in cold weather areas. Clogging is another major concern, as it adversely affects the permeability of pervious concrete. It was found that pervious concrete samples with a void ratio over 33% were not affected by clogging. Mixes with 10% and 20% fly ash replacement are used to achieve better salt-scaling resistance. The standard test method of abrasion resistance is ASTM C944. A small-size aggregate and/or adding latex and fiber, as well as latex paint and an epoxy coating, generally improved the abrasion resistance of pervious concrete.

- Pervious concrete placing procedures are different from conventional concrete placing procedures, since most pervious concrete mixes are not flowable. The compaction of pervious concrete is critical, since it affects the void ratio, permeability, strength, and durability of pervious concrete.

CHAPTER 3.0 DEVELOPING CEMENTITIOUS BINDER WITH 100% FLY ASH

3.1 Introduction

Significant quantities of fly ash, a by-product of coal-fired power plants, are generated every year. In 2013, the United States produced 115 million tons of coal ash. Only 45% was used beneficially; nearly 64 million tons were disposed of (Minkara 2015). In an effort to recycle fly ash from industrial waste and reduce the demand for Portland cement, fly ash has been used as a partial cement replacement in concrete for years. However, fly ash is typically used at a replacement ratio of less than 35% due to concerns about possible low early-age strength and the potential issue of freeze–thaw resistance (Minkara 2015).

ASTM C618 defines two categories of fly ash: Class F fly ash (FFA) and Class C fly ash (CFA). Class F fly ash is produced from the burning of anthracite or bituminous coal and generally contains less than 10% CaO, so it is pozzolanic in nature. Class F fly ash requires a cement agent or activators to produce cementitious pastes. Palomo et al. (1999) demonstrated the great potential of alkali-activated FFA as a cement for the future. The glassy silica and alumina contents from FFA were transformed into well-cemented composites by alkali activation.

Class C fly ash is produced from the burning of lignite or subbituminous coal and generally contains more than 20% CaO. In addition to pozzolanic properties, CFA has some self-cementing properties. Some researchers (Xie et al. 2015; Roskos 2011; Berry et al. 2011; Roskos et al. 2015) demonstrated that certain selected CFA can be used solely as a binder, with similar mechanical and durability performance as that of Portland cement.

In the last decade, a majority of researchers (Antiohos and Tsimas 2004; Fernández-Jiménez et al. 2005; Fernández-Jiménez and Palomo 2005; Shi and Day 2000) focused on alkali-

activated fly ash binders. This is a process that involves mixing fly ash with certain alkaline activators. The mixture is cured at a relatively high temperature. One patent (Davidovits 1982) described the alkali activation of metakaolin, which is similar to the alkali activation of fly ash, in a polymerical model as following the general formula:

$$M_n [- (Si\text{-}O_2)_z - Al - O].wH_2O \qquad \text{(Formula 1)}$$

where *M* is the alkaline element, *n* is the degree of polymerization, and *z* is 1,2, or 3. Fernández-Jiménez et al. (2005) developed a descriptive model for alkali-activated fly ash cement. In these two models, alkali activators facilitate the dissolution of aluminosilicates from fly ash and the polymerization of reaction products.

Typically, FFA and ground-granulated blast furnace slag (GGBFS) are preferred as alkali-activated binder precursors. Class F fly ash lies somewhere in between FFA and GGBFS in terms of chemical composition; therefore, CFA shows the potential of being a binder. Although some high-reactive CFA possesses excellent self-cementitious properties (Xie et al. 2015), a large portion of CFA still shows limited self-cementing ability or pozzolanic qualities. Research (Guo et al. 2010; Tishmack et al. 1999; Winnefeld et al. 2010; Tishmack et al. 2001) has been conducted on CFA binders. All CFA binders that have been studied require a high curing temperature to achieve desirable mechanical properties. In this study, the authors assume that the high CaO content of CFA could compensate for the requirement of high curing temperature for FFA, since Ca^{2+} typically is a network modifier to disrupt the aluminosilicates structure in CFA (Li et al. 2010).

The first set of experiments revealed limited strength in fly ash mortar without activation. This led to a second set of experiments in which fly ash was activated by a combination of chemical activators. With chemical activation and other additives, low-reactive CFA is able to

form an environmentally friendly binder at room temperature, which can replace Portland cement and reach desirable strength and durability. Recently, the use of younger lignite or subbituminous coal has substantially increased, and large quantities of CFA have been produced from this kind of coal (Guo et al. 2010). Our objective is to recycle CFA from industrial waste and contribute to the understanding of this by-product for future applications.

3.2 Experimentation

3.2.1 Materials

Three types of fly ash were obtained from three power plants in the western United States. Fly ash compositions, examined by X-ray fluorescence (XRF) analysis, are presented in Table 3.1. Class F fly ash 3 was used as a control, since it has been well studied (Xie et al. 2015). As described in Table 3.2, CFA 1 can be considered a *low-reactivity, high-calcium* fly ash, whereas CFA 3 is a *high-reactivity, high-calcium* fly ash. Although all can be considered fly ash, with Type II glass phase ($CaO + MgO + Na_2O + K_2O \approx 27\%$), the reactivity still varies according to the criteria in Table 3.2. ASTM C144 siliceous sands were used as fine aggregates.

Table 3.1 Chemical composition of the fly ash (% wt.)

	SiO_2	Al_2O_3	Fe_2O_3	Na_2O	K_2O	TiO_2	MgO	CaO	MnO	L.O.I*	Origin
CFA 1	23.5	13.8	4.8	6.3	0.4	1.3	4.2	23.2	0.1	0.15	OR
FFA 2	33.3	14.9	5.4	3.7	1.2	1.1	4.7	14.5	0.1	1.8	WA
CFA 3	20.6	14.5	4.7	2.5	0.3	1.4	6.2	29.9	0.1	0.32	MT

* Loss on ignition

Table 3.2 Fly ash spheres reactivity (adopted from Enders 1995)

	CaO (% wt.)	$Al_2O_3/(Al_2O_3+SiO_2)$	Reactivity
High-Ca-spheres	>25	± 0.45	High
Low-Ca-spheres	<25	± 0.45	Low
Ca-free-spheres	± 0	<0.45	Inert

The two groups of laboratory experiments featured different mix designs, as detailed below. The aim of using these mix designs was to develop a viable environmentally friendly binder made at room temperature with coal fly ash.

Group 1: CFA1, FFA2, and admixtures designed to improve the properties of mortar.

- Nanoclay (PGW, 98% montmorillonite, bulk density 0.678 g/cm^3, Nanocor Inc.): to improve strength and reduce the permeability of hardened mortar.
- Styrene-butadiene rubber (SBR) latex (Euclid Chemical Company): to improve bond strength and reduce the chloride permeability of hardened mortar.
- Borax ($Na_2B_4O_7$) was used mainly as a set retarder.
- Air-entraining (AE) agent (BASF MB-AE 90): to improve freeze–thaw durability.
- Triethanolamine (TEA): to improve early-age strength of hardened mortar.

Group 2: CFA1 only, and chemical activators designed to facilitate dissolution of fly ash particles and polymerization of hydration products.

- Water glass, i.e., sodium silicate ($Na_2SiO_3.9H_2O$).
- Sodium sulfate ($Na_2SO_4.10H_2O$).
- Quicklime (CaO).
- Calcium chloride ($CaCl_2.2H_2O$).

3.2.2 Fabrication of fly ash mortar and testing methods

For evaluating the fly ash binder, mortar samples made from CFA binder were tested using a MTS hydraulic compression test machine. According to ASTM C270 and C780 standards, the as-received fly ash was mixed with sand, water, and other admixtures or activators, based on a statistical design of experiments (DoEs), which will be discussed later. The ratio of binder/sand was 1:2.5 by volume. In order to achieve reasonable workability and

mechanical strength, the water/binder ratio was determined at 0.2–0.32 by mass based on extensive trial and error. After mixing, mortar was cast into a 2-by-4-inch cylindrical mold. The mortar cylinders (**Figure 3.1**) were demolded after 24 hours and cured in a controlled environment (temperature = 18°C–22°C, relative humidity = 98%). Compressive strength and split tensile strength were tested at 3-day, 7-day, 14-day, and 28-day curing ages following ASTM C109 and C496 standards, which provided a macroscopic indication of the cementing ability of fly ash binder. Each reported f'_c value was averaged from three duplicate specimens.

Figure 3.1 Mortar cylinders, 2 inch× 4 inch in size

A high-range water reducer (BASF MasterGlenium 7920) was employed to improve the workability of all fresh mortars. As such, a mini slump flow test (**Figure 3.2**) was adopted to examine the workability of the fresh mortar. The water reducer gives a slump flow value by measuring the average of the final spread diameter of the mortar under self-weight. The amount of water reducer was adjusted so that the final spread diameter could achieve a minimum of 200 mm (8 in.) without apparent segregation or bubbling (Jin 2002).

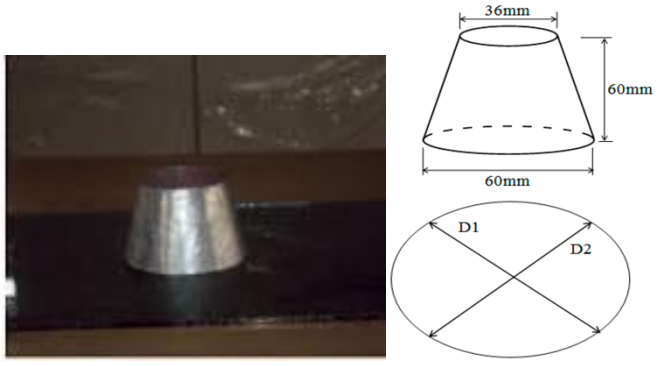

Figure 3.2 Mini slump test kit

In addition, a surface resistivity test (**Figure 3.3**) was conducted on selected mortars according to AASHTO TP95. Tested at the saturated surface dry (SSD) condition, surface resistivity provides an indirect indication of the microstructure of water-saturated mortar and has proven to correlate well with its resistance to chloride ion penetration (Polder 2001). The device (Giatec SurfTM) can automatically measure surface resistivity around the concrete or mortar specimen using four channels of a four-probe array (located at 90° from each other).

Figure 3.3 Surface resistivity test setup (reprinted from GIATEC)

To examine the fly ash binder at the microlevel, scanning electron microscopy (SEM) was carried out; information about surface morphology and the amorphous and crystalline structure of the samples was obtained by using a JEOL JXA-8500F electron microprobe. The beam conditions used were as follows: 15 kV accelerating voltage, 50 nA beam current, and focused beam diameter. Specifically, secondary electron imaging (SEI) and backscattered electron imaging (BSE) were the two modes of the instrument used to obtain high-resolution images from microscopic areas of interest on each sample.

3.2.3 Statistical design of experiment

For the mix design of both groups of mortar samples, a uniform design (UD) scheme was adopted to design experiments to investigate the effects of admixtures (Group 1) or chemical activators (Group 2) on compressive strength and other properties of these unconventional

mortars. The use of a statistical design of experiment (DoE) enabled the exploration of a large domain of unknown factors and their interactions with a limited number of experiments, in light of resource constraints. The UD is such that the experimental points are uniformly scattered in the domain of experiments (Fang et al. 2000). Known as good lattice points, the experimental points are representative of the domain. Compared with orthogonal factorial design, UD can significantly reduce how many experiments are performed when dealing with a large number of parameters at different levels. Table 3.3 presents the five design factors and their values at three different levels for each group of mortar samples, respectively. These specific values for each design factor were determined based on existing knowledge in the published domain along with cost considerations. Note that the dosage of water reducer by mass of binder is yet another factor that varied, based on trial and error, to achieve reasonable workability of fresh mortar; as such, it was not a design factor but a documented factor.

Table 3.4 presents the UD table, 5 factors at 3 levels with 27 runs, used for the DoE, which was adopted from standard Uniform Design Tables (http://sites.stat.psu.edu/~rli/DMCE/UniformDesign/). Once coupled with Table 3.3, Table 3.4 was translated to experimental points in Table 3.5 and Table 3.7.

Table 3.3 DoE factors and levels for Group 1 and 2 mortars

DoE 1 factors	Nanoclay/FAC1 ratio	SBR/FAC1 ratio	FAF2/FAC1 ratio	Water/binder ratio	Air-entraining agent dosage
	X_1	X_2	X_3	X_4	X_5
Level 1	0%	0%	0%	20%	0 ml/kg
Level 2	0.6%	6%	10%	22%	25 ml/kg
Level 3	1.2%	12%	20%	24%	50 ml/kg

DoE 2 factors	Na_2SiO_3/FAC1 ratio	CaO/FAC1 ratio	$CaCl_2$/FAC1 ratio	Na_2SO_4/FAC1 ratio	Water/binder ratio
	X_1	X_2	X_3	X_4	X_5
Level 1	1%	2%	0.5%	1%	28%
Level 2	3%	5%	1%	2%	30%
Level 3	7%	10%	2%	3%	32%

*Borax dosage = 0.2 wt.% of binder, TEA dosage = 1.2ml/one-liter water for all DoE 1 and 2 mortars
*Water reducer dosage was adjusted to achieve desirable spread diameter
*All ratios were by mass

Table 3.4 The uniform design scheme

Run no.	Factor X_1 level	Factor X_2 level	Factor X_3 level	Factor X_4 level	Factor X_5 level
1	2	2	3	2	1
2	2	2	2	2	2
3	1	3	2	2	1
4	3	2	3	1	2
5	2	3	1	1	1
6	1	3	3	1	2
7	1	2	2	2	2
8	2	1	2	1	3
9	2	2	1	3	1
10	3	2	1	3	3
11	1	1	1	2	3
12	1	1	3	1	1
13	3	3	1	2	2
14	3	3	3	3	1
15	1	2	3	3	3
16	1	1	2	3	1
17	3	2	2	1	1
18	3	3	2	1	3
19	2	1	3	3	2
20	2	3	3	2	3
21	2	3	2	3	3
22	2	1	1	1	2
23	3	1	1	2	1
24	1	3	1	3	2
25	1	2	1	1	3
26	3	1	3	2	3
27	3	1	2	3	2

Once the DoE was implemented and experimental values were recorded, an algebraic function of factors was developed to characterize the response variable as a function of influential factors. This step allows the prediction of response with the influential factors varying at intermediate levels, which were not experimentally studied. Predictive models enable the optimization of a given response under given constraints (Muthukumar and Mohan 2004), such as determining the lowest cost fly ash binder with 28-day f'_c greater than a designed value.

3.3 Results and Discussions

3.3.1 Environmentally friendly fly ash mortars without activation (Group 1 additives)

The average values for 3-day, 7-day, 14-day, and 28-day compressive strength and spread diameter are presented in Table 3.5, along with the water reducer dosage (ml/one-liter water). The surface resistivity of samples was recorded as well. The amount of water reducer was adjusted so that the final spread diameter could achieve 8 inches, since it is considered to be an important property of SCC (Jin 2002). All fly ash mortar samples showed surface resistivity between 104 and 241 kΩ-cm, which can be categorized into a very low chloride permeability group according to AASHTO T59 and is consistent with a previous study (Xie et al. 2015). This low permeability is associated with lower conductivity of hydration products, lower amount of ions in the pore solution, and lower porosity.

Table 3.5 DoE 1 – Properties of fresh and hardened mortar with Group 1 additives

Run	3-day f_c' (psi)	7-day f_c' (psi)	14-day f_c' (psi)	28-day f_c' (psi)	Spread diameter (in.)	Water reducer (ml/l)	Surface resistivity kΩ-cm (28-d)
1	1177.6	1554.0	1840.2	2191.8	9.4	15	170
2	720.6	1018.5	1228.5	1443.8	9.3	15	161
3	242.9	383.25	490.9	528	9.0	20	208
4	490.0	913.5	1000.2	1102.5	9.1	15	191
5	494.1	682.5	774.4	1021.2	9.2	20	241
6	286.2	480.4	535.5	603.8	8.9	20	232
7	586.8	879.4	1147.2	1317.8	9.2	15	157
8	1459.7	2155.8	2459.6	2690.6	9.4	20	142
9	557.9	1102.5	1231.4	1333.5	11.2	15	130
10	660.9	1084.2	1215.4	1370.4	12.3	15	124
11	1338.2	1842.8	2173.5	2226.0	10.0	10	119
12	1393.8	2073.8	2307.4	2583.0	8.8	15	152
13	312.9	540.8	624.8	727.2	11.6	20	210
14	475.6	674.7	714	876.8	8.8	25	180
15	405.6	614.3	708.8	790.2	9.3	15	143
16	821.5	1286.3	1393.9	1580.3	12.0	10	120
17	531.2	787.5	863.7	1055.3	9.4	20	192

Run	3-day f_c' (psi)	7-day f_c' (psi)	14-day f_c' (psi)	28-day f_c' (psi)	Spread diameter (in.)	Water reducer (ml/l)	Surface resistivity kΩ-cm (28-d)
18	255.3	443.7	506.7	556.5	9.0	20	142
19	903.8	1304.6	1601.3	1840.2	11.9	10	113
20	331.5	595.9	656.3	753.4	8.7	20	109
21	236.8	380.7	391.2	420.0	8.9	20	177
22	1566.8	2325.8	2682.8	2974.9	12.6	10	142
23	1420.6	2084.3	2438.6	2651	11.3	15	109
24	280.0	477.8	506.7	532.9	9.1	20	175
25	957.4	1312.5	1452.4	1557.4	10.2	15	192
26	932.6	1580.3	1724.6	1916.3	11.4	15	117
27	1027.4	1585.5	1737.8	1785.0	11.9	10	104

Model derivation and visualization

By conducting analysis of variance (ANOVA) and regression analysis, data in Table 3.5 were used to develop compressive strength models for DoE 1 with Group 1 additive.

Since all compressive models show a two-way interaction, ***three-dimensional (3D) contour plots*** were provided to show response surface plots, which help to identify the type of interactions between test variables on the response in **Figure 3.20**–**Figure 3.23**. Comparison between test results and predicted results were provided as well in the figures. Three-day, 7-day, 14-day, and 28-day compressive strength models were developed as follows:

*f_c' (3-day)= 938.7 – 474.2 * X2 – 116.9 * X4 – 201.8 * X1^2 – 153.9 * X3X5*

*f_c' (7-day)= 1102.2 – 641 * X2 – 145.8 * X4 – 146 * X1^2 + 166.4 * X3^2 + 162.8 * X2X4*

*f_c' (14-day)= 1291.6 – 738 * X2 – 169.8 * X4 – 204.6 * X1^2 + 117.2 * X3^2 + 177.5 * X2X4*

*f_c' (28-day)= 1552.6 – 834 * X2 – 210.8 * X4 – 292.5 * X1^2 + 218.9 * X3^2 + 192 * X2X4*

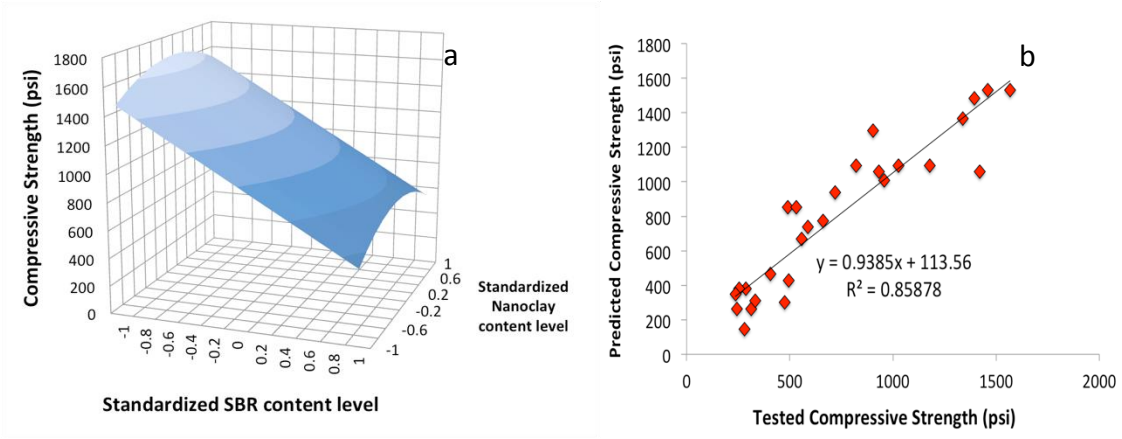

Figure 3.4 (a) 3D contour diagram of 3-day *fc'* model; (b) 3-day *fc'* test data vs. model prediction

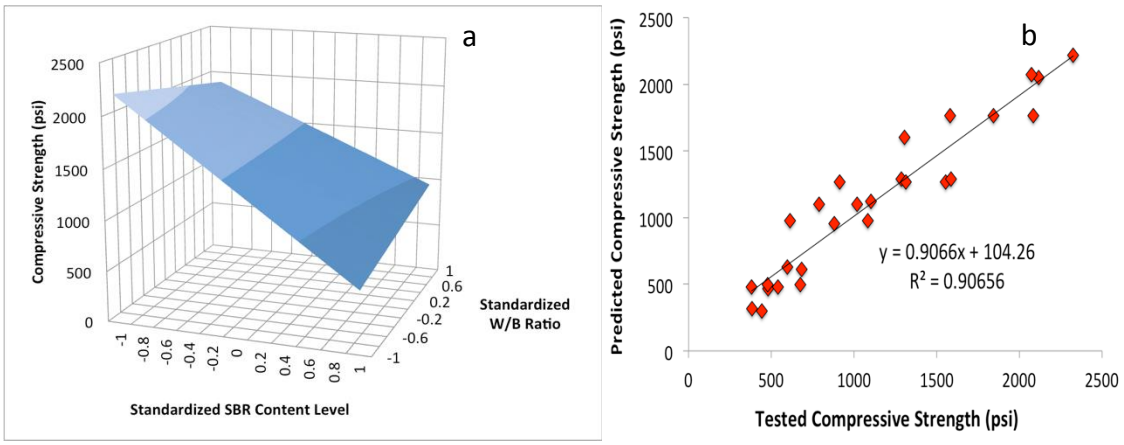

Figure 3.5 (a) 3D contour diagram of 7-day *fc'* model; (b) 7-day *fc'* test data vs. model prediction

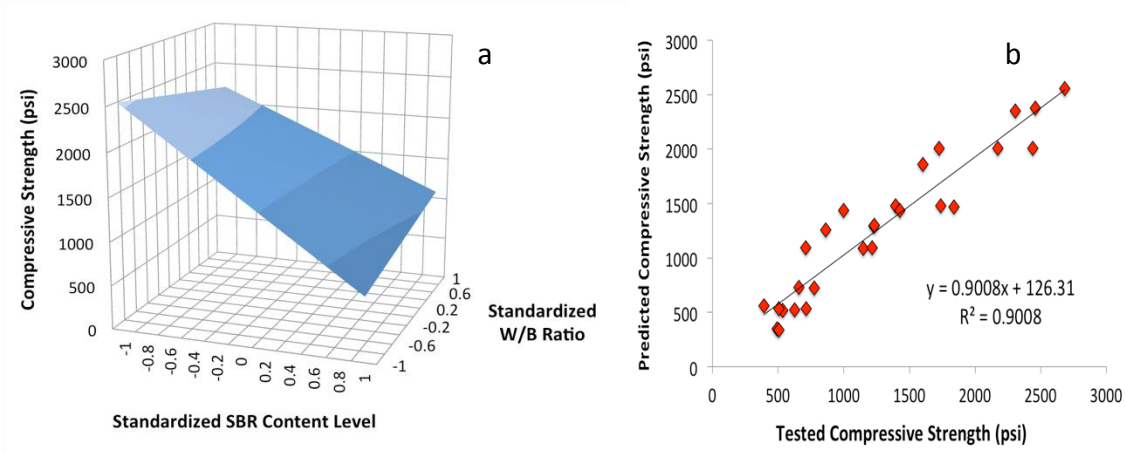

Figure 3.6 (a) 3D contour diagram of 14-day *fc'* model; (b) 14-day *fc'* test data vs. model prediction

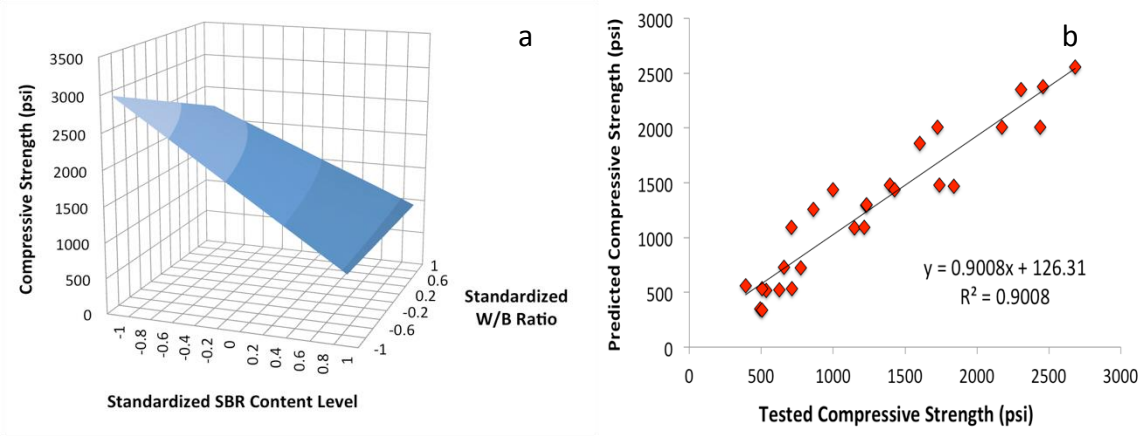

Figure 3.7 (a) 3D contour diagram of 28-day *fc'* model; (b) 28-day *fc'* test data vs. model prediction

Model verification

Analysis of variance (ANOVA) was conducted to verify the models; R^2 gives a correlation between the test response and the predicted response. Adjusted R^2 is a modified version of R^2, which ignores some insignificant model terms. For the model to be fit, R^2 and adjusted R^2 should have good agreement, since adjusted R^2 will penalize models by adding insignificant terms. Table 3.6 presents the model summary statistics for all four models. The values of R^2 for the four models are all higher than 0.9, which indicates a high degree of correlation between models and experiments results. In addition, the adjusted R^2 value is in good agreement with the R^2 value for each model. The *F*-value shows the ratio of explained errors to unexplained errors, which should be low enough for a model to be significant. *P*-value is the probability that the model will not explain the experimental response. It is observed that the *F*-values are low and the *p*-values are all less than 0.1%, indicating that all four models are highly significant.

Table 3.6 ANOVA Summary of DoE 1

Model	R^2	Adjusted R^2	Degree of freedom (D.F.)	Residual D.F.	*F*-value	*p*-value
3-day f_c'	0.93	0.86	4	22	33.44	<0.001
7-day f_c'	0.95	0.91	5	21	40.75	<0.001
14-day f_c'	0.95	0.90	5	21	38.14	<0.001
28-day f_c'	0.95	0.89	5	21	37.47	<0.001

Normal probability plots of the residuals (shown in Figure 3.8 and Figure 3.9) were used to assess model errors. The residuals are the deviations of the observed data values from the fitted values, which are assumed random and normally distributed. As shown in these figures, resulting residuals follow a linear trend.

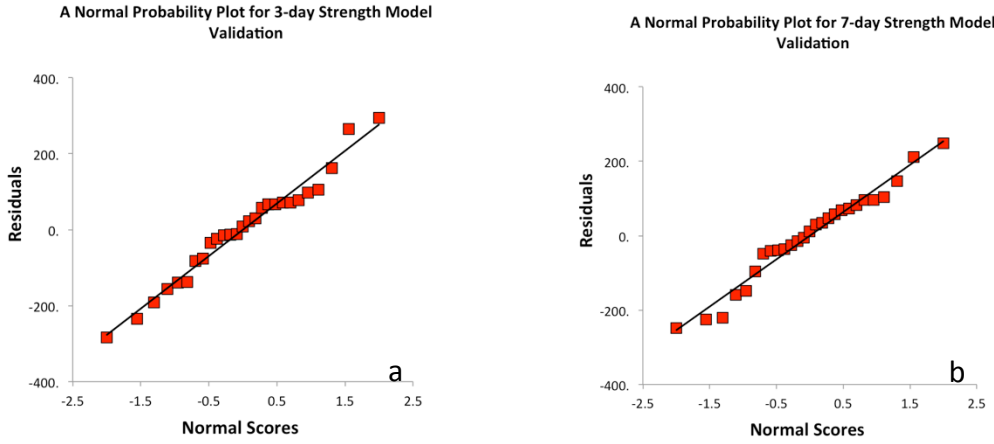

Figure 3.8 Normal probability plot for (a) 3-day *fc'* model; (b) 7-day *fc'* model

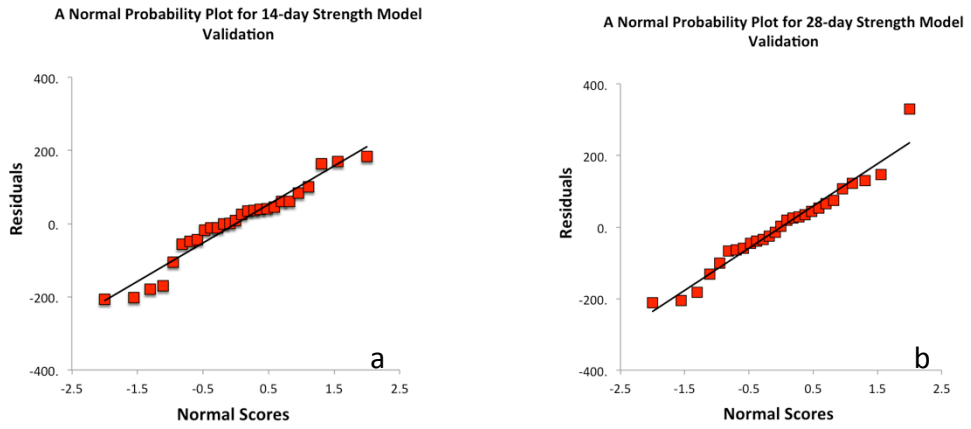

Figure 3.9 Normal probability plot for (a) 14-day *fc'* model; (b) 28-day *fc'* model

Trace plots indicate the effect of changing each mixture component while holding all other mixture components in a constant ratio. The trace plots are shown in Figure 3.10 and Figure 3.11.

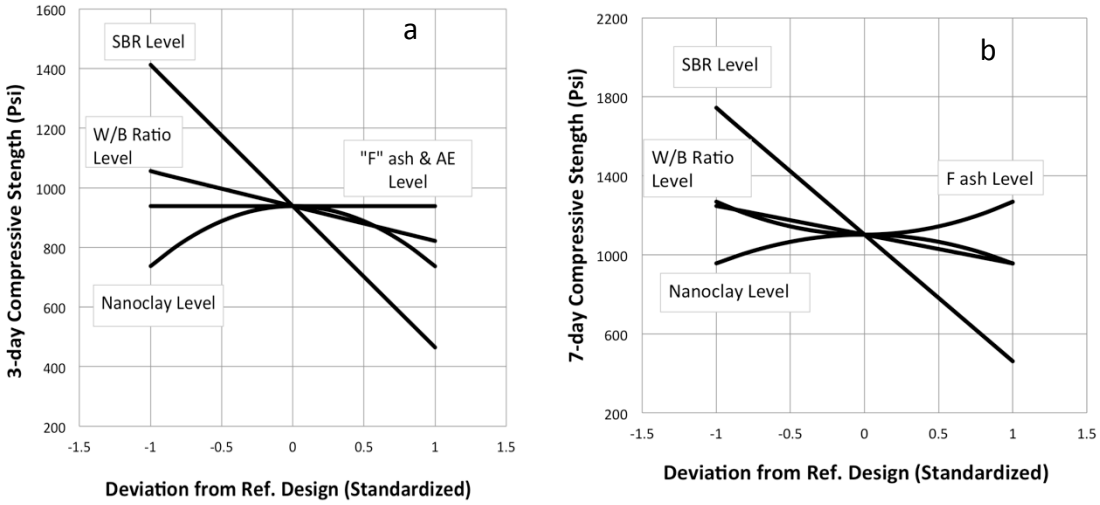

Figure 3.10 Trace plot for (a) 3-day *fc'* model; (b) 7-day *fc'* model

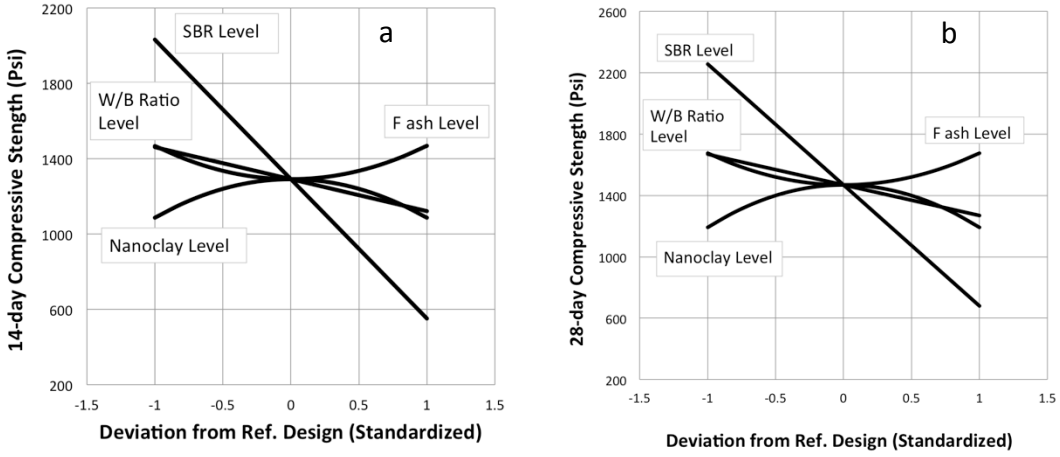

Figure 3.11 Trace plot for (a) 14-day *fc'* model; (b) 28-day *fc'* model

3.3.2 Environmentally friendly pure fly ash mortars with activation (Group 2 additives)

Similar to DoE 1, the average values for 7-day, 14-day, and 28-day compressive strength, split tensile strength, and spread diameter are shown in Table 3.7, along with the water reducer dosage and surface resistivity of all samples. All fly ash mortar samples showed a surface resistivity between 117 and 157 kΩ-cm, which can be categorized into a very low chloride permeability group as well. However, the variance of surface resistivity in DoE 1 is more than that of DoE 2, which could be attributed to the function of the additives in Group 1.

Table 3.7 DoE 2 – Properties of fresh and hardened mortar with Group 2 additives

Run	7-d f_c' (psi)	14-d f_c' (psi)	28-d f_c' (psi)	Spread diameter (in)	Water reducer (ml/l)	28-d Surface resistivity (kΩ-cm)
1	2014.7	2532.2	2787.2	10.3	10	142
2	2312.4	2769.2	2988.3	9.8	20	151
3	2562.4	2766.3	3212.1	9.9	20	154
4	2187.0	2988.1	3467.3	9.6	20	155
5	2588.2	3199.0	3756.7	9.7	10	139
6	2185.9	2727.8	3112.3	8.9	5	146
7	2395.2	2877.1	3289.0	10.7	20	150
8	2380.2	2988.2	3522.5	10.3	20	142

Run	7-d f_c' (psi)	14-d f_c' (psi)	28-d f_c' (psi)	Spread diameter (in)	Water reducer (ml/l)	28-d Surface resistivity (kΩ-cm)
9	2609.4	3289.2	3876.2	9.1	25	130
10	1910.6	2756.5	3100.2	10.0	10	133
11	2162.6	2256.2	2431.9	9.2	15	152
12	2563.3	3302.0	3771.1	9.8	25	139
13	1867.5	2729.4	3087.0	9.6	5	149
14	2407.1	2987.1	3652.1	9.7	10	140
15	2807.1	3421.2	3987.6	10.0	10	143
16	2797.7	3102.1	3566.4	9.4	20	120
17	2117.7	3212.0	3411.2	9.8	25	139
18	2352.9	3388.3	3762.0	9.9	15	142
19	2383.5	3554.9	4011.7	9.4	20	123
20	2557.7	3411.8	4156.4	9.7	5	119
21	2357.7	2998.0	3456.3	9.3	5	157
22	2376.5	3400.1	4231.2	10.6	20	142
23	2705.9	3721.1	4877.9	11.0	20	119
24	2658.8	4010.4	4412.0	9.9	5	145
25	2235.3	2612.2	2766.6	9.7	15	142
26	1882.4	2488.8	2988.3	10.2	15	117
27	2009.4	2780.3	3277.0	9.3	20	124

3.3.3 Model derivation and visualization

By using ANOVA and regression analysis, data in Table 3.7 were used to develop compressive strength models for DoE 2 with Group 2 additive as well. For two-way interactions identified in models, three-dimensional (3D) contour plots were provided to show the response surface plots in Figure 3.12, Figure 3.13, and Figure 3.14. For three-way interactions identified in models, three-way interaction charts were adopted to show the synergetic effects of three different activators (Figure 3.16, Figure 3.17, Figure 3.18, and Figure 3.19). Comparisons between test results and predicted results are provided as well. Seven-day, 14-day and 28-day compressive strength models were developed by running regression analyses:

f_c' (7-day) = 2342.9 – 182.5 * X1 + 108.2 * X1X2 + 230.5 * X3X5 + 308.4 * X1X2X3

f_c' *(14-day)= 3067.6 + 227.0* X1X2 + 344.6 * X3X5 + 626.7 * X1X2X3 – 457.6 * X2X3X4*

f_c' *(28-day)= 3356.4 + 222.9* X2^2 + 233.6* X1X2 + 581.3 * X3X5 + 713.9 * X1X2X3 – 397.1 * X2X3X4*

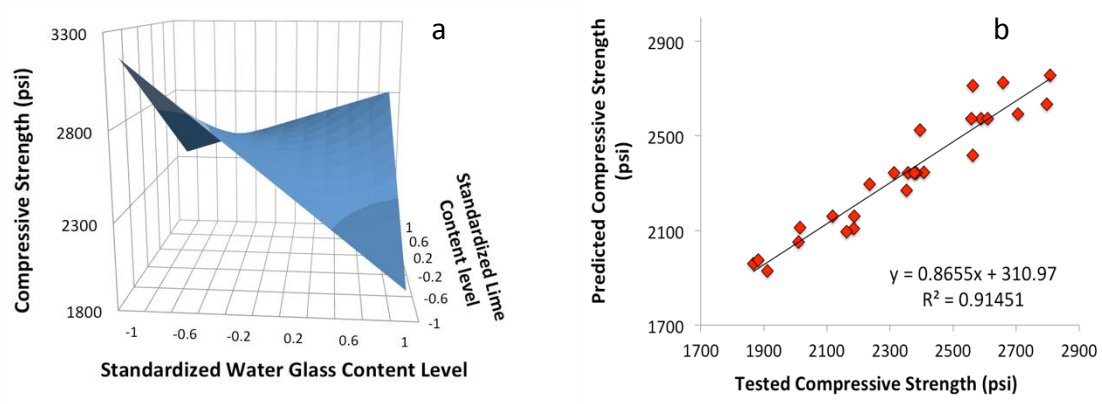

Figure 3.12 (a) 3D contour diagram of 7-day *fc'* model; (b) 7-day *fc'* test data vs. model prediction

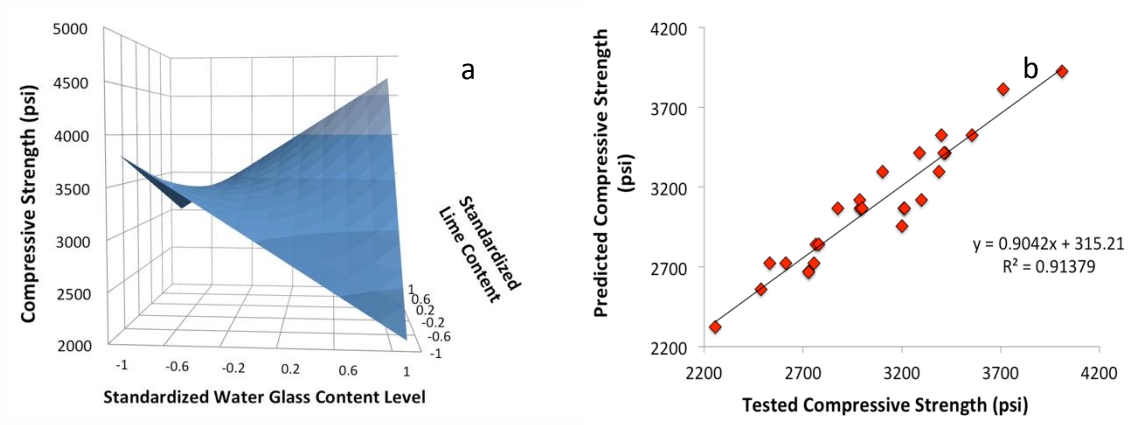

Figure 3.13 (a) 3D contour diagram of 14-day *fc'* model; (b) 14-day *fc'* test data vs. model prediction

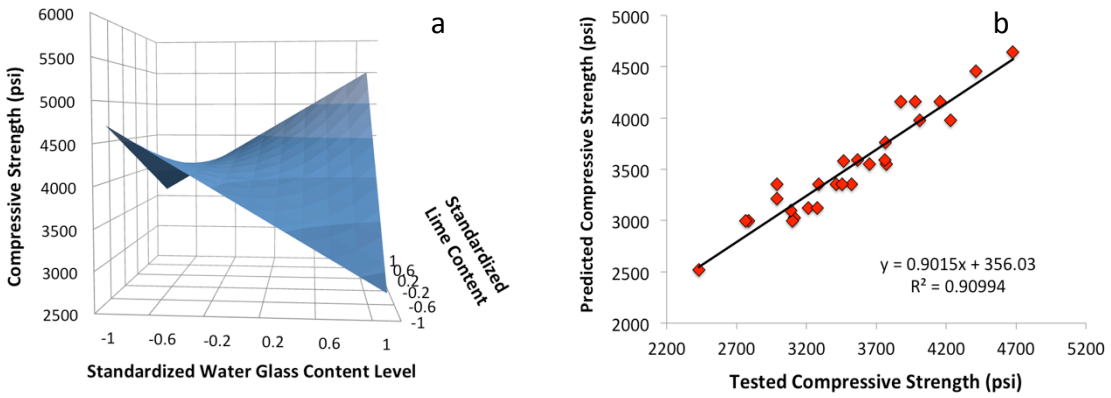

Figure 3.14 (a) 3D contour diagram of 28-day *fc'* model; (b) 28-day *fc'* test data vs. model prediction

Model verification

In Table 3.8, observe that the *F*-values are low and the *p*-values are all less than 0.1%, indicating that all three models of DoE 2 are highly significant.

Table 3.8 ANOVA summary of DoE 2

Model	R^2	Adjusted R^2	Degree of freedom (D.F.)	Residual D.F.	F-value	*p*-value
7-day f_c'	0.94	0.89	4	22	42.99	<0.001
14-day f_c'	0.93	0.88	4	22	39.90	<0.001
28-day f_c'	0.95	0.90	4	22	38.52	<0.001

Normal probability plots of the residuals (shown in Figure 3.15) are used to assess the model errors of DoE 2.

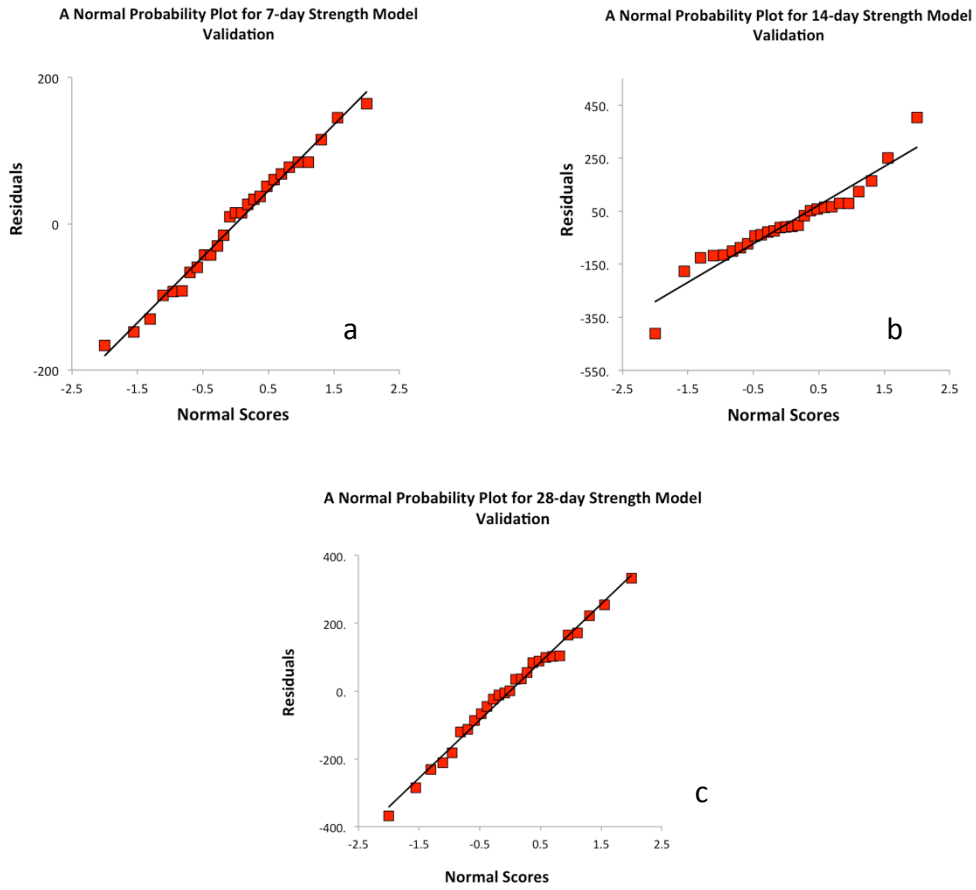

Figure 3.15 Normal probability plot for (a) 7-day *fc'* model; (b) 14-day *fc'* model; (c) 28-day *fc'* model

Three-way interaction charts show synergetic effects of activators.

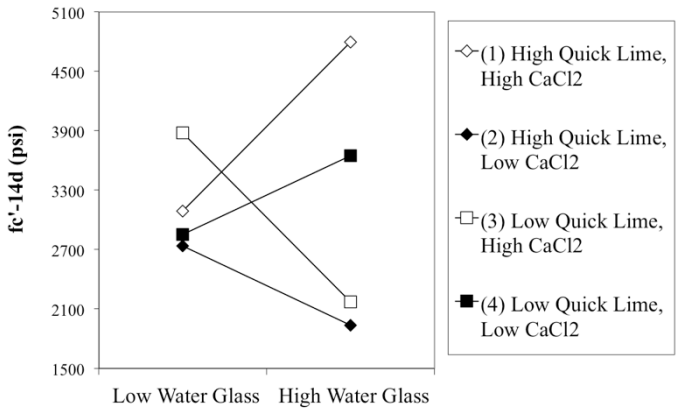

Figure 3.16 Synergetic effect of quick lime, $CaCl_2$ and water glass in 14-day *fc'* model. (Factor X_1, X_2, and X_3)

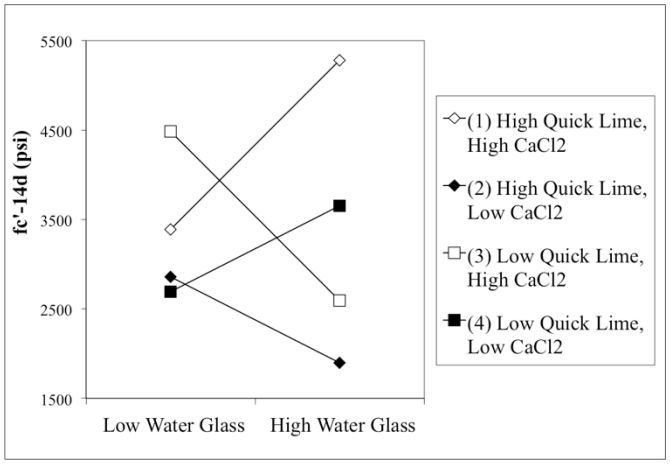

Figure 3.17 Synergetic effect of quick lime, $CaCl_2$ and water glass in 28-day *fc'* model. (Factor X_1, X_2, and X_3)

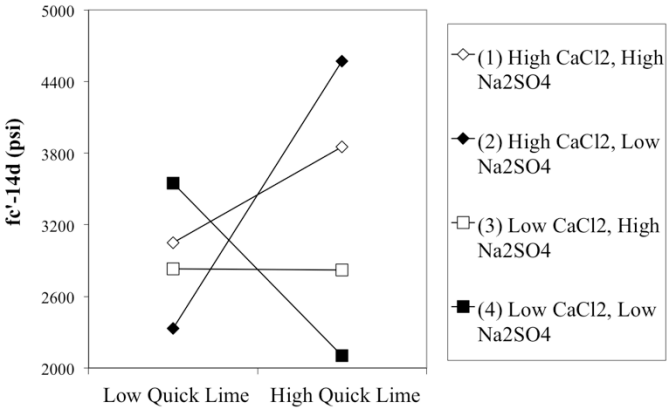

Figure 3.18 Synergetic effect of quick lime, $CaCl_2$ and Na_2SO_4 in 14-day *fc'* model. (Factor X_2, X_3, and X_4)

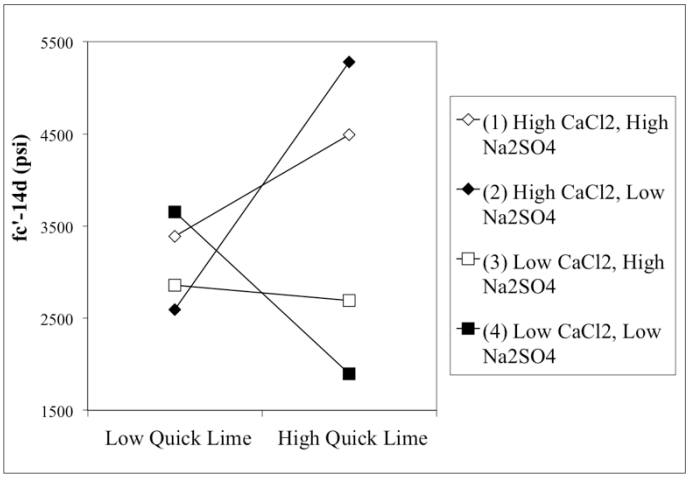

Figure 3.19 Synergetic effect of quick lime, $CaCl_2$ and Na_2SO_4 in 28-day *fc'* model. (Factor X_2, X_3, and X_4)

3.4 Microscopic Investigation

A microscopic investigation was conducted to obtain more insights on the effects of chemical activators, using the SEI and BSE modes of the electron microprobe. For comparison, mortar mix #22 of DoE 1 and mortar mix #23 of DoE 2 were examined at the age of 35 days, as they performed the best in their group in terms of compressive strength development. As shown in Figure 3.20a, most of the fly ash spheres remained smooth and spherical, implying that the degree of fly ash hydration was relatively low for mortar mix #22 of DoE 1 without activation. In contrast, Figure 3.20c suggests that many of the fly ash spheres in mortar mix #23 of DoE 2 were dissolved. While SEI micrographs provide only morphological information, BSE images provide morphological and compositional information by discriminating between heavy and light atoms. Figure 3.20b confirms that most of the fly ash spheres remained barely reacted. As such, in mortar #22 of DoE 1, the fly ash particles mainly served as micro-aggregates and nucleation centers for the precipitation of hydration products (Schaefer et al. 2009). In contrast, Figure 3.20d reveals more dissolution of fly ash spheres and the formation of more homogenous phases. Fly ash spheres in Figure 3.20d (mortar #23 of DoE 2) clearly exhibit different levels of

dissolution: some spheres were totally dissolved, some collapsed, and some were only at the onset of dissolution. Figure 3.20e and Figure 3.20f further illustrate these phenomena at higher spatial resolution. Figure 3.20e reveals that hydration only occurred at the surface layer of fly ash spheres in the absence of activation. Fly ash is the principal source of aluminosilicates for DoE 1 mortars. These low-activity fly ash spheres were only able to provide a submicron-thin layer of hydration products, which explains the low compressive strength of DoE 1 fly ash mortars. In contrast, Figure 3.20f reveals that hydration products covered the fly ash spheres and that some interlacing fibrous structures formed among the spheres. It is reasonable to assume that these hydration products and fibrous structures provided additional mechanical strength. Since the dissolution of fly ash spheres was improved significantly with chemical activation, more aluminosilicates were provided to form C-S-H gel.

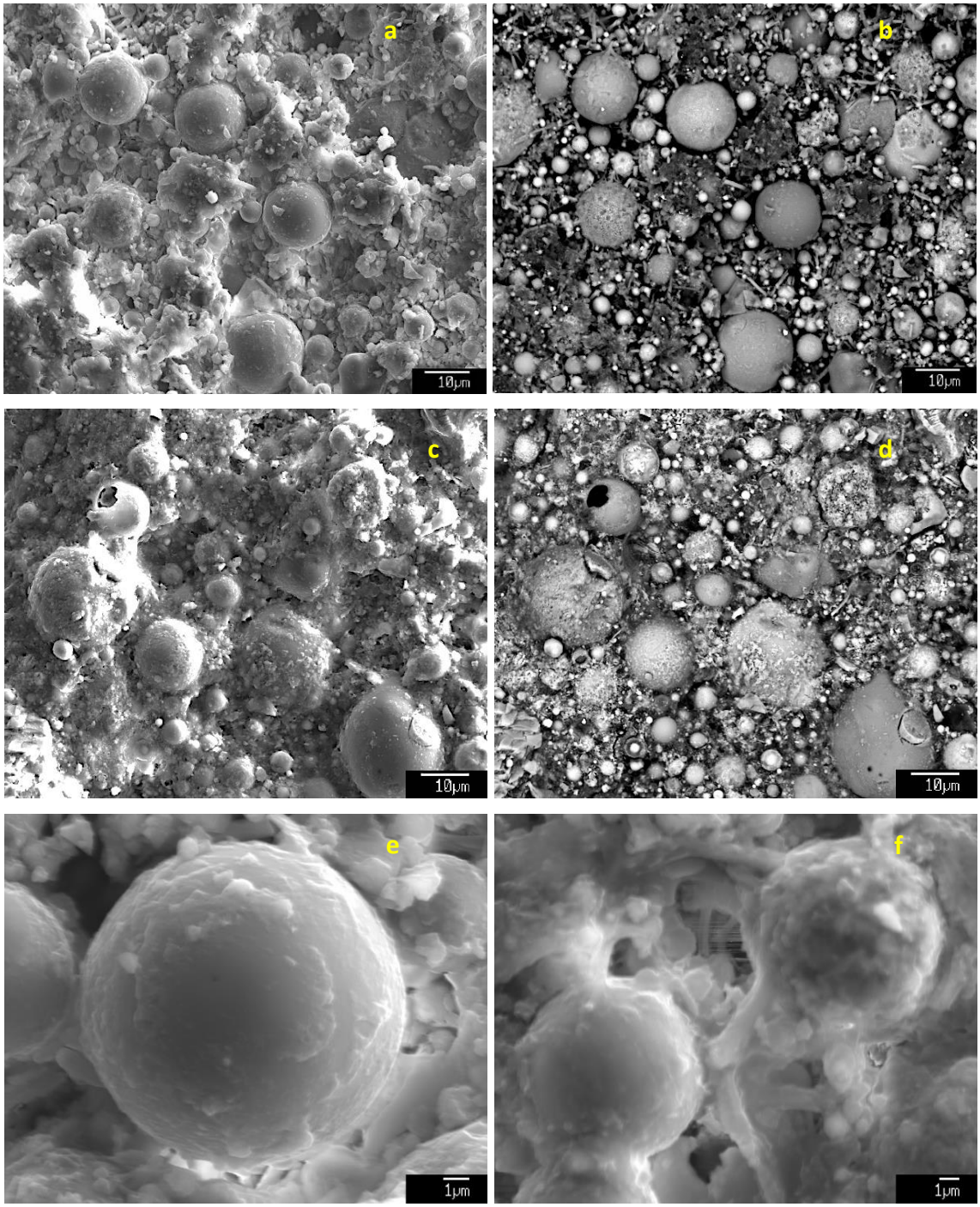

Figure 3.20 Micrograph of 28-day mortar surfaces:
(a) SEI, *DoE 1 Mortar #22*; (b) BSE, *DoE 1 Mortar #22*; (c) SEI, *DoE 2 Mortar #23*;
(d) BSE, *DoE 2 Mortar #23*; (e) SEI, *DoE 1 Mortar #22*; (f) SEI, *DoE 2 Mortar #23*

3.5 Investigation of Graphene Oxide Modified Mortar

Previous studies ((Lv et al. 2014; Gong et al. 2015; Ranjbar et al. 2015) indicate that graphene oxide (GO) can significantly improve the overall performance of cement mix by regulating cement hydration, providing a crack branching and bridging mechanism, and acting as nanofillers. Therefore, GO shows significant potential for practical application in fly ash-based cementitious materials of high strength and durability.

The GO used in this study was produced by using a modified Hummer's method, which mainly involves chemical oxidation of the graphite (Li et al. 2008). The as-produced GO was pasty, which was diluted with deionized water first and then sonicated for 45 minutes by using a Branson digital sonifier (S-450D, 400 W, 50% amplitude) to produce stable GO suspension (max. 3g/L) (Figure 3.21). The GO suspension with designed GO content (by weight) was then ready for the production of GO-fly ash or GO-cement binder.

Figure 3.21 Ultrasonification of GO suspension

Since mortar mix #23 of DoE 2 was the best performer in terms of compressive strength, it was chosen to study the effects of GO on fly ash mortar. The mix design of mortar #23 (shown in Table 3.3 and

Table 3.4) was modified with the addition of 0.03% (by weight of fly ash binder) GO. The same mix and curing procedures described in Section 3.2.2 were used to produce this GO-modified mortar.

After 28 days, the GO-modified fly ash mortar #23 of DoE 2 was compared with the regular fly ash mortar #23 of DoE 2 and the regular cement based mortar. The surface condition of mortar usually indicates to some extent the degree of polymerization of hydration products. By visual inspection, the smoothness of the GO-modified mortar surface was much better than the regular fly ash mortar, while the Portland cement mortar showed the smoothest surface (Figure 3.22), which indicates that the polymerization degree of GO-modified fly ash hydration products was higher than the regular fly ash hydration products, but lower than the cement hydration products.

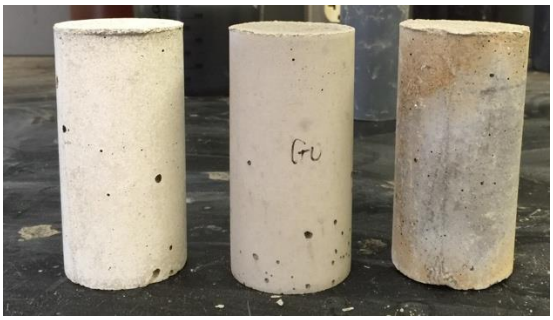

Figure 3.22 Mortar cylinders, 2 inch × 4 inch in size:
cement mortar (left); GO-modified fly ash mortar (middle); fly ash mortar (right)

The compressive strength of GO-modified fly ash mortar was measured using the same method described in Section 3.2.2. Table 3.9 shows the effect of GO on the strength of fly ash mortar. Observe that an increase of 23% in the 28-day compressive strength of fly ash mortar was achieved by incorporating 0.03% (by weight of fly ash) GO. Gong et al. (2015) indicated in a similar study that the introduction of 0.03% by weight GO sheets increased the compressive strength of cement paste by more than 40%. Another study by Ranjbar et al. (2015) found that

the compressive strength of fly ash-based geopolymer was improved 1.44 times by adding 1% by weight graphene nanoplatelet.

Table 3.9 Comparison of compressive strength

	0.03% GO-modified fly ash mortar	Regular fly ash mortar	Compressive strength increase
7-day f_c' (psi)	3353.2	2705.9	24%
14-day f_c' (psi)	4688.0	3721.1	26%
28-day f_c' (psi)	5998.2	4877.9	23%

A microscopic investigation was conducted to obtain additional insights on the effects of GO. Chemical element maps of the polished mortar sections were generated by using electron probe micro-analysis/wavelength dispersive X-ray spectroscopy (EPMA/WDS), which visualizes chemical element distributions in the analyzed area. For comparison, mortar mix #23 of DoE 2 and the GO-modified mortar mix #23 of DoE 2 were examined at the age of 14 days. Mapping of two selected elements (Ca and Si) is shown in Figure 3.23.

Figure 3.23 confirms that the fly ash particles are rich in Si and Ca elements, which is consistent with the chemical composition analysis of the fly ash used (Table 3.1). Figure 3.23 also suggests that the fly ash particles were not fully reacted at the age of 14 days, since many fly ash particles remained spherical shapes. It is clear from Figure 3.23b that the sand particles (very rich in Si) can be easily discriminated based on the difference in chemical composition between sand and paste.

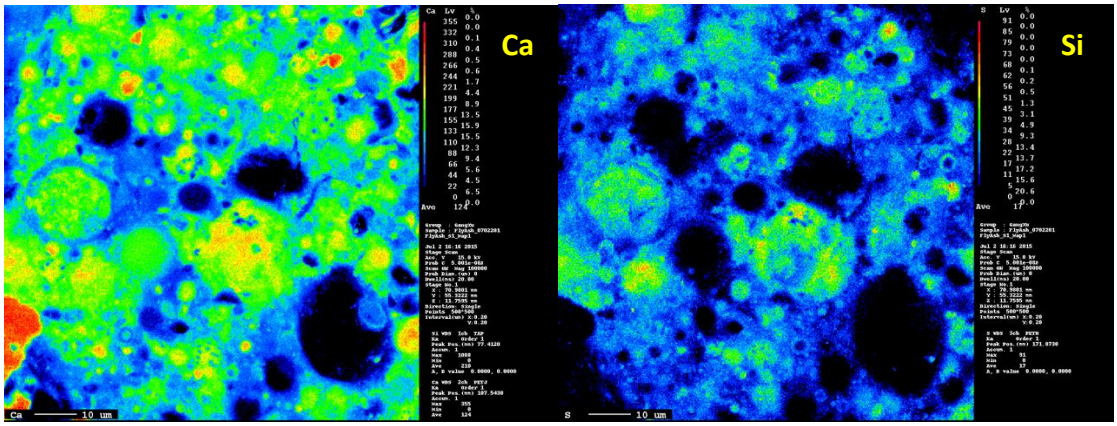

(a)

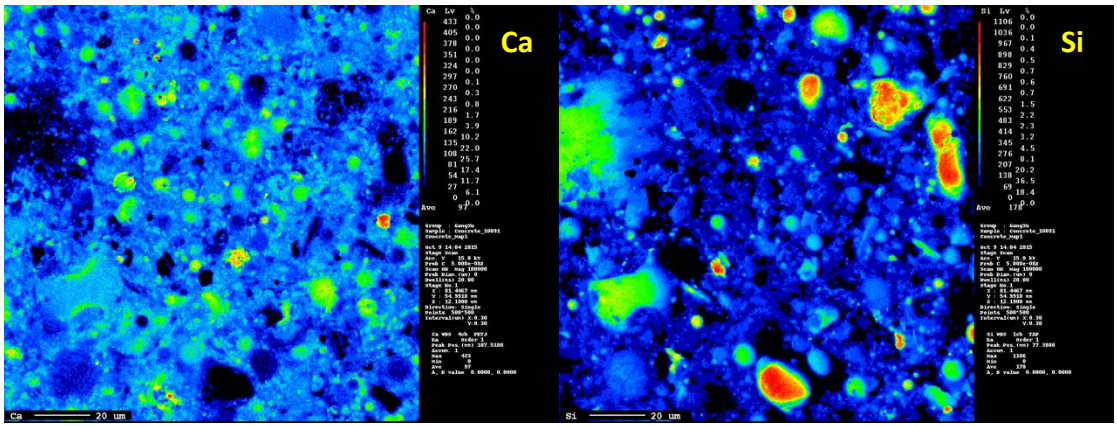

(b)

Figure 3.23 Element mapping (Ca and Si)
(a) #23 mortar of DoE 2; (b) GO-modified #23 mortar of DoE 2

ImageJ software was used to generate element ratio maps by processing the EPMA/WDS data from the element mapping in Figure 3.23. As show in Figure 3.24a, the Ca/Si mole ratio of regular fly ash mortar varies from 0 to 4, whereas the Ca/Si mole ratio of GO-modified fly ash mortar ranges from 0 to 5. The Ca/Si mole ratio maps indicate that the Ca-rich phase is conglomerated at spotted areas in the GO-modified fly ash mortar. On the contrary, the Ca-rich phase in the fly ash mortar is evenly dispersed with a low Ca/Si mole ratio. This finding was further confirmed by the histogram analysis of two Ca/Si mole ratio maps. As shown in Figure 3.25, the Ca/Si mole ratio of regular fly ash mortar features a mean value of 0.926 with a standard deviation of 1.281, whereas GO-modified fly ash mortar has a higher mean value of

1.384 with a standard deviation of 2.111. All these observations suggest that the phases present in fly ash mortar could be some form of CSH (calcium silicate hydrate). However, this CSH form with low Ca/Si ratio (average = 0.926 and 1.384) is different from the one produced by the hydration of Portland cement. Gan (Gan 1997) stated that the average bulk Ca/Si ratio of CSH in Portland cement paste falls between 1.5 and 1.7. A similar study by Brough and Atkinson (2002) found that CSH in KOH (potassium hydroxide)-activated slag mortar has a well-defined Ca/Si ratio of approximately 1.1, which is closer to the Ca/Si ratio in this study.

The average bulk Ca/Si ratio was increased from 0.926 to 1.384 in the GO-modified fly ash mortar, which indicates that the addition of 0.03% GO could facilitate the leaching of Ca^{2+} from fly ash particles. Meanwhile, since a higher standard deviation of Ca/Si ratio was observed in the GO-modified fly ash mortar, it is likely that GO nanosheets dispersed in fly ash paste act as growth points to form hydration products with a higher Ca/Si ratio. Abdolhosseini Qomi et al. (2014) studied the effect of Ca/Si ratio on the mechanical properties of CSH at nanoscale. They found that the CSH prepared at Ca/Si ratio = 1 to 1.1 exhibits superior stiffness and hardness on average, and that the CSH at low and high Ca/Si ratios behaved differently, which could explain why GO-modified fly ash mortar has a higher compressive strength than regular fly ash mortar.

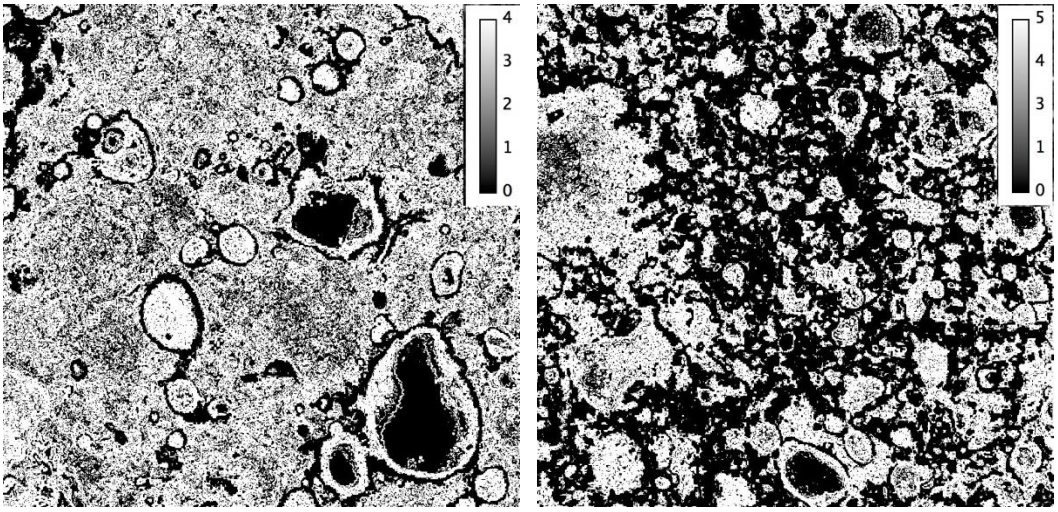

(a) (b)

Figure 3.24 Ca/Si mole ratio mapping
(a) #23 mortar of DoE 2; (b) GO modified #23 mortar of DoE 2

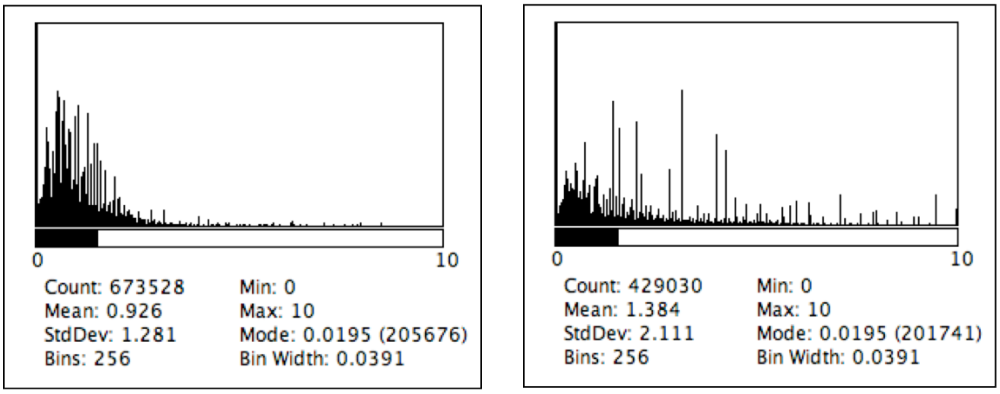

(a) (b)

Figure 3.25 Histogram of Ca/Si mole ratio mapping
(a) #23 mortar of DoE 2; (b) GO-modified #23 mortar of DoE 2

3.6 Summary and Conclusions

The laboratory study in this chapter explores the beneficial use of low-reactivity coal fly ash as cementitious binder in mortars, without heat activation. A uniform design scheme was employed for the statistical design of experiments. Predictive models were developed based on the experimental data to quantify the influence of mix design parameters on the compressive

strength of fly ash mortars at various ages. The models were verified and then employed for predictions.

The first group of mortar samples was fabricated using a low-reactivity Class C and Class F coal fly ash as well as admixtures intended to improve the strength and durability of hardened mortar. In the absence of chemical activation, these fly ash mortars exhibited a relatively low 28-day compressive strength in the range of 420–2975 psi, whereas a high-calcium, high-reactivity fly ash mortar (CFA3) can develop a compressive strength of 4000 psi at 28-d. The SBR latex exhibited a negative impact on the compressive strength of fly ash mortars. Admixing a small amount of the montmorillite nanoclay (0.6% by mass of Class C fly ash) significantly improved the compressive strength of fly ash mortars.

The second group of mortar samples was fabricated using the same low-activity Class C fly ash along with the following chemical activators: sodium silicate, quicklime, calcium chloride, and sodium sulfate. Admixing chemical activators into fly ash mortars led to noticeable improvement in their mechanical properties, with a 28-day compressive strength in the range of 2432–4878 psi. These activators showed a high level of synergetic effects. The highest 28-day compressive strength can be achieved by using high levels of water glass, quicklime, and $CaCl_2$, but a low level of Na_2SO_4. In addition, it was found that that the benefit of admixed sodium sulfate on compressive strength could be compromised in the presence of quicklime and calcium chloride.

Microscopic examination was conducted to shed light on the hydration behavior of selected fly ash mortars, using an electron probe micro-analyzer. Without activation, the fly ash spheres were only covered by a submicron-thin layer of hydration products and served mainly as micro-aggregates. With chemical activation at room temperature, hydration products covered the

fly ash spheres, and some interlacing fibrous structures formed among the spheres. This explains the observed difference in the two groups of fly ash mortars and points to a direction for further improving the development of such unconventional mortars and concretes.

The effect of GO on the strength of activated fly ash mortar was also studied. It was observed that an increase of 23% in the 28-day compressive strength of fly ash mortar was achieved by incorporating 0.03% (by weight of fly ash) GO. A microscopic investigation was conducted to obtain more insights on the effects of GO. It was found that the Ca/Si mole ratio of the regular fly ash mortar featured a mean value of 0.926 with a standard deviation of 1.281, whereas that of GO-modified fly ash mortar presented a higher mean value of 1.384 with a standard deviation of 2.111. The increased average bulk Ca/Si ratio, from 0.926 to 1.384, by GO indicated that the addition of 0.03% GO could facilitate the leaching of Ca^{2+} from fly ash particles. Meanwhile, since a higher standard deviation of Ca/Si ratio was observed in the GO-modified fly ash mortar, it is likely that the GO nanosheets dispersed in fly ash paste act as growth points to form hydration products with a higher Ca/Si ratio due to GO's higher surface energy and template effect.

It is concluded that low-reactivity fly ash can be used as a sole binder to form a paste with desirable strength by adopting chemical activation and GO modification at room temperature. This pure fly ash binder was applied to pervious concrete for further investigation, which will be discussed in Chapter 4.

CHAPTER 4.0 DEVELOPING PERVIOUS CONCRETE WITH 100% FLY ASH

4.1 Introduction

In Chapter 3, mortar with fly ash as a binder was tested for the following reasons (Jin 2002):

1. In pervious concrete, the binder provides a bond between coarse aggregates and provides suitable workability of the concrete. The binder requires properties similar to those of mortar, that is, strong overall strength to ensure bonding, stable paste without segregation, sufficient setting time, etc.

2. Mortar contains all the mixing materials of pervious concrete, except that in pervious concrete, the fine aggregates are scaled up to the coarse aggregates. Therefore, a mortar test reflects the properties of pervious concrete to some extent.

3. The scale of an experiment for mortar is much smaller than that for pervious concrete. Therefore, the variables of a mortar test can be controlled in a laboratory. With mortar tests, the design of the experiment can include investigation of many combinations of variables with reasonable effort. A small-scale test can be repeated more readily and can provide more accurate results.

4. Based on the literature review, there is agreement among many researchers that successful fabrication of mortar should be achieved before concrete application and that an understanding of mortar behavior is of importance itself.

This chapter describes our investigation into the performance of pervious concrete with fly ash as a cementitious binder, using the method developed in Chapter 3. Based on the proven binding strength and durability of a pure fly ash paste (described in previous chapters), an innovative pervious concrete mix design of a pure fly ash binder modified by graphene oxide

(GO) was developed with the desired workability and with overall strength and durability. This mix design was compared with control groups. Laboratory tests that simulated many years of field service were conducted to investigate the durability of pervious concrete; the tests included evaluations of salt scaling and freeze–thaw damage.

4.2 Experimentation

4.2.1 Materials

Class F fly ash (CFA) 1, a low-reactivity fly ash described in Chapter 3, was used along with activators (water glass, sodium silicate, sodium sulfate, quicklime, calcium chloride) as a fly ash binder for a pervious concrete mix design. The GO used in the pervious concrete was prepared using the procedures described in Section 3.4. The 0.03% (by weight of binder) GO for each mix design was sonicated to stable suspension before being subjected to any applications.

One type of single-sized coarse aggregate (crushed limestone 3/8-inch in size with 100% passing the 1/2-inch sieve and 100% retained on the 3/8-inch sieve) was used. The dry-rodded unit weight, specific gravity, and water absorption of this coarse aggregate are listed in Table 4.1. One commercially available glass powder, recycled from industrial feedstocks, was used as a microfiller. The properties of this glass powder are listed in Table 4.2. The main composition of the glass powder is amorphous calcium aluminosilicate formed by the fusion of calcia, silica, and alumina, with lesser amounts of boron oxide and magnesium oxide. It has been found that glass powder, 75μm or less in size, can act as an effective supplementary material, preventing alkali-silica reaction (Sukamal Kanta Ghosh et al. 2015). The intent of using glass powder in this study was to mitigate the excessive alkalinity of activators in the fly ash binder or the alkali-silica reaction in the cement binder. A type I/II cement (ASTM C150) was used in the mix design of control groups. Cement properties provided by the manufacturer are listed in Table 4.2.

Table 4.1 Properties of aggregate used in the pervious concrete

Aggregate type	Crushed limestone
Aggregate size	3/8 inch
Unit wight (lb/ft^3)	90.2
Specific gravity	2.6
Water absorption	2.5%

Table 4.2 Physical and chemical properties of glass powder and cement

	Glass powder	Cement
Specific gravity	2.5	3.2
Bulk density (lb/ft^3)	43	76
d_{98} top size (μm)	40	--
D_{50} median size (μm)	8–9	--
SiO_2 (wt.%)	50–55%	21%
CaO (wt.%)	20–25%	65%
Al_2O_3 (wt.%)	14–20%	4%
Fe_2O_3 (wt.%)	<1%	3.5%
Na_2O+K_2O (wt.%)	8–14%	<0.9%
Loss on ignition (wt.%)	<0.5%	<1.1%
Tricalcium silicate C_3S (wt.%)	--	55%
Tricalcium aluminate C_3A (wt.%)	--	6.2%

4.2.2 Mix proportions

Four groups of pervious concrete were designed based on the best performer of fly ash mortar in Chapter 3 and the suggested proportion values in Table 2.2. The fly ash binder from #23 mortar of DoE 2 was used as a pervious concrete binder. These four groups of pervious concrete were designed to investigate the performance of fly ash-based pervious concrete and how the addition of GO content influences the void ratio, strength, water permeability, and Young's modulus of pervious concrete. The proportions of four mixes are shown in Table 4.3.

4.2.3 Specimen fabrication

The pervious concrete for the four mix designs (see Table 4.3) was prepared in four separate batches. Cylinders 4 in. in diameter, 8 in. in height and cylinders 6 in. in diameter, 12 in. in height were prepared by using an improved standard concrete mixing procedure, because it was found that when the standard concrete mixing procedure was used, pervious concrete samples failed at the interface between the cement binder and the aggregate under compression. The improved mixing procedure was adopted to improve the bonding between the cement/fly ash paste and the aggregate (Vernon R. Schaefer et al. 2006). The coarse aggregate was sieved and washed, and then air-dried. The additional amount of water was calculated to reach a saturated surface dry (SSD) condition of coarse aggregates. The "butter batch" was mixed in the rotating drum before mixing the pervious concrete. Then a small amount of cement/fly ash and GO suspension liquid (<5% by mass) was mixed with the aggregate for 1 minute to coat the surface of the aggregate. The remaining cement/fly ash, GO suspension liquid, and water with admixtures were added to the rotating drum and mixed for 3 minutes. The mixture was allowed to rest for 3 minutes, and then was mixed again for additional 2 minutes. Before casting, a pervious concrete ball was made with a handful of pervious concrete mix. If the sample was able to maintain the ball shape, then the mix was considered acceptable. If the sample of pervious concrete mix was too dry or too wet, it would not form a ball.

Table 4.3 Pervious concrete material proportions used in this study

Mix Design	Agg. Size (inch)	Agg. (kg/m^3) [a/b]	Cement (kg/m^3)	Fly ash CFA1 (kg/m^3)	Water (kg/m^3) [w/b]	$NaSO_4$ (kg/m^3)	CaO (kg/m^3)	$CaCl_2$ (kg/m^3)	Water Glass (kg/m^3)	GO (g/100kg binder)	TEA (ml/100 kg binder)	HRWR (ml/100 kg binder)	AE (ml/100 kg binder)
Cement	3/8	1425 [4.45]	320	--	80 [0.25]	--	--	--	--	--	40	300	30
Cement + GO	3/8	1425 [4.45]	320	--	80 [0.25]	--	--	--	--	96	40	300	30
Fly ash	3/8	1435 [4.0]	--	358	97 [0.27]	3.6	17.9	3.6	25	--	40	1000	30
Fly ash + GO	3/8	1435 [4.0]	--	358	97 [0.27]	3.6	17.9	3.6	25	108	40	1000	30

* 2% (by weight of cement or fly ash) glass powder used for all mix designs
* a/b = aggregate-binder-ratio
* w/b = water-binder-ratio
* 1 lb/yd^3 = 0.5933 kg/m^3
* 1 fl oz/cwt = 65.2 mL/100 kg

All 4 in. by 8 in. cylinder specimens were prepared in two layers, with each layer compacted by ten blows of a standard 2.5 kg Protocol hammer. The 6 in. by 12 in. cylinders were prepared in three layers. The specimens were struck off at the top surface before being covered with caps. The specimens were demolded after 24 hours and cured according to ASTM C192. To ensure that the pervious concrete cylinders had smooth, parallel, uniform bearing surfaces to the applied axial load during compression testing, the cylinders were capped with a sulfur capping compound according to ASTM C617 (Figure 4.1). A close-up view of sample surfaces is shown in Figure 4.2.

Figure 4.1 Pervious concrete cylinders with capping:
(left to right) cement, cement + GO, fly ash, fly ash + GO

Figure 4.2 Close-up view of sample surface:
(left to right) cement, cement + GO, fly ash, fly ash + GO

4.3 Tests and Results

4.3.1 Density and Void Ratio

ASTM C1754 was used to determine the density of hardened pervious concrete. The average length of the specimen was recorded to the nearest 0.25 mm (0.01 in.) by using the jaw caliper. The average diameter of the specimen was recorded to the nearest 0.25 mm (0.01 in.) by averaging two diameters measured at right angles to each other at about mid-height of the specimen. To measure the dry mass, the specimen was first dried in an oven at a temperature of 38°C for 24 hours. The specimen was removed from the oven to record the mass. Then the specimen was put back in the oven for 24 hours before again determining the mass. These two steps must be repeated until the difference between any two subsequent mass measures is less than 0.5%. The density of the hardened pervious concrete of different mix at 28 days was calculated by dividing the dry mass of the sample by it volume. The results are shown in Table 4.4 and Figure 4.3.

Table 4.4 Density of hardened pervious concrete at 28 days (unit: Kg/m^3)

	Cement	Cement + GO	Fly ash	Fly ash + GO
Sample 1	1873.3	1857.5	1926.5	1965.7
Sample 2	1897.6	1885.3	1896.2	1944.7
Sample 3	1860.2	1803.2	1885.6	1990.4
Sample 4	1900.2	1869.4	1912.3	1983.6
Average	1882.8	1853.9	1905.2	1971.1

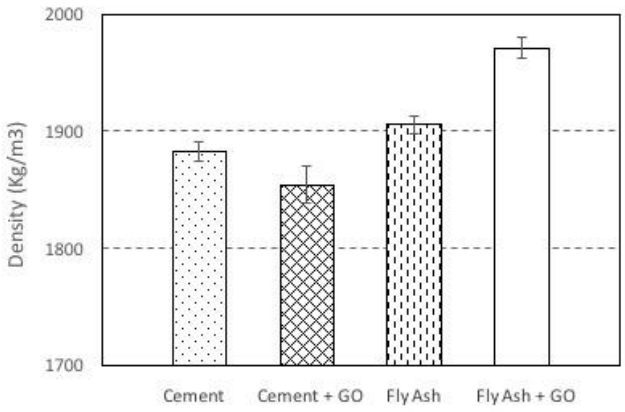

Figure 4.3 Density of hardened pervious concrete at 28 days

ASTM C1754 was used to determine the void ratio of hardened pervious concrete. The specimen was submerged completely in a water bath for 30 minutes, with water temperature at 20±3°C. A rubber mallet was used to tap the side of the specimen ten times below the water to release the trapped air bubbles inside the pervious concrete. The specimen was rotated after each tap so that taps were equally spaced around the circumference of the specimen. The submerged mass was recorded to the nearest 0.5 g (0.001 lb). The void ratio of the hardened pervious concrete of difference mix at 28 days was calculated according to Equation 2 and is shown in Table 4.5 and Figure 4.4. All the samples showed void ratios between 20% and 31%, which are within an acceptable range (Montes et al. 2005). The incorporation of GO in the binder resulted in a decreased average void ratio of fly ash pervious concrete ranging from 24.9% to 21.2%, whereas the average void ratio of Portland cement pervious concrete increased from 27.4% to 28.9%.

$$\text{Void ratio} = \left(1 - \frac{W_d - W_w}{\rho_w V}\right) \times 100\% \qquad (2)$$

where W_d = oven dry mass of sample
W_w = submerged mass of sample
ρ_w = density of water
V = volume of sample

Table 4.5 Void ratio of hardened pervious concrete at 28 days

	Cement	Cement + GO	Fly ash	Fly ash + GO
Sample 1	27.8%	29.3%	23.2%	21.5%
Sample 2	26.3%	27.8%	25.9%	22.1%
Sample 3	28.3%	30.8%	25.5%	20.2%
Sample 4	27.1%	28.0%	24.8%	21.1%
Average	27.4%	28.9%	24.9%	21.2%

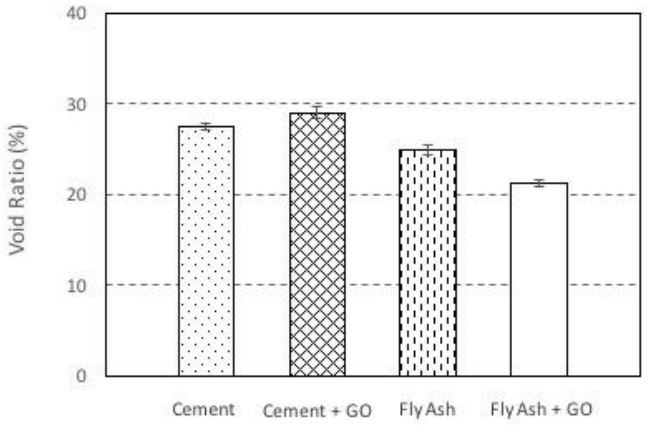

Figure 4.4 Void ratio of hardened pervious concrete at 28 days

4.3.2 Compressive and split tensile strength test

The compression test was performed on Day 7 and Day 28 following ASTM C39. Before testing, the diameter of each specimen was measured at the top, middle, and bottom of the specimen's length. The cross-section area was calculated based on the average diameter. The loading rate used was between 24 psi/sec and 40 psi/sec. The compression test was stopped when the load started decreasing rapidly, or there was an obvious sign of damage on samples. The compressive strength of the hardened pervious concrete from different mix designs is shown in Table 4.6 and Figure 4.5. All values in Table 4.6 are the average of three test results. For four pervious concrete mixes, the development of compressive strength as a function of time is shown in Figure 4.6.

Table 4.6 Compressive strength results

Mix design	7-day f_c' (psi)	28-day f_c' (psi)
Cement	1363	1822
Cement+GO	1381	2256
Fly ash	893	1447
Fly ash+GO	1457	2220

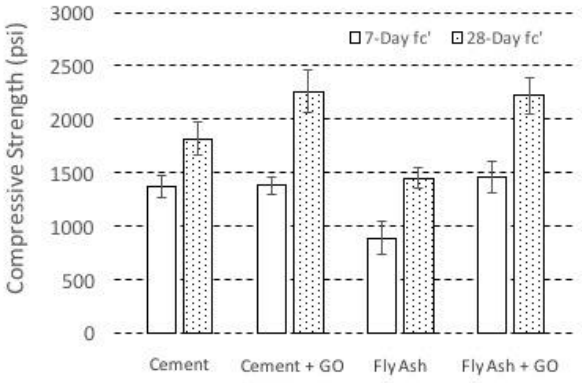

Figure 4.5 Compressive strength test results

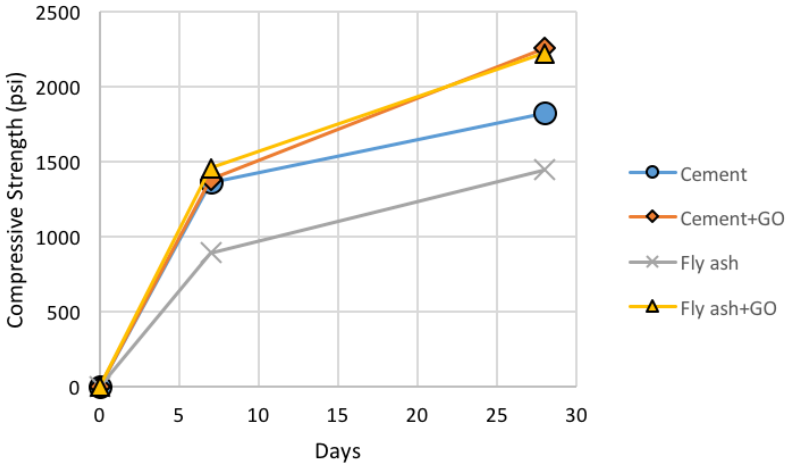

Figure 4.6 Compressive strength development with time

Figure 4.7 shows the relationship between the void ratio and compressive strength. There is no overall correlation found between the void ratio and compressive strength, since each mix used a different binder system. However, for each binder system, the general trend is that compressive strength decreases as the void ratio increases.

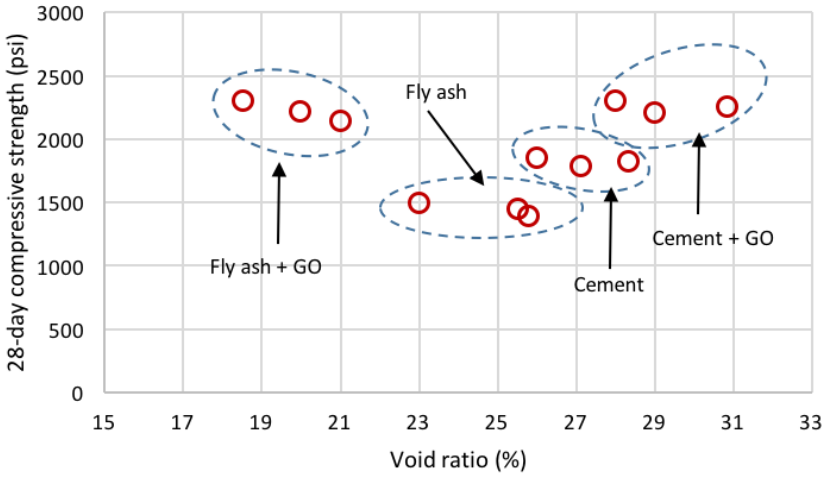

Figure 4.7 Relationship between void ratio and 28-day compressive strength

The addition of 0.03% (by weight of binder) GO improved the average 7-day compressive strength of fly ash pervious concrete by 63% (from 893 psi to 1457 psi), but the 0.03% GO only increased the average 7-day compressive strength of cement pervious concrete from 1363 psi to 1381 psi (1%). The average 28-day compressive strength varied from 1447 psi to 2256 psi. The incorporation of 0.03% GO in the binder showed that the average 28-day compressive strength of fly ash pervious concrete was improved from 1447 psi to 2220 psi (by 53%), while the average 28-day compressive strength of cement pervious concrete was improved from 1822 psi to 2256 psi (by 24%).

In summary, the addition of 0.03% GO increased both 7-day and 28-day compressive strength of fly ash pervious concrete by more than 50%. However, for cement pervious concrete, GO only increased the 28-day compressive strength by 24% and had little effect on early

strength development. Note that all samples produced from the improved mixing procedure described in Section 4.2.1 failed through the aggregate after compression tests (see Figure 4.8), which eliminated the weak interface zone between the paste and aggregates.

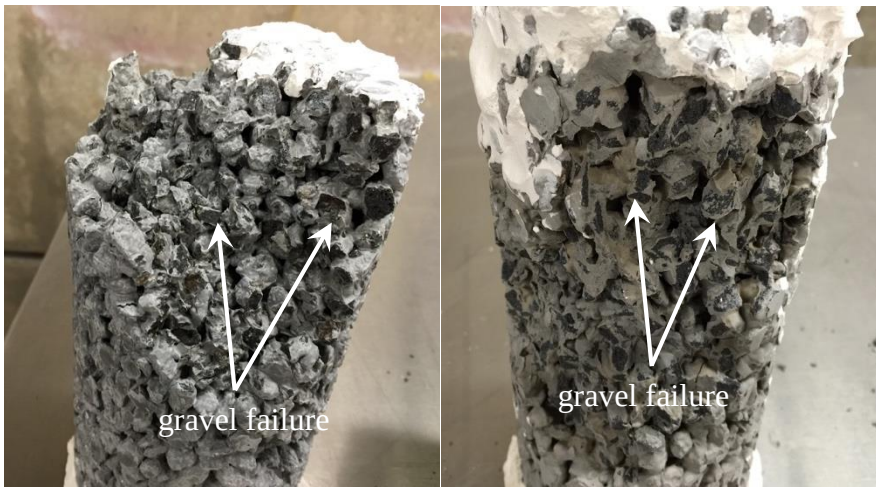

Figure 4.8 Failure surface of samples after compression tests on 7-day: cement + GO (left); fly ash + GO (right)

The split tensile strength test was performed by applying a line load along the cylinder length. Since there are no standard test methods for measuring the split tensile strength of pervious concrete, ASTM C496 was used. Before testing, the diameter of each specimen was measured at the top, middle, and bottom of the specimen length. The cross-section area was calculated based on the average diameter. The loading rate for this test was between 100 psi/min and 150 psi/min, and the test was stopped when an obvious sign of damage occurred on samples (see Figure 4.9). The split tensile strength of hardened pervious concrete was calculated based on Equation 3 and is shown in Table 4.7 and Figure 4.10. All values in Table 4.7 are the average of three test results.

$$\text{Split tensile strength} = 2P/\pi ld \quad (3)$$

where P = maximum applied load
l = length
d = diameter

Figure 4.9 Failure surface of samples after split tensile strength tests at 7-day: cement + GO(left); fly ash + GO(right)

Table 4.7 Split tensile strength results

Mix design	7-day f_t' (psi)	28-day f_t' (psi)
Cement	168.7	240.9
Cement+GO	180.6	283.1
Fly ash	125.9	200.5
Fly ash+GO	181.8	274.2

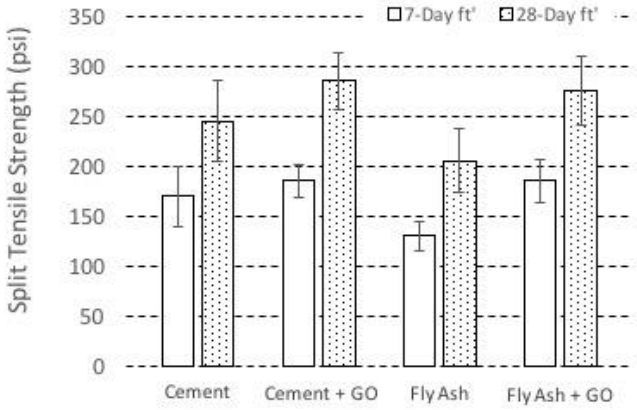

Figure 4.10 Split tensile strength test results

The addition of 0.03% GO improved the average 7-day split tensile strength of fly ash pervious concrete by 44% (from 126 psi to 182 psi); it increased the average 7-day split tensile

strength of Portland cement pervious concrete by 7% (from 169 psi to 181 psi). The average 28-day split tensile strength varied from 200.5 psi to 283.1 psi. The incorporation of 0.03% GO into the binder showed that the average 28-day split tensile strength of fly ash pervious concrete was improved from 200.5 psi to 274.2 psi (by 37%), while the average 28-day split tensile strength of cement pervious concrete was improved from 240.9 psi to 283.1 psi (by 18%). Figure 4.11 shows the relationship between the 28-day compressive strength and 28-day split tensile strength of pervious concrete, which is a linear relationship. The split tensile strength is approximately equal to 12% of the compressive strength for all the pervious concrete mixes.

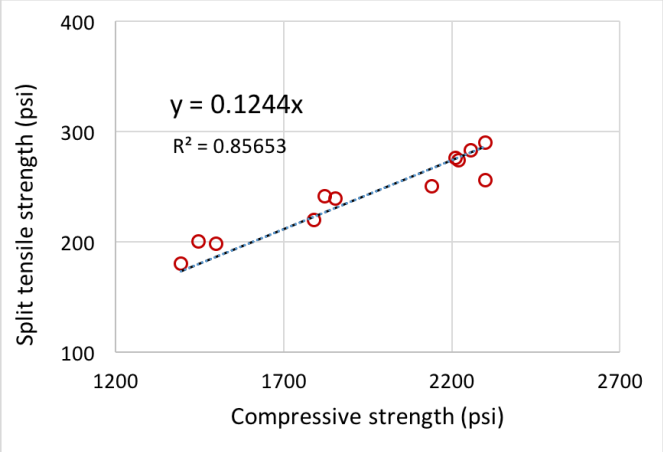

Figure 4.11 Relationship between split tensile strength and compressive strength at 28 days

4.3.3 Young's modulus

Young's modulus (E) is an important property used for pervious concrete design. At the date of compressive strength tests, two samples of each mix design were used to determine the Young's modulus of pervious concrete according to ASTM C 469. A compressometer was used to measure the longitudinal strain of samples during the loading (Figure 4.12). The loading rate for this test was between 28 psi/sec and 42 psi/sec. The specimen was loaded three times, and the data from the first loading were not used. The test was stopped when the load reached 40% of the average ultimate load of the specimens from the same mix design. The Young's modulus of the

hardened pervious concrete was calculated based on Equation 4 and is shown in Table 4.8 and Figure 4.13. All values in Table 4.8 are the average of two test results.

$$E = (S_2 - S_1)/(\varepsilon_2 - 0.000050) \quad (4)$$

where S_2 = stress corresponding to 40% of ultimate load
S_1 = stress corresponding to a longitudinal strain of 50 millionths
ε_2 = longitudinal strain produce by stress S_2

Figure 4.12 Compressometer setup

Table 4.8 Young's modulus (E) of pervious concrete

Mix design	*E* at 7 days (ksi)	*E* at 28 days (ksi)
Cement	2450	2450
Cement+GO	2500	2550
Fly ash	2900	2950
Fly ash+GO	2950	3150

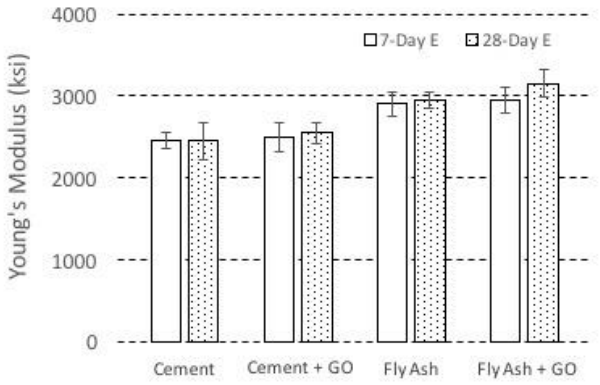

Figure 4.13 Young's modulus (E) of pervious concrete

Based on test results, the fly ash pervious concrete has a higher E of 2950 ksi than that of Portland cement pervious concrete (E = 2450 ksi) at 28 days. At 28 days, the incorporation of 0.03% GO increased the E of the fly ash pervious concrete by 6.8% (from 2950 ksi to 3150 ksi), while it increased the E of the Portland cement pervious concrete by 4.1% (from 2450 ksi to 2550 ksi).

4.3.4 Infiltration test

The test method proposed by Flores et al. (2007) was adopted to evaluate the permeability of pervious concrete. A 4 in. by 8 in. (10 × 20 cm) pervious concrete cylinder was used in this method. The perimeter surface of cylinder was covered with a waterproof and non-absorbing material. A plastic cap was attached to the top of the specimen to get a constant 1 cm water head at the top surface of the pervious concrete. This test recorded the time that the given volume of water needs to flow through the entire specimen. The infiltration rate of the hardened pervious concrete was calculated based on Equation 5 and is shown in Table 4.9 and Figure 4.14.

$$\text{Infiltration rate} = Q/At \quad (5)$$

where Q = volume of water for the test
A = cross-section area of specimen
t = recorded time for water to flow through the entire specimen

Table 4.9 Infiltration rate of hardened pervious concrete at 28 days

	Cement (in./hr)	Cement + GO (in./hr)	Fly ash (in./hr)	Fly ash + GO (in./hr)
Sample 1	1249	1590	623	729
Sample 2	1166	1521	583	795
Sample 3	1093	2082	950	625
Sample 4	1561	1682	776	515
Average	1267	1719	733	666

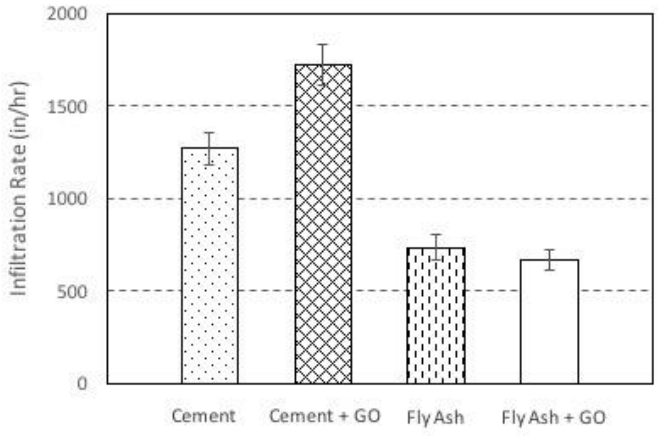

Figure 4.14 Infiltration rate of hardened pervious concrete at 28 days

For all mixes, the infiltration rate ranges from 515 in./hr to 2082 in./hr. Low infiltration mixes are those with fly ash as a binder. The Portland cement pervious concrete has a higher infiltration rate compared with those of fly ash groups. It is likely that the fly ash pervious concrete needs a greater volume of binder, which yields a less void and tortuous structure, to achieve similar strength of the cement pervious concrete. While GO reduced the infiltration rate of the fly ash pervious concrete, it significantly improved the infiltration rate of the Portland

cement pervious concrete. Further investigation is needed to understand the effects of GO on the void ratio and permeability of pervious concrete.

Previous studies (Vernon R. Schaefer et al. 2006; Joung 2008) found that the infiltration rate was highly correlated to the void ratio. Figure 4.15 shows the relationship between the void ratio and the infiltration rate for all the pervious concrete samples in this study, where the infiltration rate increased exponentially as a function of void ratio.

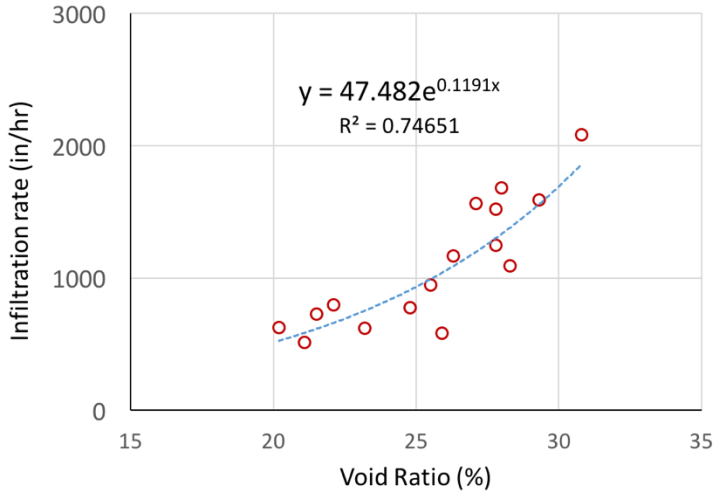

Figure 4.15 Relationship between void ratio and infiltration rate of the pervious concrete

4.3.5 Freeze-deicer salt scaling resistance test

Sixteen pervious concrete specimens in 4 in. by 4 in. cylinders were tested at 28 days, and labeled as four groups: C (cement), Cg (cement + GO), F (fly ash), and Fg (fly ash + GO). Each group has four cylinder samples (Figure 4.16). The test was conducted at the cold lab at Montana State University. The pervious concrete cylinders were immersed in a plastic container containing 3% NaCl solution for 24 hours. The concrete cylinders were then surface-dried with paper towels and weighed. Next, all the cylinders were placed in a closed container and transferred with solution into the freezer at -20 ± 1°C for 24 hours. After this freezing stage, the specimens (along with the plastic box) were placed in the laboratory environment at 23 ± 2°C

and with a RH ranging from 45–55% for 12 hours. Once the ice in the plastic container was completely thawed, the cylinders were transferred onto a wood plate and dried for 12 hours, at which time each of the specimens was weighed and its mass recorded. This freeze/thaw and wet/dry cycle was repeated 15 times. After drying at 3, 7, 10, 13, and 15 cycles, the mass change of each concrete cylinder was tested. Note that a sufficiently low temperature (-20° C) and sufficient amount of time (24 h) are crucial to ensure complete freezing of the concrete pore solution. By design, this test protocol simulated salt scaling of the field concrete in an accelerated manner. For concrete structures in the field environment, often the number of their freeze/thaw cycles is estimated from the number of times the ambient air temperature crosses the 0°C threshold (divided by two). This method tends to substantially overestimate the actual number of freeze/thaw cycles that occurred inside the concrete, especially when the presence of deicer solution significantly reduces the freezing point of the pore solution.

Figure 4.16 Pervious concrete samples before freeze-deicer salt scaling test

The test results are presented in Figure 4.17 and Table 4.10. The freezing rate at the sample core was also recorded (Figure 4.18). After the third cycle, the cement pervious concrete had a weight loss of 2.06% and 5.35%, whereas the fly ash pervious concrete had a weight loss of approximately 15% (Figure 4.19). The initial weight loss of fly ash pervious concrete was much higher, because there was still a certain amount of the unhydrated fly ash binder at 28

days. Due to slow hydration progress, fly ash pervious concrete typically performs more strongly at later ages. The incorporation of GO increased the salt scaling resistance for all groups. Although ordinary fly ash pervious concrete did not show better salt scaling resistance than other groups, it is noteworthy that the GO-modified fly ash pervious concrete was the only group that survived after the fifth cycle with 57% weight loss, which indicated that GO-modified hydration products from the fly ash had better salt scaling resistance than the conventional cement hydrates.

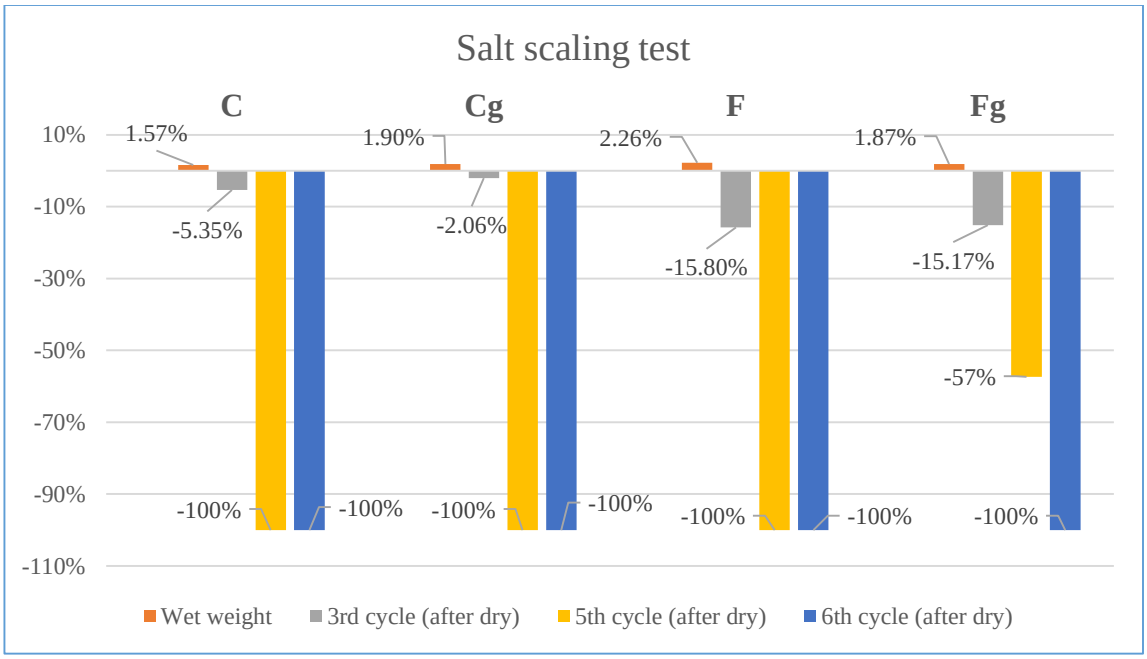

Figure 4.17 Weight loss during freeze-deicer salt scaling test

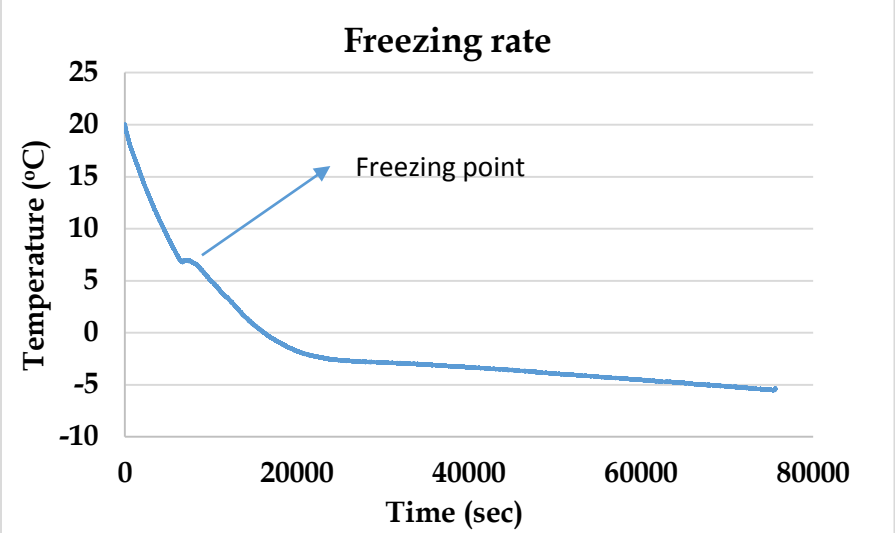

Figure 4.18 Freezing rate of pervious concrete immersed in 3% NaCl

Table 4.10 Freeze-deicer salt scaling test results

Sample	Dry weight - Initial	Wet weight	Increase in weight		3rd cycle (after dry)	Loss of weight compared to Initial weight		5th cycle (after dry)	Loss of weight compared to Initial weight		6th cycle (after dry)	Loss of weight compared to Initial weight
4x4 Cyl.	2902	3008	3.65%	3.65%	*	100%	100%	*	-100%	-100.00%	*	100.00%
c-1	1569	1586	1.08%	1.57%	1400	10.77%	-5.35%	*	-100%	-100%	*	-100%
c-2	1484	1512	1.89%		1401	5.59%		*	-100%		*	
c-3	1399	1428	2.07%		1350	3.50%		*	-100%		*	
c-4	1438	1456	1.25%		1416	1.53%		*	-100%		*	
Cg -1	1587	1618	1.95%	1.90%	1561	1.64%	-2.06%	*	-100%	-100%	*	-100%
Cg -2	1464	1492	1.91%		1439	1.71%		*	-100%		*	
Cg -3	1454	1486	2.20%		1414	2.75%		*	-100%		*	
Cg -4	1492	1515	1.54%		1460	2.14%		*	-100%		*	
F-1	1379	1415	2.61%	2.26%	1251	9.28%	-15.80%	*	-100%	-100%	*	-100%
F-2	1478	1509	2.10%		1250	15.43%		*	-100%		*	
F-3	1491	1528	2.48%		1195	19.85%		*	-100%		*	
F-4	1399	1425	1.86%		1138	18.66%		*	-100%		*	
Fg-1	1623	1655	1.97%	1.87%	1584	2.40%	-15.17%	824	-49.23%	-57%	*	-100%
Fg-2	1570	1601	1.97%		1011	35.61%		460	-70.70%		*	
Fg-3	1560	1588	1.79%		1442	7.56%		654	-58.08%		*	
Fg-4	1557	1584	1.73%		1322	15.09%		753	-51.64%		*	

Note:

1. Unit of weight is grams
2. ***** Disintegrated
3. By the end of the 6th cycle all the samples are completely disintegrated

Figure 4.19 Pervious concrete samples after the third cycle during freeze-deicer salt scaling test (top to bottom) cement, cement + GO, fly ash, fly ash + GO

4.3.6 Degradation resistance test

At 90 days, three samples of each mix design were used to determine the degradation resistance of pervious concrete according to ASTM C1747. A Los Angeles abrasion machine was used for this test. The weight loss during the test was calculated to characterize the degradation resistance of each mix design. The GO-modified fly ash pervious concrete samples before and after the test are shown in Figure 4.20 The test results for all samples are shown in Figure 4.21.

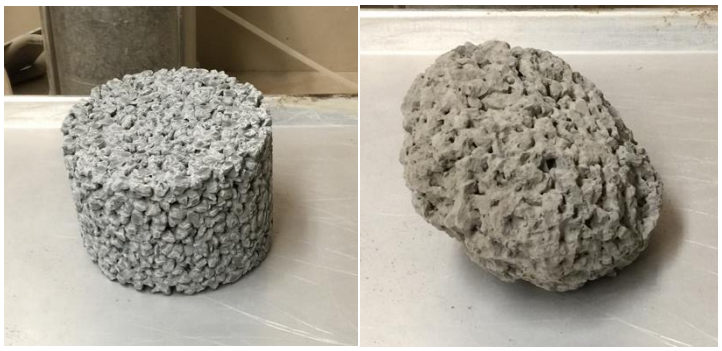

(a) (b)

Figure 4.20 Samples before and after degradation test. (a) before test; (b)after test

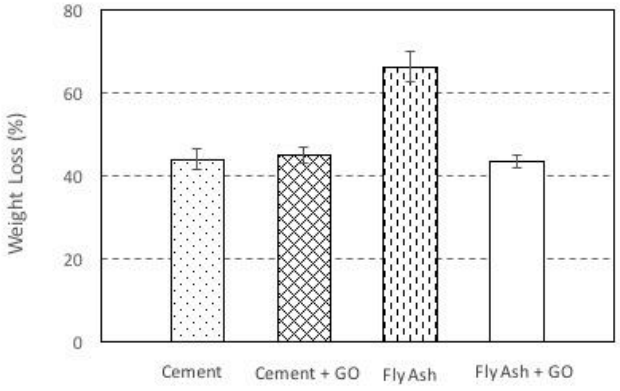

Figure 4.21 Degradation test results

The weight loss values for all samples were within the range of 38% to 72% at 90days. A similar test performed on the cement pervious concrete had weight loss between 35% to 80%

(Qiao Dong et al. 2013). After the test, the fly ash pervious concrete had the highest weight loss of 66%. However, the incorporation of GO decreased the weight loss of fly ash pervious concrete significantly (from 66% to 44%). The GO-modified cement pervious concrete showed similar weight loss (44%) as the cement samples (45%). This test indicated that the GO-modified fly ash pervious concrete had comparable degradation resistance to the cement pervious concrete at later age. It is recommended that the durability test for fly ash concrete be performed at later ages due to its later strength development.

4.4 Summary and Conclusions

With proven binding strength and durability of a pure fly ash paste, as described in the previous chapter, an innovative pervious concrete mix design of a pure fly ash binder modified by graphene oxide (GO) was developed. All hardened pervious concrete samples exhibited a density ranging from 1803 Kg/m^3 to 1990 Kg/m^3, but fly ash pervious concrete typically had a higher density than the cement pervious concrete. All the samples had values of void ratio between 20% and 31%. By incorporating GO into the binder, the average void ratio of fly ash pervious concrete was reduced from 24.9% to 21.2%, whereas the average void ratio of Portland cement pervious concrete was increased from 27.4% to 28.9%.

The average 28-day fc' for fly ash pervious concrete was1447 psi, and 2256 psi for GO-modified fly ash pervious concrete. The addition of 0.03% GO (by weight of binder) increased both 7-day and 28-day fc' of fly ash pervious concrete by more than 50%, while for Portland cement pervious concrete, the 0.03% GO increased the 28-day fc' by 24% and had little effect on early strength development.

It is noted that all samples produced from the improved mixing procedure described in Section 4.2.1 failed through the aggregate after compression tests (see Figure 4.8), which eliminated the weak interface zone between the paste and aggregates.

The average 28-day ft' for the fly ash pervious concrete was 200 psi, and 274 psi for GO-modified fly ash pervious concrete. The incorporation of 0.03% GO (by weight of binder) into the binder showed that the average 28-day ft' of fly ash pervious concrete was improved from 200.5 psi to 274.2 psi (by 37%), while the average 28-day ft' of cement pervious concrete was improved from 240.9 psi to 283.1 psi (by 18%). The split tensile strength was approximately equal to 12% of the compressive strength for all the pervious concrete mixes at 28 days.

The fly ash pervious concrete had a higher E of 2950 ksi than that of Portland cement pervious concrete (E = 2450 ksi) at 28 days. At 28 days, the incorporation of 0.03% GO increased the E of the fly ash pervious concrete by 6.8%, while it increased the E of the Portland cement pervious concrete by 4.1%.

For all mixes, the measured infiltration rate ranged from 515 in./hr to 2082 in./hr. Portland cement pervious concrete had a higher infiltration rate than fly ash groups. While the GO reduced the infiltration rate of the fly ash pervious concrete, it significantly improved the infiltration rate of the Portland cement pervious concrete. The infiltration rate was found to increase exponentially as a function of void ratio.

The freeze-deicer salt scaling resistance test was conducted at 28 days; the initial weight loss of fly ash pervious concrete was much higher than that of cement pervious concrete due to the slow hydration of fly ashes. The incorporation of GO increased the salt scaling resistance for all groups, but the improvement for the cement pervious concrete was marginal. The GO-modified fly ash pervious concrete was the only group that survived after the fifth cycle with

57% weight loss, which indicated that GO-modified hydration products from the fly ash had a better salt scaling resistance than the conventional cement hydrates.

At 90 days, the degradation resistance of pervious concrete was tested according to ASTM C1747. The results indicated that the GO-modified fly ash pervious concrete had a comparable degradation resistance to the cement pervious concrete at later age. The incorporation of GO decreased the weight loss of fly ash pervious concrete significantly (from 66% to 44%) during the degradation test. It is recommended that the durability test for fly ash concrete be performed at later ages due to its later strength development.

It is concluded that the GO-modified fly ash pervious concrete developed in this study is comparable to ordinary cement pervious concrete, with the desirable density, void ratio, strength, infiltration rate, and degradation resistance. However, the freeze-deicer salt scaling resistance of fly ash pervious concrete is not as good as ordinary cement pervious concrete due to its high initial loss. Further investigation is needed to improve its hydration degree at early ages.

CHAPTER 5.0 CONCLUSION

5.1 Summary

The laboratory study reported here explores the beneficial use of coal fly ash as cementitious binder without heat activation. Based on the literature review, high-calcium fly ash shows the potential of being a sole binder in making moderate strength concrete such as pervious concrete. The study began with a small-scale mortar test. A *uniform design* scheme was employed for the statistical design of experiments. Predictive models were developed later based on the experimental data to quantify the influence of mix design parameters on the compressive strength of fly ash mortars at various ages. The models were verified and then employed for predictions.

The first group of mortar samples was fabricated using a low-reactivity, high-calcium fly ash and a low-calcium fly ash, as well as admixtures intended to improve the strength and durability of hardened mortar. In the absence of chemical activation, these fly ash mortars exhibited a relatively low 28-day compressive strength in the range of 420–2975 psi, whereas a high-calcium, high-reactivity fly ash mortar developed a 28-day compressive strength of 4000 psi at 28 days. The styrene–butadiene rubber (SBR) latex exhibited a negative impact on the compressive strength of fly ash mortars. Admixing a small amount of montmorillite nanoclay (0.6% by mass of Class C fly ash) significantly improved the compressive strength of fly ash mortars.

The second group of mortar samples was fabricated using the same low-activity, high-calcium fly ash along with the following chemical activators: sodium silicate, quicklime, calcium chloride, and sodium sulfate. Admixing chemical activators with fly ash mortars led to a

noticeable improvement in the mechanical properties of the fly ash, with a 28-day compressive strength in the range of 2432–4878 psi. These activators also showed a high level of synergetic effects.

Microscopic examination was conducted to shed light on the hydration behavior of selected fly ash mortars. Without activation, the fly ash spheres were only covered by a submicron-thin layer of hydration products and served mainly as micro-aggregates. With chemical activation at room temperature, fly ash spheres dissolved, and some interlacing fibrous structures formed among the spheres, which contributed to strength improvement of the mortars. This explains the observed difference in the two groups of fly ash mortars and points to a direction for further improving the development of such unconventional mortars and concretes.

The effect of graphene oxide (GO) on the strength of activated fly ash mortar was also studied. It is observed that an increase of 23% in the 28-day compressive strength of fly ash mortar was achieved by incorporating 0.03% (by weight of fly ash) GO. A microscopic investigation was also conducted to obtain more insights on the effects of GO. It was found that the Ca/Si mole ratio of the regular fly ash mortar featured a mean value of 0.926 with a standard deviation of 1.281, whereas that of GO-modified fly ash mortar had a higher mean value of 1.384 with a standard deviation of 2.111. The increased average bulk Ca/Si ratio, from 0.926 to 1.384, by GO indicated that the addition of 0.03% GO could facilitate the leaching of Ca^{2+} from fly ash particles. Meanwhile, since a higher standard deviation of the Ca/Si ratio was observed in the GO-modified fly ash mortar, it is likely that the GO nanosheets dispersed in fly ash paste act as growth points to form hydration products with a higher Ca/Si ratio due to their higher surface energy and template effect.

With the proven binding strength and durability of a pure fly ash paste, an innovative pervious concrete mix design of pure fly ash binder modified by GO was developed. All hardened pervious concrete samples from different mix designs had a density that ranged from 1803 Kg/m^3 to 1990 Kg/m^3 with a void ratio between 20% and 31%.

The average 28-day *fc'* for fly ash pervious concrete was 1447 psi, and 2256 psi for GO-modified fly ash pervious concrete. The average 28-day *ft'* for fly ash pervious concrete was 200 psi, and 274 psi for GO-modified fly ash pervious concrete. It was found that split tensile strength was equal to 12% of compressive strength for all pervious concrete mixes at 28 days. Young's modulus was measured. Fly ash pervious concrete had a higher E of 2950 ksi than that of Portland cement pervious concrete (E = 2450 ksi) at 28 days. The incorporation of 0.03% GO increased the E of the fly ash pervious concrete by 6.8%. While the incorporation of 0.03% GO increased the overall mechanic performance of fly ash pervious concrete, it reduced the infiltration rate of fly ash pervious concrete.

As part of the durability tests, the freeze-deicer salt scaling resistance test was conducted at 28 days. The results showed that the initial weight loss of fly ash pervious concrete was much higher than that of cement pervious concrete due to the slow hydration of fly ash, but the complete hydration products of GO-modified fly ash pervious concrete showed the best salt scaling resistance among all samples. The incorporation of GO increased the salt scaling resistance for all groups. Since the salt scaling test suggested that durability tests for fly ash concrete should be performed at later ages due to its later strength development, the degradation resistance of pervious concrete was tested according to ASTM C1747 at 90 days. The results indicated that GO-modified fly ash pervious concrete had comparable degradation resistance to

cement pervious concrete at a later age. The incorporation of GO decreased the weight loss of fly ash pervious concrete significantly (from 66% to 44%) during the degradation test.

It is concluded from the laboratory study that GO-modified fly ash pervious concrete is comparable to ordinary cement pervious concrete with the desirable density, void ratio, strength, infiltration rate, and degradation resistance. However, the freeze-deicer salt scaling resistance of fly ash pervious concrete is not as good as ordinary cement pervious concrete due to its high initial loss. Further investigation is needed to improve its hydration degree at early ages.

This study demonstrated an example of beneficial use of fly ash, which not only diverts fly ash from the waste stream to a building material application, but also shows the potential of fly ash for reducing the CO_2 footprint of the concrete industry by replacing Portland cement.

5.2 Findings

In addition to being categorized as Class C and Class F, fly ash can be divided into *high-calcium* fly ash (CaO content > 10%) and *low-calcium* fly ash (CaO content < 10%), based on CaO content difference. The reactivity of fly ash is determined by the content of CaO, Al_2O_3, and SiO_2. As defined in Table 3.2, fly ash can be categorized into *high-reactivity, low-reactivity,* and *inert* groups.

High-calcium, high-reactivity fly ash is cementitious in nature. *High-calcium, low-reactivity* fly ash is both pozzolanic and cementitious in nature, which requires activation for complete hydration. *Low-calcium* fly ash is generally pozzolanic.

In order to activate the *high-calcium, low-reactivity* fly ash used in this study, sodium silicate, quicklime, calcium chloride, and sodium sulfate were chosen as chemical activators. Admixing chemical activators into fly ash mortars led to a noticeable improvement in their

mechanical properties and durability. These activators also showed a high level of synergetic effects.

Graphene oxide improved the overall performance of pervious concrete significantly by regulating hydration, providing a crack branching and bridging mechanism, and acting as nanofillers.

Normally, the hydration degree for fly ash binder is relatively low at early ages. However, the GO-modified hydration products of fly ash showed better freeze-deicer salt scaling resistance than cement hydrates during the salt scaling test. The degradation test performed at later ages showed that GO can decrease the weight loss of fly ash pervious concrete significantly.

It was noted that samples produced from the improved mixing procedure, described in Section 4.2.3, failed through the aggregate after compression tests (see Figure 4.8), which eliminated the weak interface zone between the paste and aggregates.

5.3 Recommendations

In Phase I of this project, many of the results suggested the potential of fly ash in its application to pervious concrete. Some areas still need study and evaluation in Phase II.

- Water treatment tests should be conducted to evaluate the effectiveness of the filtration function provided by fly ash pervious concrete. These tests can also address the concerns about heavy metal leaching from fly ash itself, which can cause water contamination.
- The performance of fly ash at early ages must be improved. Due to slow hydration, fly ash concrete typically shows better performance at later ages. To address this issue, some mechanical or chemical techniques, such as reinforcing fibers and better activators, are needed to improve early strength.
- More studies are needed to characterize fly ash hydration products with GO. Some

advanced tools can be used to determine chemical compositions, mineralogy, and degree of polymerization of hydrates, such as NMR, FI-IR, XRD, and XRF.

- The abrasion resistance of pervious concrete needs to be improved at early ages, which is a concern at locations where there is significant turning traffic, snow plows, and studded tire application.
- Since fly ash binder is fundamentally different from cement binder, some other environmental benefits from fly ash pervious concrete, such as heat-island effects and acoustic absorption effects, need evaluation.

Pervious concrete is a green concrete, which has many environmental benefits. Using fly ash from industrial waste in pervious concrete is an added environmental benefit. The successful development of fly ash pervious concrete provides a template to incorporate even more waste to reduce the need for consuming natural resources in building materials. Various types of recycled materials can be incorporated into this kind of pervious concrete in the future.

CHAPTER 6.0 REFERENCES

Abdolhosseini Qomi, M. J., Krakowiak, K. J., Bauchy, M., Stewart, K. L., Shahsavari, R., Jagannathan, D., Brommer, D. B., Baronnet, A., Buehler, M. J., Yip, S., Ulm, F.-J., Van Vliet, K. J., and Pellenq, R. J.-M. (2014). "Combinatorial molecular optimization of cement hydrates." *Nature Communications*, 5, 4960.

Amde, A. M., and Rogge, S. (2013). *Development of High Quality Pervious Concrete Specifications for Maryland Conditions*.

Anderson, I., Suozzo, M., and Dewwoolkar, M. (2013). *Laboratory & Field Evalua ons of Pervious Concrete*. TRC Report.

Antiohos, S., and Tsimas, S. (2004). "Activation of fly ash cementitious systems in the presence of quicklime." *Cement and Concrete Research*, 34(5), 769–779.

Ashbrook, Sharon. (2006). "Nuclear Magnetic Resonance in Mineralogy." University of St Andrews.

Berry, M., Stephens, J., and Cross, D. (2011). "Performance of 100% fly ash concrete with recycled glass aggregate." *ACI Materials Journal*, 108(4).

Bin Tong. (2011). "Clogging effects of portland cement pervious concrete." Iowa State University.

Brough, A. R., and Atkinson, A. (2002). "Sodium silicate-based, alkali-activated slag mortars: Part I. Strength, hydration and microstructure." *Cement and Concrete Research*, 32(6), 865–879.

Brouwers, H. J. H., and Eijk, V. R. J. (2003). "Chemical reaction of fly ash." *Proceedings of the 11th International Congress on the Chemistry of Cement (ICCC)*, Durban, South Africa.

Bury, M. A., Mawby, C. A., and Fisher, D. (2006). "Making Pervious Concrete Placement Easy Using a Novel Admixture System." *Concrete inFOCUS*, (Fall).

C09 Committee. (2012). *Specification for Coal Fly Ash and Raw or Calcined Natural Pozzolan for Use in Concrete*. ASTM International.

Crouch, L. K., Pitt, J., and Hewitt, R. (2007). "Aggregate Effects on Pervious Portland Cement Concrete Static Modulus of Elasticity." *Journal of Materials in Civil Engineering*, 19(7), 561–568.

Das, B., and Sobhan, K. (2013). *Principles of Geotechnical Engineering*. Cengage Learning.

Davidovits, J. (1982). "Mineral polymers and methods of making them, USA patent 4,349,386 A."

Diamond, Sidney. (1981). "The characterization of fly ashes." *MRS Annual Meeting*, Boston.

Duxson, P., and Provis, J. L. (2008). "Designing Precursors for Geopolymer Cements." *Journal of the American Ceramic Society*, 91(12), 3864–3869.

Enders, M. (1995). "Microanalytical characterization (AEM) of glassy spheres and anhydrite from a high-calcium lignite fly ash from Germany." *Cement and Concrete Research*, 25(6), 1369–1377.

Fang, K.-T., Lin, D. K. J., Winker, P., and Zhang, Y. (2000). "Uniform Design: Theory and Application." *Technometrics*, 42(3), 237–248.

Fan, W.-J., Wang, X.-Y., and Park, K.-B. (2015). "Evaluation of the Chemical and Mechanical Properties of Hardening High-Calcium Fly Ash Blended Concrete." *Materials*, 8(9), 5933–5952.

Fernández-Jiménez, A., and Palomo, A. (2005). "Composition and microstructure of alkali activated fly ash binder: Effect of the activator." *Cement and Concrete Research*, 35(10), 1984–1992.
Fernández-Jiménez, A., Palomo, A., and Criado, M. (2005). "Microstructure development of alkali-activated fly ash cement: a descriptive model." *Cement and Concrete Research*, 35(6), 1204–1209.
Flores, J. J., Martínez, B., and Uribe, R. (2007). "Analysis of the behavior of filtration vs. compressive strength ratio in pervious concrete." *Pervious Concrete Symposium Proceedings*.
Gan, M. S. J. (1997). *Cement and Concrete*. CRC Press.
Ghafoori, N., and Dutta, S. (1995). "Laboratory Investigation of Compacted No-Fines Concrete for Paving Materials." *Journal of Materials in Civil Engineering*, 7(3), 183–191.
Gong, K., Pan, Z., Korayem, A. H., Qiu, L., Li, D., Collins, F., Wang, C. M., and Duan, W. H. (2015). "Reinforcing Effects of Graphene Oxide on Portland Cement Paste." *Journal of Materials in Civil Engineering*, 27(2).
Guo, X., Shi, H., and Dick, W. A. (2010). "Compressive strength and microstructural characteristics of class C fly ash geopolymer." *Cement and Concrete Composites*, 32(2), 142–147.
Harwalkar, A., and Awanti, S. (2014). "Laboratory and Field Investigations on High-Volume Fly Ash Concrete for Rigid Pavement." *Transportation Research Record: Journal of the Transportation Research Board*, 2441, 121–127.
Haselbach, L., and Freeman, R. (2006). "Vertical Porosity Distributions in Pervious Concrete Pavement." *Materials Journal*, 103(6), 452–458.
Hemmings, R. T., and Berry, E. E. (1987). "On the Glass in Coal Fly Ashes: Recent Advances." *Symposium Q – Fly Ash and Coal Conversion By-Products IV*, MRS Online Proceedings Library Archive.
Hendrik G. van Oss. (2015). "USGS Cement Production in 2014." USGA.
Holland, Terence. (2005). *Silicafume Users Manual*. Technical Report.
Huang, B., Wu, H., Shu, X., and Burdette, E. G. (2010). "Laboratory evaluation of permeability and strength of polymer-modified pervious concrete." *Construction and Building Materials*, 24(5), 818–823.
Iribarne, J., Iribarne, A., Blondin, J., and Anthony, E. J. (2001). "Hydration of combustion ashes — a chemical and physical study." *Fuel*, 80(6), 773–784.
Jin, J. (2002). "Properties of mortar for self-compacting concrete." University of London.
Joseph Davidovits. (1994). "Properties of geopolymer cements." Kiev Ukraine.
Joshi, R. C. (1970). "Pozzolanic reactions in synthetic fly ashes."
Joung, Y. (2008). "Evaluation and optimization of pervious concrete with respect to permeability and clogging." Texas A&M University.
Kevern, J., and Sparks, J. (2013). "Low-Cost Techniques for Improving the Surface Durability of Pervious Concrete." *Transportation Research Record: Journal of the Transportation Research Board*, 2342, 83–89.
Kevern, J. T., Wang, K., and Schaefer, V. R. (2010). "Effect of Coarse Aggregate on the Freeze-Thaw Durability of Pervious Concrete." *Journal of Materials in Civil Engineering*, 22(5), 469–475.
Kevern, J., Wang, K., Suleiman, M. T., and Schaefer, V. R. (2006). "Pervious concrete construction: Methods and quality control." *Submitted to Concrete Technology Forum-*

Focus on Pervious Concrete, National Ready Mix Concrete Association, Nashville, TN, May, 23–25.
Kim, H. K., and Lee, H. K. (2010). "Acoustic absorption modeling of porous concrete considering the gradation and shape of aggregates and void ratio." *Journal of Sound and Vibration*, 329(7), 866–879.
Koehler, E., Offenberg, M., Malone, J., and Jeknavorian, and A. A. (2009). "Chemical Admixture System for Pervious Concrete." *Special Publication*, 262, 273–286.
Kutchko, B. G., and Kim, A. G. (2006). "Fly ash characterization by SEM–EDS." *Fuel*, 85(17–18), 2537–2544.
Lee, C., Wei, X., Kysar, J. W., and Hone, J. (2008). "Measurement of the Elastic Properties and Intrinsic Strength of Monolayer Graphene." *Science*, 321(5887), 385–388.
Lee, H., Cody, R. D., Cody, A. M., and Spry, P. G. (2000). "Effects of various deicing chemicals on pavement concrete deterioration." *Mid-Continente Transportation Symposium Proceedings*.
Li,Chao. (2011). "Research on the glass phase of slag, high calcium fly ash and low calcium fly ash and their hydration mechanism." Doctor of Engineering, Tsinghua University.
Li, C., Sun, H., and Li, L. (2010). "A review: The comparison between alkali-activated slag (Si + Ca) and metakaolin (Si + Al) cements." *Cement and Concrete Research*, 40(9), 1341–1349.
Li, D., Mueller, M. B., Gilje, S., Kaner, R. B., and Wallace, G. G. (2008). "Processable aqueous dispersions of graphene nanosheets." *Nature nanotechnology*, 3(2), 101–105.
Lv, S., Ting, S., Liu, J., and Zhou, Q. (2014). "Use of graphene oxide nanosheets to regulate the microstructure of hardened cement paste to increase its strength and toughness." *CrystEngComm*, 16(36), 8508–8516.
Marchand, J., Pigeon, M., Bager, D., and Talbot, C. (1999). "Influence of Chloride Solution Concentration on Deicer Salt Scaling Deterioration of Concrete." *Materials Journal*, 96(4), 429–435.
McCarthy, G. J., and Solem-Tishmack, J. K. (1994). "Hydration Mineralogy of Cementitious Coal Combustion By-Products." ASCE, 103–121.
Meininger, Richard C. (1988). "No-Fines Pervious Concrete for Paving." *Concrete International*, 10(8), 20–27.
Minkara, R. (2015). "Beneficial Use of Ash in Concrete.pdf." North Carolina Coal Ash Management Commission.
Montes, F., Valavala, S., and Haselbach, L. M. (2005). "A new test method for porosity measurements of Portland cement pervious concrete." *Journal of ASTM International*, 2(1), 13.
Muthukumar, M., and Mohan, D. (2004). "Optimization of mechanical properties of polymer concrete and mix design recommendation based on design of experiments." *Journal of Applied Polymer Science*, 94(3), 1107–1116.
National Ready Mixed Concrete Association (NRMCA). (2004). *Freeze-Thaw Resistance of Pervious Concrete*. Silver Spring, Maryland.
Neithalath, N. (2004). "Development and characterization of acoustically efficient cementitious materials." *Theses and Dissertations Available from ProQuest*, 1–245.
NeithAlAth, Na., Bentz, D. P., and Sumanasooriya, M. S. (2010). "Predicting the Permeability of Pervious Concrete." *Concrete international*, 35.

Neithalath, N., Weiss, J., and Olek, J. (2006). “Predicting the permeability of pervious concrete (enhanced porosity concrete) from non-destructive electrical measurements.” *United States: Purdue University*.

Olek, J., Cohen, M., Scholer, C., and Mandrekar, D. (2003). “Use of Modulus of Rupture, Fatigue Resistance and Maturity in Determining Opening to Traffic Time for Concrete Pavements.” *Joint Transportation Research Program*, 218.

Palomo, A., Grutzeck, M. W., and Blanco, M. T. (1999). “Alkali-activated fly ashes: A cement for the future.” *Cement and Concrete Research*, 29(8), 1323–1329.

Park, S. B., Seo, D. S., and Lee, J. (2005). “Studies on the sound absorption characteristics of porous concrete based on the content of recycled aggregate and target void ratio.” *Cement and Concrete Research*, 35(9), 1846–1854.

Polder, R. B. (2001). “Test methods for on site measurement of resistivity of concrete — a RILEM TC-154 technical recommendation.” *Construction and Building Materials*, Near Surface Testing of, 15(2–3), 125–131.

Putman, B. J., and Neptune, A. I. (2011). “Comparison of test specimen preparation techniques for pervious concrete pavements.” *Construction and Building Materials*, 25(8), 3480–3485.

Qiao Dong, Hao Wu, Baoshan Huang, Xiang Shu, and Kejin Wang. (2013). “Investigation into Laboratory Abrasion Test Methods for Pervious Concrete.” *Journal of Materials in Civil Engineering*, 25(7), 886–892.

Qin, Y., Yang, H., Deng, Z., He, J., Qin, Y., Yang, H., Deng, Z., and He, J. (2015). “Water Permeability of Pervious Concrete Is Dependent on the Applied Pressure and Testing Methods, Water Permeability of Pervious Concrete Is Dependent on the Applied Pressure and Testing Methods.” *Advances in Materials Science and Engineering, Advances in Materials Science and Engineering*, 2015, 2015, e404136.

Ramezanianpour, A. A. (2014). “Fly Ash.” *Cement Replacement Materials*, Springer Berlin Heidelberg, Berlin, Heidelberg, 47–156.

Ranjbar, N., Mehrali, M., Mehrali, M., Alengaram, U. J., and Jumaat, M. Z. (2015). “Graphene nanoplatelet-fly ash based geopolymer composites.” *Cement and Concrete Research*, 76, 222–231.

Roskos, C. (2011). “BUILDING GREEN: DEVELOPMENT AND EVALUATION OF AN ENVIRONMENTALLY FRIENDLY CONCRETE.” Masters of Science, MONTANA STATE UNIVERSITY.

Roskos, C., White, T., and Berry, M. (2015). “Structural Performance of Self-Cementitious Fly Ash Concretes with Glass Aggregates.” *Journal of Structural Engineering*, 141(3), B4014010.

Roy, D. M., and Ldorn, G. M. (1982). “Hydration, Structure, and Properties of Blast Furnace Slag Cements, Mortars, and Concrete.” *Journal Proceedings*, 79(6), 444–457.

Schaefer, V. R., Kevern, J. T., and Wang, K. (2009). “Pervious concrete mix design for wearing course applications.” *Proceedings of the Mid-Continent Transportation Research Symposium, Ames, Iowa*.

Schaefer, V. R., Suleiman, M. T., Wang, K., Kevern, J. T., and Wiegand, P. (2006). “An overview of pervious concrete applications in stormwater management and pavement systems.” *Civil, Construction and Environmental Engineering, Iowa State University, Ames, IA*, 50011.

Schneider, M., Romer, M., Tschudin, M., and Bolio, H. (2011). "Sustainable cement production—present and future." *Cement and Concrete Research*, Special Issue: 13th International Congress on the Chemistry of Cement, 41(7), 642–650.
Shi, C., and Day, R. L. (2000). "Pozzolanic reaction in the presence of chemical activators: Part I. Reaction kinetics." *Cement and Concrete Research*, 30(1), 51–58.
Sukamal Kanta Ghosh, Ananya Chaudhury, Rohan Datta, and D.K.Bera. (2015). "A REVIEW ON PERFORMANCE OF PERVIOUS CONCRETE USING WASTE MATERIALS." *International Journal of Research in Engineering and Technology*, 04(13), 105–115.
Tejaswi, S Sai, Rao, R Chinna, Vidya, B, and Renuka, J. (2015). "Experimental Investigation of Waste Glass Powder as Partial Replacement of Cement and Sand in Concrete." *IUP Journal of Structural Engineering*, 8(4), 14–22.
Tennis, P. D., Leming, M. L., and Akers, D. J. (2004). *Pervious concrete pavements*. Portland Cement Association, Skokie, Ill.
Thomas, M. D. A. (2007a). *Optimizing the use of fly ash in concrete*. Portland Cement Association Skokie, IL, USA.
Thomas, M. D. A. (2007b). *Optimizing the use of fly ash in concrete*. Portland Cement Association Skokie, IL.
Tishmack, J. K., Olek, J., and Diamond, S. (1999). "Characterization of high-calcium fly ashes and their potential influence on ettringite formation in cementitious systems." *Cement Concrete and Aggregates*, 21, 82–92.
Tishmack, J. K., Olek, J., Diamond, S., and Sahu, S. (2001). "Characterization of pore solutions expressed from high-calcium fly-ash–water pastes." *Fuel*, 80(6), 815–819.
Tung, V. C., Allen, M. J., Yang, Y., and Kaner, R. B. (2009). "High-throughput solution processing of large-scale graphene." *Nature Nanotechnology*, 4(1), 25–29.
Vassilev, S. V., Menendez, R., Borrego, A. G., Diaz-Somoano, M., and Rosa Martinez-Tarazona, M. (2004). "Phase-mineral and chemical composition of coal fly ashes as a basis for their multicomponent utilization. 3. Characterization of magnetic and char concentrates." *Fuel*, 83(11-12), 1563–1583.
Vassilev, S. V., and Vassileva, C. G. (2005). "Methods for Characterization of Composition of Fly Ashes from Coal-Fired Power Stations: A Critical Overview." *Energy & Fuels*, 19(3), 1084–1098.
Vernon R. Schaefer, Keijin Wang, Muhannad T. Suleiman, and John T. Kevern. (2006). *Mix Design Development for Pervious Concrete In Cold Weather Climates*. Iowa State University.
Wang, R., Lackner, R., and Wang, P.-M. (2011). "Effect of Styrene-Butadiene Rubber Latex on Mechanical Properties of Cementitious Materials Highlighted by Means of Nanoindentation: Nano/Macro-Mechanical Properties of Latex-Modified Concrete." *Strain*, 47(2), 117–126.
Wanielista, M., and Manoj Chopra. (2007). *Performance Assessment of Portland Cement Pervious Pavement*. University of Central Florida.
Winnefeld, F., Leemann, A., Lucuk, M., Svoboda, P., and Neuroth, M. (2010). "Assessment of phase formation in alkali activated low and high calcium fly ashes in building materials." *Construction and Building Materials*, 24(6), 1086–1093.
Xie, N., Shi, X., Dang, Y., and Pace, A. (2015). "Up-cycling of waste materials: A 'green' binder prepared with pure coal fly ash."

Yang, Z., Shi, X., Creighton, A. T., and Peterson, M. M. (2009). "Effect of styrene–butadiene rubber latex on the chloride permeability and microstructure of Portland cement mortar." *Construction and Building Materials*, 23(6), 2283–2290.

Zhao, Y., Zhang, J., Tian, C., Li, H., Shao, X., and Zheng, C. (2010). "Mineralogy and Chemical Composition of High-Calcium Fly Ashes and Density Fractions from a Coal-Fired Power Plant in China." *Energy & Fuels*, 24(2), 834–843.

Zhong, S., and Chen, Z. (2002). "Properties of latex blends and its modified cement mortars." *Cement and Concrete Research*, 32(10), 1515–1524.